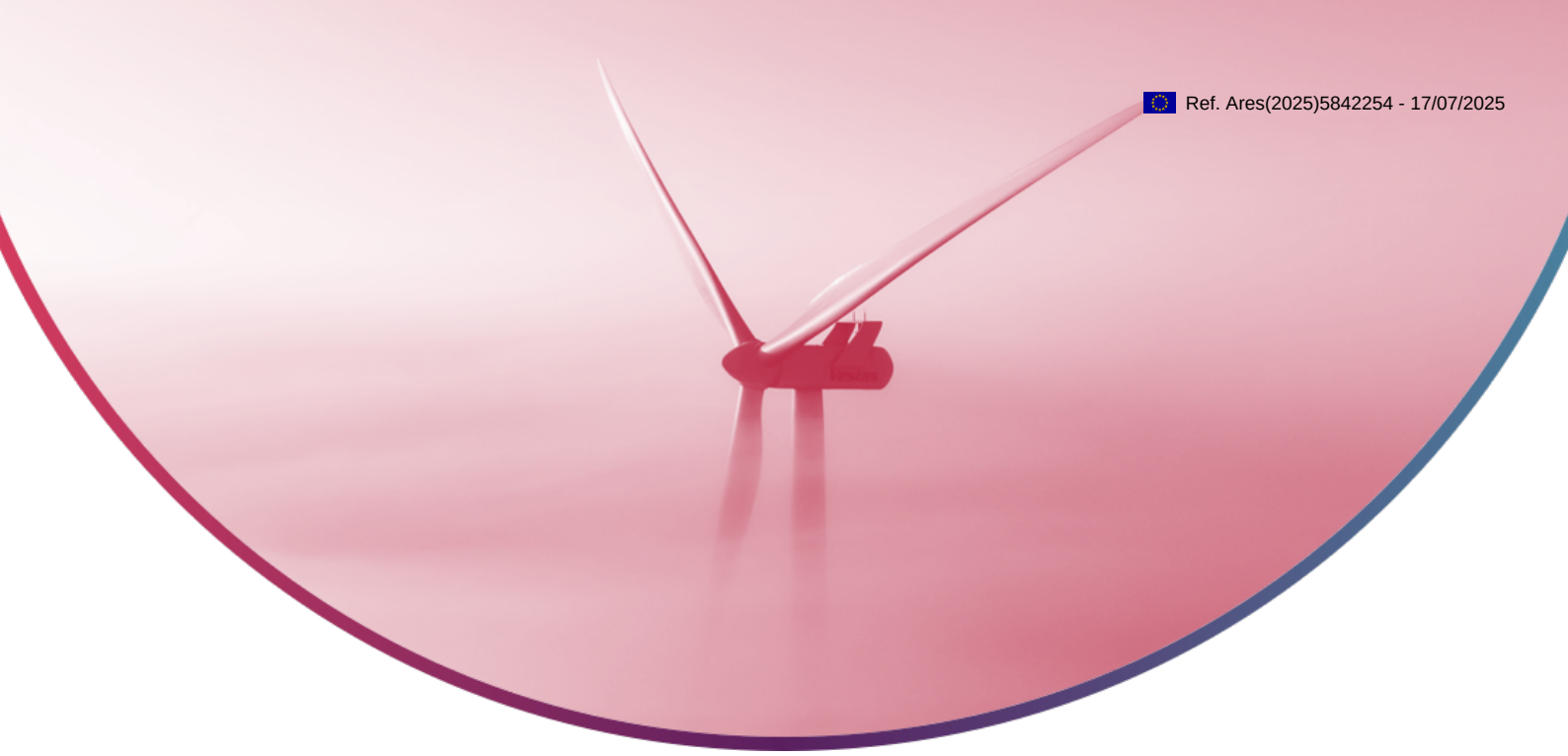

AiRE

D3.1- Mesoscale and wake model development for atmospheric flow of wind including precipitation and site characteristics

Development and extension of numerical models

DOCUMENT INFORMATION

PROJECT INFORMATION	
GRANT AGREEMENT NUMBER	101083716
PROJECT TITLE	Advanced study of the atmospheric flow Integrating REal climate conditions to enhance wind farm and wind turbine power production and increase components durability
PROJECT ACRONIM	AIRE
FUNDING SCHEME	HORIZON-RIA
PROJECT COORDINATOR	CENER
START DATE OF THE PROJECT	1 January 2023
DURATION	48 months
CALL IDENTIFIER	HORIZON-CL5-2021-D3-03
PROJECT WEBSITE	https://aire-project.eu/

DELIVERABLE INFORMATION	
DELIVERABLE N° & TITLE	D3.1- Mesoscale and wake model development for atmospheric flow of wind including precipitation and site characteristics
WP LEADER	VTT
DELIVERABLE CREATOR	Fraunhofer IWES
CONTRIBUTING PARTNERS	Fraunhofer IWES, CENER, VTT,
AUTHORS	Balthazarr Sengers, Irene Eguinoa, Jonas Schulte, Jennifer Carreiro Spencer, Guillén Campaña, Maria Aparicio-Sanchez, Alvaro Olcoz-Alonso, Elena Cantero, Iñaki Sandua-Fernández, Beatriz Méndez, Hassan Kassem,
REVIEWERS	Ásta Hannesdóttir (DTU) Beatriz Méndez (CENER) Laia Mencía (Inveniam)
CONTRACTUAL DEADLINE	2025-06-30
DELIVERY DATE TO EC	2025-07-17
DISSEMINATION LEVEL	public

DISCLAIMER

Funded by the European Union

CONTENTS

LIST OF FIGURES

LIST OF TABLES

1. EXECUTIVE SUMMARY

Atmospheric flow conditions are the main driving factors of erosion and blade surface damage. Understanding these factors and to be able to predict them accurately are fundamental. Therefore, in this task (Task3.1), the AIRE team across multiple leading industries and research institutes puts a great effort in assessing and developing models for predicting atmospheric conditions with a sharp focus on rain and precipitation forecasting. Due to the multi-scale nature of atmospheric flow, this task focused on the meso-scale modelling (AIRE modelled phenomena 1) and the micro-scale level (AIRE modelled phenomena 2). Addressing such a wide range of scales dictates a fine-tuned approach at each level. Hence, the AIRE methodology in this task followed a diverse approach in terms of techniques and methods, using different codes and tools.

On the largest scale (AIRE modelled phenomena 1), the meso-scale model WRF is used to simulate the target commercial sites with domain size of (100 km x 100km). The four sites cover a wide range of conditions and the produced time series is necessary for the development of the erosion risk atlas in WP4 and the case studies in WP5. In order to build up confidence in the model, in-depth sensitivity analysis is necessary. Previous wind atlases which are designed for wind energy applications, like the New European Wind Atlas (NEWA), focus primarily on wind speed and wind direction at the hub-height, while not taking any special care of precipitation. In this task, we are taking the NEWA-WRF setup to the next level by extending the evaluation matrix to cover wind and rain, and subsequently blade damage increments, by assessing WRF's sensitivity to its microphysics schemes. The sensitivity study is based on data from four sites, consisting of data obtained in AIRE as well as from publicly available data sets. These sites are independent of the target commercial sites in WP4 and WP5 which add an extra layer of confidence in the results and avoiding any site-specific tuning. This exercise resulted in a new model configuration that more accurately the most damaging conditions, i.e. high rain rates in combination with high wind speed, than the standard model setup. Using this setup, the production runs of the four commercial sites were conducted for one representative year of rain and wind across Europe.

Moving to the micro-scale level (AIRE modelled phenomena 2), it was apparent from the beginning that multiple fidelity approaches were needed to address these different phenomena such as wakes, complex terrain flow and turbulence. In pursuit in addressing this, the work was split into three sub-tasks, namely rain effect on wakes, flow in complex terrain and high-fidelity turbulent simulations.

Based on a literature review, it was concluded that there are two main ways how rain can influence wakes, and therefore AEP. Firstly, the atmospheric conditions such as turbulence level, thermal stratification, wind speed and wind direction can change during rain events, impacting the wind turbine wake. Secondly, the blade surface erosion, hence the level of the surface damage, affects the turbine's performance which is also reflected in the wakes. After extensive cleaning and filtering of the windfarm data of multiple sites, in-depth studies of windfarm performance under rain and no rain conditions were performed using two open-source windfarm analysis tools (FOXES and FLORIS). It became evident that isolating the effect of rain on wakes is extremely challenging, considering that other atmospheric conditions might change during rain events. Moreover, the quality of the datasets have to be very high with the lowest uncertainty possible. Although some small changes were detected, it was concluded that longer time series with more rain events are needed to achieve statistical significance. Nevertheless, a complete workflow with clear guidelines was developed which shall be used later in WP5. Additionally, an initial implementation in FOXES was carried out to include the damage level as input and adjust the power and thrust curves accordingly. That paves the way for coupling FOXES with the windfarm controller in WP4.

Since AIRE is targeting both onshore and offshore windfarms, addressing the flow in complex terrain is inevitable. The research site Alaiz was chosen for this task, starting with a grid sensitivity study over the complex terrain and the wake regions using the open-source code OpenFOAM. Then moving to an essential yet challenging topic in CFD, namely turbulence modelling. Two turbulence models were used, and the results were compared. Finally, a validation study was conducted at the target measurements points with and without wakes.

To complete the work, this task addresses the mid-fidelity turbulence modelling using the open-source code FAST.Farm at Batskar the site based on the previous research project TUTTE. After careful data analysis, FAST.Farm models were implemented, and a wide range of turbulent atmospheric conditions using Turbsim were simulated. The results were validated against the wind farm production data and showed a very good agreement overall.

This deliverable is the cornerstone of AIRE's flow modelling challenge. In this report, all the above-mentioned points are discussed in great details. The findings of this work are already affecting other tasks within the project and provide the basis for the analysis to be performed in the project´s WP5 defining different case studies. While all originally proposed questions were addressed, more questions and challenges became more apparent, going far beyond the scope of this task and the entire project. Hence, potential improvements and follow-up studies are highlighted.

2. INTRODUCTION

As mentioned above this task has main modelling parts, namely Meso-scale model, wakes and wind farm models, flow in complex terrain and FAST.Farm models. This is naturally reflected on the structure of the this deliverable.

In Chapter 3, Fraunhofer IWES introduces the meso-scale sensitivity analysis and the production run of the WRF model. The sensitivity study is based on four sites reflecting different site conditions. Chapter 4 starts with a short literature review done by Fraunhofer IWES exploring the potential influence of rain on wakes. Then CENER demonstrate using FLORIS code in-depth analysis of wind data and operation data of a commercial wind farm. It is followed by an investigation done by Fruanhofer IWES using FOXES code for commercial farms too. The main objective of these two studies is to isolate the rain effect on wakes qualitatively and quantitively. Chapter 4 ends with short verification of FOXES code including the damage level influence on wind turbine performance.

Chapter 5 presents the sensitivity and validation case of flow in complex terrain Alaiz done by CENER. The sensitivity and validation includes the wake modelling using two different turbulence models. Then in Chapter 6, VTT gives a complete overview of Batskar wind farm dataset. Additionally, a wide range of conditions were modelled using FAST.Farm. In Chapter 7 CENER demonstrate the erosion effect on the windfarm level. Finally, Chapter 8 concludes this report with some general conclusions and findings.

3. MESOSCALE MODELS WITH WRF

3.1 Introduction

Mesoscale models are a standard tool used in wind resource assessment [19] and have in recent years been used to develop regional Erosion Risk Atlases [28, 12]. Within the AIRE project, in Task 4.2 an Erosion Risk Atlas will be developed and in WP5 the mesoscale model results will be used to assess the operational data. In this chapter, sensitivity tests are carried out with a range of model configurations to determine a set-up optimized for both precipitation and wind conditions. For this, in situ measurements of rain at the surface and wind at approximately the hub height were needed. To avoid having to wait for all WP2 campaigns to conclude, the sensitivity tests were not carried out for the four sites used in WP5 case studies. Rather, four different sites and data sets were used for the sensitivity tests: two from open access data sets (Cabauw and Falkenberg), and two from other AIRE sites (Alaiz and Risø). This also widen the scope and validity of the study, as any site-specific tuning is avoided.

3.2 Methods

3.2.1 Validation data

The following gives a very brief description of the sites used for validation. Their locations are displayed in Figure 1.

Cabauw: 51.971°N, 4.927°E; 0.7 m MSL
Located in a flat, rural area that consists mainly of pasture and grasslands. The climate is temperate maritime with precipitation throughout the year. Met mast is 213m tall with wind sensors at several heights, which here are linearly interpolated to 100m. Data are available for the year 2019.

Falkenberg: 52.167°N, 14.122°E; 73 m MSL
Located in a flat, rural region characterized by agricultural land. The climate is temperate continental, with precipitation mostly occurring during convective events in warmer months. The main mast is 99 meters tall and equipped with wind sensors at 98m, which are used for analysis. Data are available for the year 2022.

Risø: 55.694°N, 12.088°E; 6 m MSL
Located in a relatively flat coastal area characterized by open fields and agricultural land and proximity to the Roskilde Fjord. The climate is temperate oceanic, with moderate precipitation throughout the year. The met mast is 123m tall with several wind sensors, interpolated to 100m. Data are available for the year 2019.

Alaiz: 42.696°N, 1.555°W; 1000+ m MSL
Located in a complex terrain area in the Sierra de Alaiz mountain range. The climate is transitional between oceanic and Mediterranean, having seasonal variability in precipitation and wind conditions influenced by orographic effects. The mast is 118m tall, with wind measurements at 98.5m used in this work. Data are available for the period of Feb 2023 to Jan 2024.

Figure 1. Sites considered in sensitivity tests.

Table 1. General WRF settings that are untouched in the sensitivity tests.

Parameter	Setting
WRF model version	4.5
Surface layer scheme	MYNN
Land surface model	Unified Noah
Radiation schemes	RRTMG
Atmospheric boundary conditions	ERA5
Sea surface conditions	OSTIA
Nudging	Grid nudging above PBL
Nesting	One-way
Horizontal resolution	18, 6 and 2 km
Vertical resolution	61 eta levels

3.2.2 Mesoscale model

General setup

The Weather Research and Forecasting Model (WRF) is a mesoscale Numerical Weather Prediction (NWP) model that solves the basic equations related to large-scale atmospheric processes on a grid resolution of several km. Subgrid-scale processes, smaller than the magnitude of a few kilometers, are included as parameterizations. The underlying model equations are described in the model documentation [65]. In this work, the simulations were carried out with WRF v4.5. Many sensitivity tests were performed. The standard setup is based on multiple years of scientific work on the best-practice in the North Sea, hence an offshore environment. Extensive sensitivity studies with various physics schemes were carried out in [26], and the best-performing configuration was used by [19] to create the New European Wind Atlas (NEWA). The work presented at [11] validated simulations using a similar setup to lidar measurements, in the scope of wind farm cluster wakes. An overview of the main model settings for the mesoscale simulations with the WRF model applied in this work can be found in Table 1.

For the simulations of the precipitation and wind conditions, three one-way nested domains were used to downscale to the area of interest. Meteorological reanalysis data from ERA5 was used to drive the mesoscale simulation. Different years are simulated for each location depending on data availability. However, all simulations consist of a single year split into chunks of 10 days plus 1 day for spin-up to limit model drift.

Table 2. Overview of sensitivity tests. All other options are consistent between simulations.

Number	PBL	MP	CU	Comment
1	5	8	1	Recommended double-moment MP from literature
2	5	2	1	
3	5	7	1	
4	1	8	1	Same MP, but using different PBL scheme
5	1	2	1	
6	1	7	1	
7	5	10	1	Recommendation External Advisory board
8	5	8	1	Corrine land use data set
9	5	8	3	Change CU. Run 10: also turned on in innermost domain
10	5	8	3	
11	5	7	3	
12	5	4	3	Single-moment MP
13	5	6	3	
14	5	4	3	Changed hardcoded droplet number concentration
15	5	8	3	

Results are available every 10 minutes with a spatial resolution of 2 km and several vertical levels in the lowest 1000m. In post-processing, the wind fields are interpolated to the altitude of the measurements. Designated WRF runs were carried out for each measurement location, with the domains centered around the measurement point. The innermost domains had a spatial resolution of 2 km and 120 grid points in each direction, covering a total area of 240x240km.

Sensitivity tests

Due to its open-source access and high level of quality-controlled data, the Cabauw site was used to perform the majority of the sensitivity tests on. Initial configurations were based on recommendations from literature. After initial results showed large (precipitation) biases, tests were carried out with other Planetary Boundary Layer (PBL) schemes, Cumulus (CU) schemes for sub-grid scale precipitation, and single-moment microphysics schemes. Lastly, tests were conducted in which the hardcoded droplet number concentration was reduced, which was expected to lead higher rain rains as droplets would be larger and more easily become rain drops that can rain out. In addition to these tests, also the original setup from the New European Wind Atlas (NEWA) was ran again for reference. Table 2 summarizes the tests carried out, approximately in chronological order.

3.3 Results

Initial results

Figure 2 shows the annual accumulated rain fall (left) and mean wind speed (right) in Cabauw during the simulated year for all sensitivity tests from Table 2. The horizontal black dashed line indicates the observed values. The initial tests showed a significant underestimation of the precipitation, which led to a search for a model configuration that produces more rain.

Funded by the European Union

Without looking too much at the details of each simulation, two main conclusions could be drawn from these tests: 1) Using the Grell-Freitas (3) CU scheme instead of the default one systematically increased rain and 2) single-moment MP schemes seemed wetter than double-moment schemes. The mean wind speed was not much affected by these tests, with the exception of the tests changing the PBL scheme. Still, the overestimation of the mean wind speed is slightly larger compared to some of the initial setups that were optimized for wind applications. Based on these results, three configurations were selected for further analysis:

- Goddard (10): Best performing double-moment scheme
- WSM5 (12): Best performing single-moments scheme
- WSM5_NC (14): Best performance overall, but with hardcoded change of droplet number concentration

These three setups, together with NEWA and ERA5, are analyzed in more detail at the four sites discussed above.

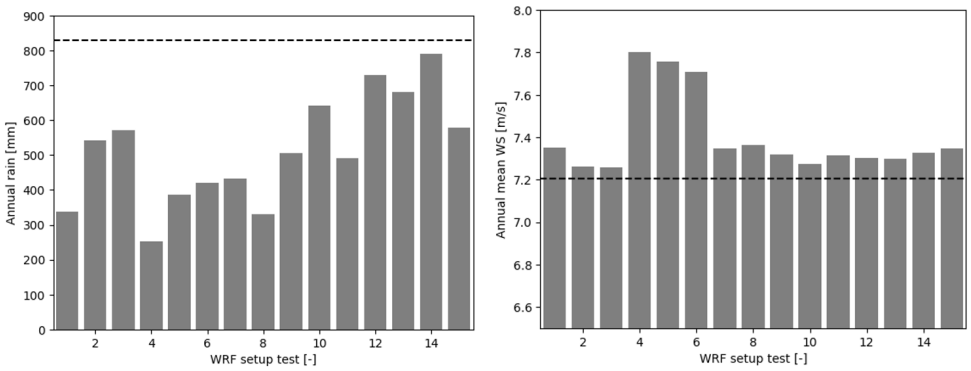

Figure 2. Initial results of all sensitivity tests compared to measurements (horizontal black dashed line) at Cabauw. (a) Annual (summed) rain and (b) annual mean wind speed.

Funded by the European Union

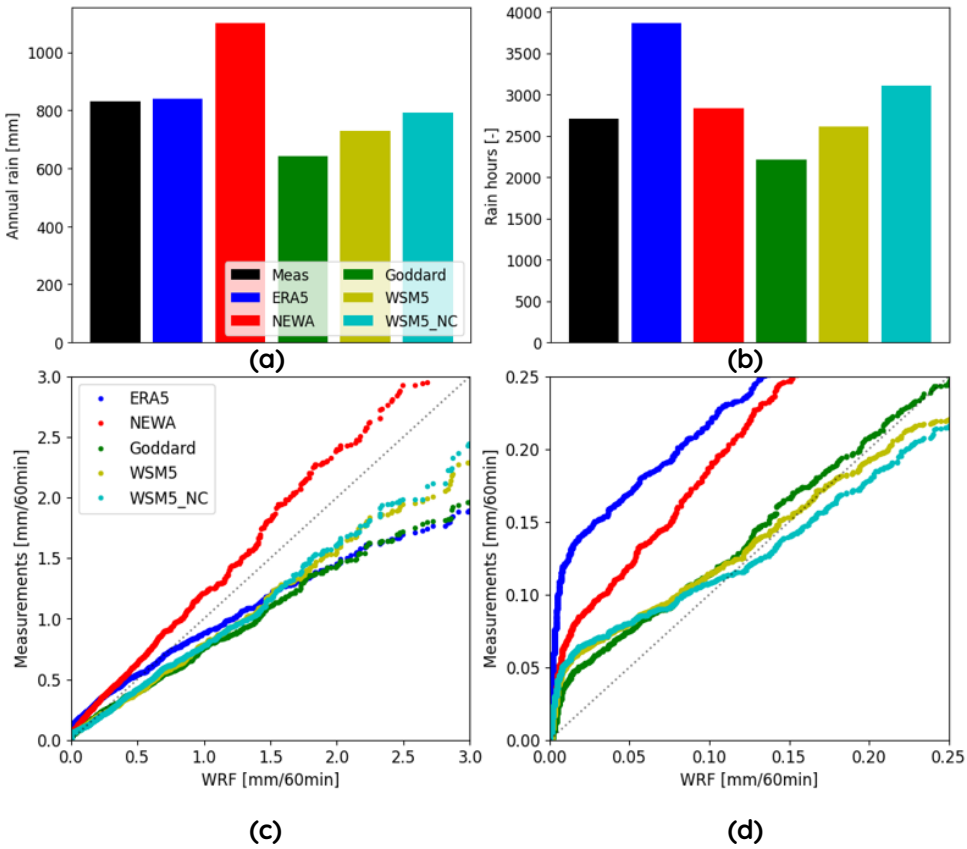

Figure 3. Comparison of measurements (black) and model results for rainfall. (a) Annual (summed) rain, (b) number of rain hours, (c) Q-Q plot of the rain rate and (d) Q-Q plot of the rain rate zoomed in to smallest values.

Detailed investigation

Figure 3a shows a measured annual rainfall of just over 800 mm, which is very well reproduced by ERA5. NEWA overestimates this by about 300 mm, while the new WRF results tend to underestimate by up to 200 mm. When looking at the number of rain hours (counting time steps with a rain rate larger than zero) in Figure 3b, one can see that ERA5 and WSM5_NC overestimate it, Goddard underestimates and NEWA and WSM5 are pretty accurate. Since ERA5 and WSM5_NC were good on total rain but overestimate the number of rain hours, this indicates that the simulated rain intensity is too low. To confirm this, Figure 3c shows Q-Q plots, with Figure 3d zooming in on the smaller values. Clearly, all simulations overestimate the low-intensity events, with most underestimating high-intensity events. Only NEWA runs parallel to the unity line, but together with an overestimation of low-intensity events, this results in an overestimation of total rain.

When looking at 100 m height wind speed, the Weibull distributions (Figure 4a) show an underestimation of mean wind speed for ERA5 and an overestimation for all other models. To estimate the impact this has on a turbine's energy production, this wind speed signal is used to estimate the Annual Energy Production (AEP) of a single IEA 15MW turbine (note that the wind speeds are taken at 100m while the hub height is 150m). Relative to the AEP calculated with the wind speed measurements (Figure 4b), it is shown that ERA5's underestimation of wind speed would result in an AEP bias of -12%, while all others result in an overestimation of 2-6%, with Goddard showing the best performance.

Funded by the European Union

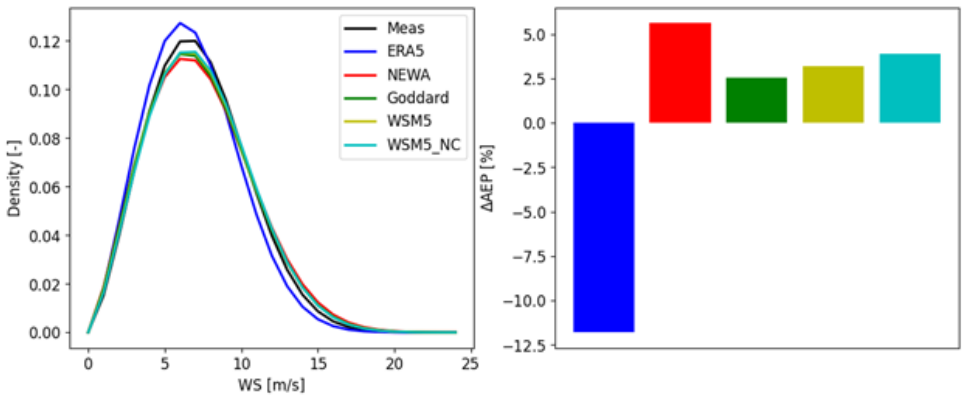

(a) (b)

Figure 4. Comparison of measurements (black) and model results for wind speed. (a) Weibull distribution, (b) Annual Energy Production (AEP) difference between models and measurements estimated from the wind speed time series for an IEA 15MW turbine.

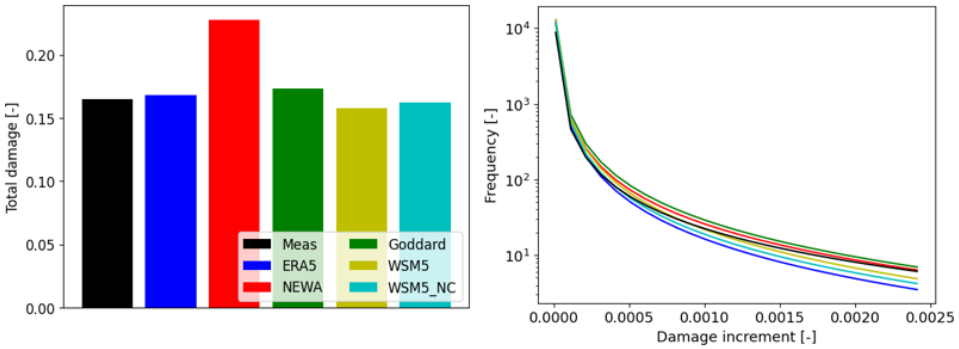

(a) (b)

Figure 5. Comparison of measurements (black) and model results for damage. (a) Total (summed) annual damage, (b) frequency of damage increments.

Finally, the blade damage model from [28] was used to estimate the damage incurred on an IEA 15MW turbine [24] during the simulated year. This is deemed a relevant metric, as it combines wind speed and precipitation estimates, and will be the eventual metric calculated in the Erosion Risk Atlas in Task 4.2.

The total damage (Figure 5a) shows that most models are quite accurate, only NEWA showing a large overestimation. Given the deviations in precipitation and wind speeds, this is quite a surprising result. To study this result in more detail, the frequency of the damage increments is shown in Figure 5b, with the high increments (most damaging events) on the far right. This shows that the models seem to contain mostly systematic differences to each other, while the measurements don't quite show the same pattern. Goddard and NEWA perform best at larger increments, while overestimating at smaller increments. All others perform better at small increments but underestimate the large increments. Since these large increments are most important for the total damage, it is argued that these should be well represented.

Funded by the European Union

3.3.1 Other sites

Alaiz

The results for annual rain in Alaiz look similar to those in Cabauw, with ERA5, WSM5 and WSM5_NC performing well, NEWA overestimating and Goddard underestimating. For wind speed and therefore AEP, ERA5 shows a huge underestimation, likely due to the complex topography that cannot be resolved at its spatial resolution. NEWA and the other WRF runs seem to perform well, with slight AEP underestimation of up to 5% and Goddard again showing the strongest performance. Looking at damage, only NEWA accurately reproduces the total damage calculated from the observations, resulting from an overestimation of precipitation and underestimation of wind speed, and the three WRF runs showing underestimations of the total damage. From the frequency distribution it can be learned that none of the models capture the large damage increments, but once again NEWA and Goddard are closest to the observations.

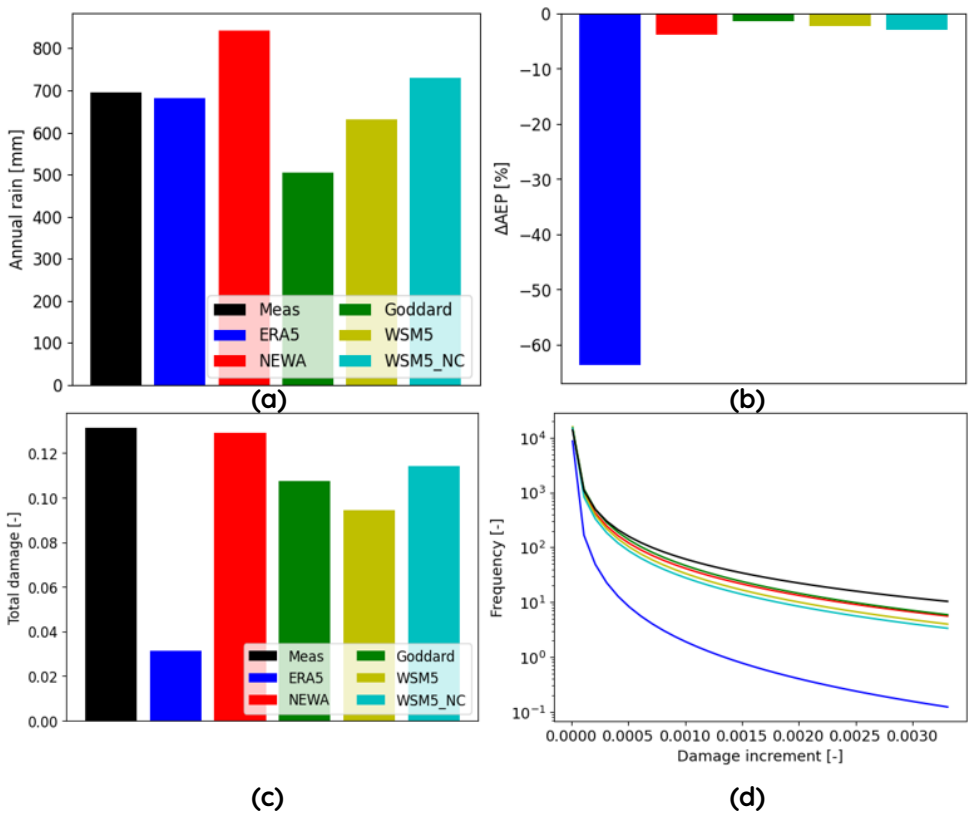

Figure 6. Similar to Figures 3-5, but for Alaiz. (a) Annual (summed) rain, (b) AEP differences relative to measurements, (c) total (summed) damage and (d) frequency of damage increments.

Funded by the European Union

Risø

At Risø, the annual precipitation is underestimated by all models except NEWA. The wind speed is rather well reproduced, except for in NEWA where AEP is overestimated by close to 20%. This in turn leads to an overestimation of total damage from NEWA, while ERA5 and the other WRF runs perform well. Interestingly, in the damage increment distribution NEWA does seem to perform best, with Goddard following.

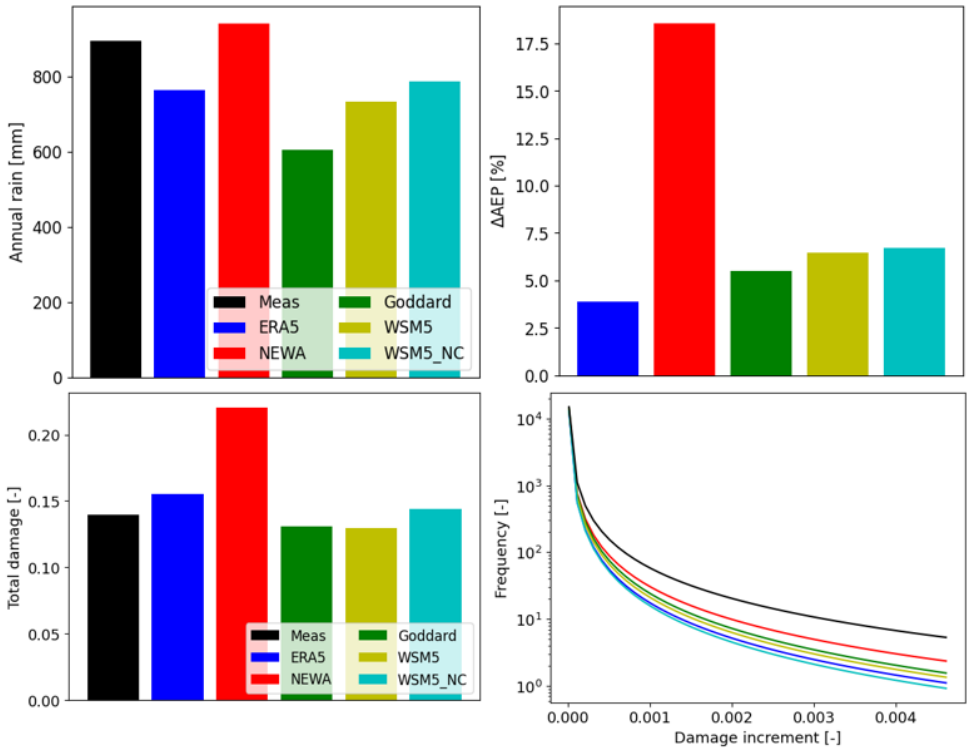

Figure 7. Like Figure 6, but for Risø.

Falkenberg

In Falkenberg, the precipitation is overestimated by ERA5 and NEWA, but pretty well reproduced by the other three WRF runs. For wind speed, ERA5 is performing well, but NEWA and the WRF runs show huge overestimations, with AEP biases in the order of +40%. It therefore comes as no surprise that the total damage is also significantly overestimated by all models, either because there is too much rain (ERA5), too much wind (WRF runs), or both (NEWA). Note that the order of magnitude is smaller than for the other sites, as Falkenberg knows a dryer climate. Looking at the distribution of damage increments, NEWA and Goddard again seem to perform best.

3.4 Conclusions

Many sensitivity tests were carried out for Cabauw, with the three promising configurations also tested at three other locations having significantly different site characteristics. While the results show that it is rather hard to accurately reproduce the measurements with the same model setup for all these locations, the following generalized conclusions could be drawn:

Funded by the European Union

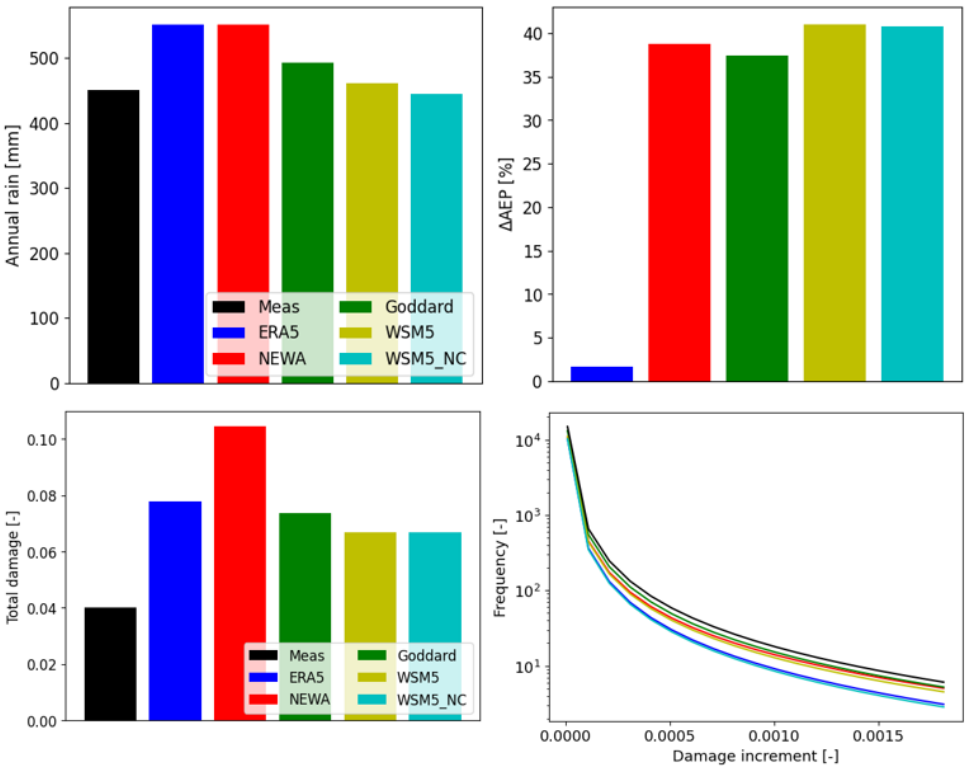

Figure 8. Like Figure 6, but for Falkenberg.

- NEWA systematically produces higher total annual rainfall than the other WRF runs. This can be traced back to the use of a product in the boundary conditions (Corrine + ESA CCI instead of MODIS). Particularly, it is expected that the soil moisture content is different between these data sets.
- ERA5 is not suited to develop a high-quality erosion atlas, mostly due to large overestimation of rain hours and inability to accurately capture the wind speed in complex terrain.
- Between the three WRF runs, WSM5 or WSM5_NC seem to estimate precipitation most accurately, with Goddard typically underestimating. However, the high intensity events are better reproduced by Goddard, as is the mean wind speed, resulting in better damage estimates.
- Between NEWA and Goddard, it seems that the distribution of damage increments is very similar. However, NEWA occasionally shows a large overestimation of the total damage. For this reason, Goddard was chosen as the setup for the production runs.

Table 3. Sites included for the evaluation of the representative year.

Name	Latitude [°N]	Longitude [°E]
Site A	45.122	3.098
Site B	40.695	15.410
Båtskär	59.959	19.954
Buseco	43.441	-6.643
Alaiz	51.971	4.927
Risø	42.696	-1.555
Levenmouth	52.167	14.122
Falkenberg	55.694	12.088
Cabauw	56.163	-3.009

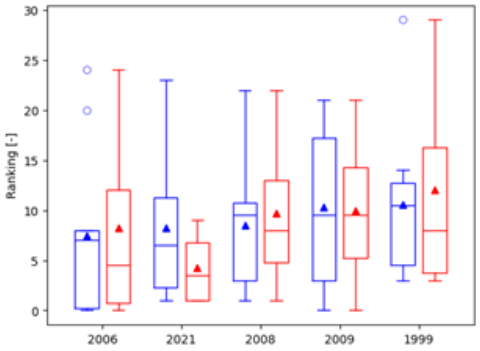

Figure 9. Ranking of the years most representative of the 30 year mean, averaged over all nine locations (blue) or only over the four sites considered in WP5 (red). The box plot displays the median (horizontal line), interquartile range (IQR, boxes) and maximum values within 1.5·IQR. Triangles indicate means and circles indicate outliers.

3.5 Production runs

Representative year

While ideally the Erosion Risk Atlas in Task 4.2 would be developed based on 30+ years of model results all over Europe, due to computational expense this is not possible. To retain a large spatial extent of the atlas, it was chosen to run for one year only using a representative year. To find a representative year in terms of inflicted erosion damage, the last 30 years of ERA5 precipitation and 100m wind speed at the locations listed in Table 3 were considered. These locations consist of the four locations of WP5, the four locations used for the sensitivity tests, and one additional site of the AIRE project.

Next, the blade damage model was employed to calculate the damage increments and subsequently the total damage. The absolute differences of each year compared to the 30 year average were summed across all locations. The five years with the smallest bias across all locations, hence the most similar to the 30 year mean, are considered in Figure 9. The boxplot illustrates the distribution of these years across all locations (blue) and the four locations considered in WP5 (red). While 2006 gives the best mean score overall, its median value is slightly higher than that of 2021. Additionally, across the four WP5 locations, 2021 seems to be better suited. For these reasons, 2021 was chosen as the representative year for the production runs.

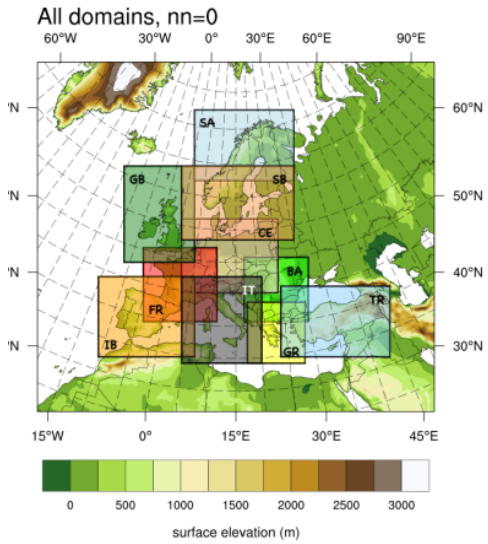

Figure 10. Domains of the New European Wind Atlas (NEWA) that are used for the production runs. (Source: [19])

Domains and execution

For the spatial extent of the production runs and subsequently the erosion risk atlas, the domain setup from NEWA was used, see Figure 10. Main benefits of using multiple domains instead of one very big domain covering all of Europe include: no large areas outside of area of interest (far offshore), controlled forcing by global dataset, and massive parallelization.

Initially the production runs were planned to have a resolution of 2 km, equal to the sensitivity tests. However, this did not only increase the computational costs, but also caused numeric instabilities in complex terrain. Changing the model configuration to fix this would results in a set-up different from the sensitivity tests, which was undesirable. Rather, an additional sensitivity test was carried out in which the effect of resolution on the annual damage at the four considered sites was studied. Results in Fig 11 indicate that there are some differences, but generally speaking the effect of resolution is small. Besides, there is no systematic influence (e.g., increased resolution always results in higher damage). For this reason, it was deemed reasonable to execute the production runs at a 3km resolution.

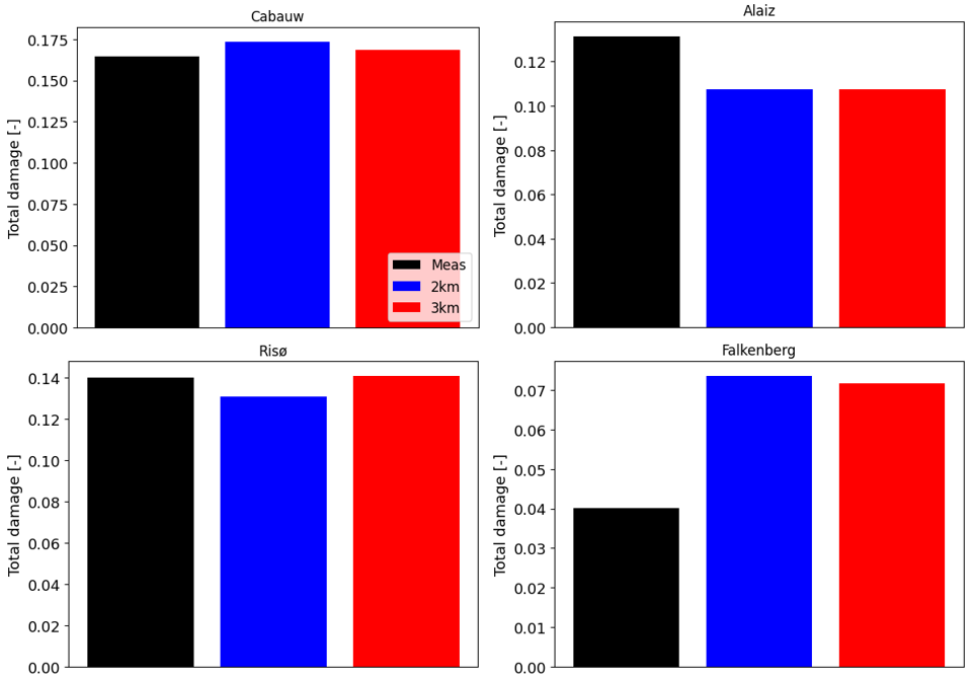

Figure 11. Total damage at all four locations, comparing resolutions of 2 km and 3 km with the measurements.

Funded by the European Union

4. WAKE AND FARM MODELS

4.1 Review

4.1.1 Aerodynamics of wet blades

The literature generally agrees the physics of the interaction between a rain drop and a moving airfoil, such as an aircraft wing or the blades of a wind turbine. Studies such as Cao Y. et al. [14], Smith Sara et al. [66] and Douvi Eleni et al. [21] describe the interaction and here we summarise it. When rain hits a blade a combination of blade wetting and rebounding of the rain drops occur. Rain drops that rebound get split into smaller droplets and may form what is known as an ejecta-fog near the leading edge of the airfoil. Droplets that remain in contact with the blade form a thin and uneven film on the blade. Further droplets hit this film, effectively making tiny craters in it which increase the roughness of the film further. The surface material of the blade has an effect on the spreading and thickness of the thin film. The increased surface-roughness due to the thin water film affects the aerodynamic performance of the blade by altering the ratio between lift and drag across the airfoil.

How much the aerodynamic performance of the blade is affected by rain depends on many factors, the most important being: rainfall intensity; angle of attack; airflow velocity; Reynolds number; airfoil shape and the rain droplet diameter. For a wind turbine, any change in aerodynamic performance is directly related to a change in power performance.

Many studies have examined the effect of rain on power performance of wind turbines [66, 21, 17, 71, 4, 20]. These studies include investigations of measured wind farm data during rain, wind tunnel simulations and computational fluid dynamic (CFD) studies. The studies cannot be directly compared to each other due to the differences in many of the factors influencing aerodynamic performance as mentioned above, however, looking at the results together gives an interesting insight, although certainly not a clear relationship. In Figure 12 the power performance results at varying rain intensities from a number of these studies are shown together and coloured by study type. A huge range in power performance change is seen across the studies: from an 80% decrease to 20% increase. Rainfall rate shows no direct relationship to power performance change, although for rainfall intensity rates above 50mm/hr a power performance decrease is always observed. It should also be kept in mind that very heavy rainfall intensity rates (above 50mm/hr [70]) do not occur for long durations in Europe, hence any power decrease caused by such rainfall is not likely to be for a large proportion of annual operating time for a turbine.

4.1.2 Blade surface damage

Blade surface damage to wind turbine blades occurs when airborne particles collide with them. Particles that can cause damage include rain, hail, dust, sand and even insects. The severity of damage caused is related to the size and composition of the particles, the rotational speed of the blade and the surface properties of the blade. Over time the damage accumulates with pits and gouges appearing on the blade and surface delamination may even occur, ultimately resulting in an increased blade surface roughness. Many strategies exist to help mitigate the rate of damage accumulation including protection tapes, coatings, reduction of tip speed and site selection. Methods also exist for predicting the life of a wind turbine blade using models based on wind and rain site data [29, 49, 30].

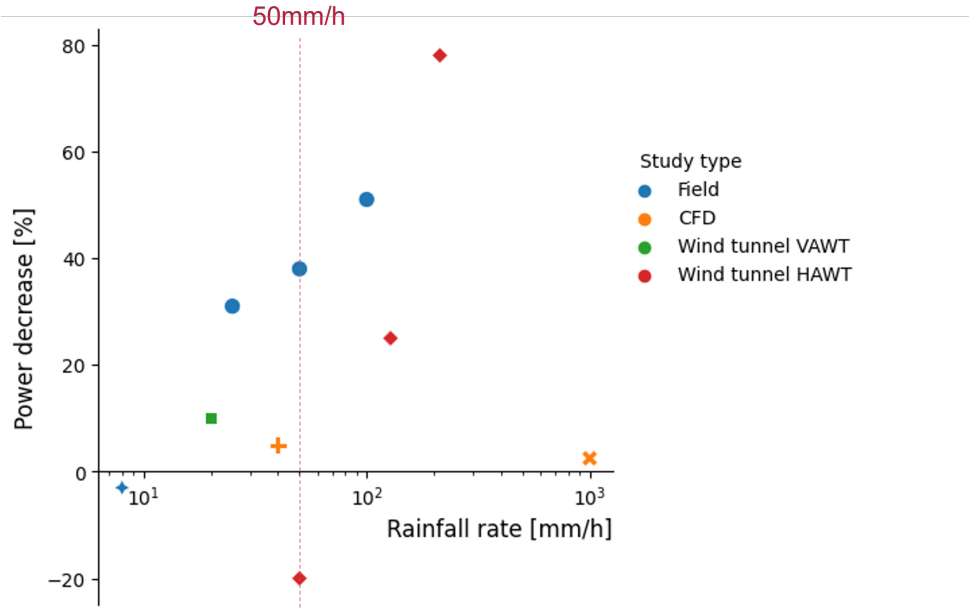

Figure 12. Results from six studies on power performance change for wind turbines during rain. Markers of the same colour are the same study type. Markers of the same shape and colour come from the same study. The red vertical line indicates 50mm/hr rainfall intensity.

As with a wet blade, the increased surface roughness of a damaged blade changes aerodynamic performance. For a damaged blade a decrease in lift and an increase in drag reduces the power performance of the blade and hence turbine as a whole. The magnitude of this power performance loss has been investigated in several studies, mostly using CFD, and is predicted to be in the range of 1% to 8% [5, 43, 27, 46, 63]. One study using severely damaged blade sections in a wind tunnel estimated power loss to be 25% [60]. It should be noted however, that blades with such extreme damage would likely have long been removed from any operational turbine. It should also be kept in mind that the amount of damage in these studies is usually qualitatively described (often using words such as light, moderate or severe) hence it is difficult to directly compare results between studies. Dependencies on airfoil type and Reynolds number also exacerbate this issue.

4.1.3 Impact on the wake

In contrast to the previous two sub-themes of this report, very little work has been done on understanding the impacts of rain on the wake of the wind turbine. One study measured velocities and turbulence statistics behind a small model turbine in a wind tunnel with and without water in the airflow [66]. Unfortunately, the results were not very conclusive and additionally it is unlikely the results would scale well to an operational turbine. Further research is needed in this area to understand if and how rain may affect the wake of an operational wind turbine. The studies examined in this literature review predict that rain has a detrimental effect on operational turbine performance during operation in heavy rain and also through accumulated damage to the blades from raindrop impacts. How exactly rain affects the wake of an operational turbine is still unclear. Further field and CFD studies designed to investigate these topics using state-of-art instruments and equipment will help broaden and solidify our understanding of the impacts of rain on wind turbines.

4.2 FLORIS analysis

4.2.1 Introduction

The exploitation of operational data from wind farms is becoming a fundamental tool to improve plant and asset management. Considering these operational data, it has been possible to move from an evaluation of assets based on generic turbine and ambient data to considering site-specific conditions in which the wind turbines operate. The wind industry is leveraging the value of data to understand physical impacts and, in later stages, develop models to reduce uncertainty. All the available information makes it possible to analyse the effect of certain situations both on the operation of the wind farm, and on the wind turbines individually.

The effect of rain in terms of its impact on performance and asset management has not been addressed in depth to date ([25, 1, 16]). Reducing the uncertainty of the effect of rainfall is one of the key points within the AIRE project ([2]). Once the impact of rainfall is identified, the wind farm simulation setup can be adapted to estimate wind farm performance more accurately.

The present study develops a methodology to carry out the assessment of rainfall impact on wind farm performance based on available operational data (rain measurements and typical 10-min SCADA), applying it to a commercial operating wind farm (Commercial Wind Farm A) as case study.

The remainder of the chapter is as follows. Section 4.2.2 briefly describes the approach followed. Section 4.2.3 introduces the wind farm where the methodology has been tested, while Section 4.2.4 focuses on the specific steps of the data analysis applied to that wind farm. Finally, conclusions are drawn in Section 4.2.5.

4.2.2 Methodology description

This work deals with the development of a methodology for the associated operational analysis, since it has not been addressed in the state of the art specifically for precipitation and there are many constraints related to the data that must be considered: types of available data, quality of the data, sample size, etc. For the sake of readability, the steps are defined in Section 4.2.4 in parallel with the study of a commercial operational wind farm (Commercial Wind Farm A), introduced in Section 4.2.3, where the different issues in the process are addressed, and the suggested procedures are verified.

This methodology is developed to analyse the impact of precipitation on a wind farm using SCADA data, i.e. the minimum available data. In addition to the usual SCADA data with ten-minute statistical information on meteorological signals and wind turbine operation, a signal identifying the precipitation is required (either included in the SCADA or another external sensor, but close to the location). For wind farm analysis, information allowing wake simulation (power curve and thrust coefficient C_T data from turbine models) is also required, as well as information on the location of each wind turbine.

After a preliminary data processing, the analysis is considered into three different levels:

- **Meteorological characteristics**: independent analysis of meteorological signals.

- **Wind turbine performance**: individual analysis by wind turbine and comparison of the performance in all of them.
- **Wind farm analysis**: the focus of this approach is on the comparison between SCADA data and wind farm simulations.

4.2.3 Site description

The wind farm area, situated in France, encompasses a non-complex region at 1100 m a.m.s.l. (above mean sea level). It benefits from the wind regime of the mistral, particularly favourable for wind energy applications. The area is mainly composed of cultivated fields, and a forest on its western part. Figure 13 shows the wind farm, which is composed of 4 wind turbines (red dots) and a 79 m meteorological mast (purple dot). It is surrounded by two neighbouring wind farms northwest (blue dots) and southeast (green dots), with 9 and 5 wind turbines, respectively.

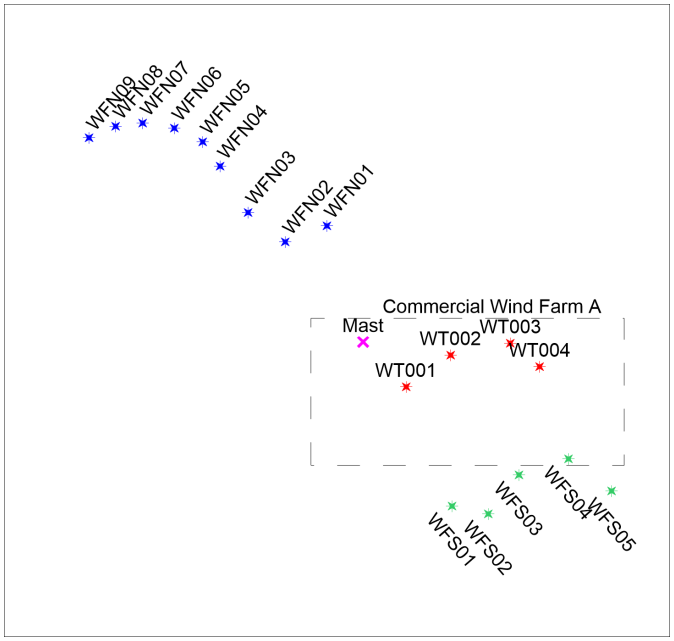

Figure 13. Location and overview of the wind farm. Wind farm turbines (red) and meteorological mast (purple), northwest (blue) and southeast (green) neighbouring wind farms.

The meteorological mast is located 550 m northwest of the first wind turbine from the wind farm. Near the mast, the terrain is open pasture for at least 3 km from west to east but there is a forest area at 400 m at south direction.

The met mast is 79 m height lattice structure, with six measurement levels oriented to 110° and 290°. Wind speed is measured at six levels (30 m, 50 m, 70 m, 78 m and 82.3 m, two anemometers at this last level), wind direction at three levels (50 m, 70 m and 77.5 m), two temperature sensors (5 and 76.5 m), one pressure sensor (5 m), one rain gauge (10 m) and one humidity sensor (76.5 m).

Figure 14 shows test site measurements timeline. The extensive measurement period (EMP) ran from May 2017 to May 2023 comprising six years of measurements from the SCADA data and 28 months from meteorological mast. The Intensive Observational Period (IOP), when all sensors had concurrent measurements, lasted for 12 months from January 2019 to December 2019.

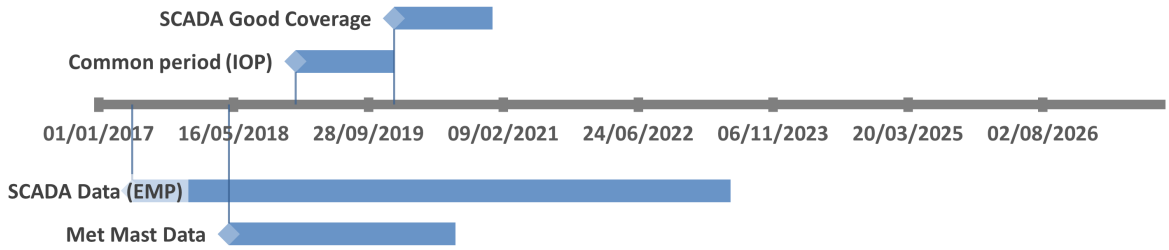

Figure 14. Test site timeline with measurement periods.

4.2.4 Dataset analysis

The steps of the methodology presented in Section 4.2.2 are applied to the study of the wind farm described in Section 4.2.3. This makes it possible to address all the practical issues in the process and to verify the suggested procedures of the methodology.

4.2.4.1 Data processing

First, a preliminary data processing is necessary to prepare the data for the analysis. This step includes:

- Cleaning and curation: processing raw SCADA data to obtain clean data.
- Operational and meteorological identification methods are used to generate additional signals that are useful for the analysis.
- Finally, the complete dataset is filtered according to the rainfall data.

CLEANING PROCESS

This step is compulsory to ensure data quality for both meteorological and operational data, as well as additional sensors related to precipitation. The verifications are carried out both at individual turbine level and at the wind farm level. This process includes the verification of:

- Additional variables, which have been calculated from the available information and operational states identification: air density, yaw misalignments, turbulence intensity, ... etc.
- Extreme values for relevant signal statistics (maximum, minimum, average and standard deviation). They are used to ensure the consistency of the original and calculated data.
- Power curve verification, taking into account the operational identification.
- Turbulence curve vs wind speed, ensuring results are within normal limits.
- Wind roses and wind distributions.

During the process, original data is corrected where necessary, or discarded if their quality is not sufficient.

OPERATIONAL AND METEOROLOGICAL IDENTIFICATION

Funded by the European Union

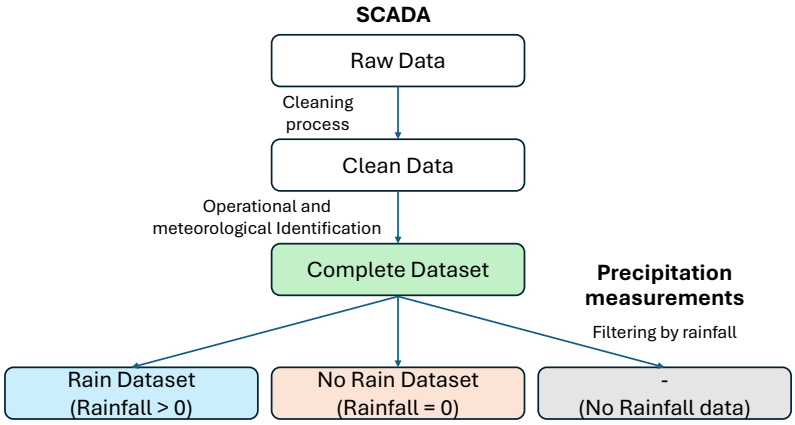

Figure 15. Diagram of data filtering into datasets.

Based on the available information from the SCADA, an identification of the operational states of each wind turbine at each sample has been carried out. The identification of the operational states of the wind turbines is crucial for the analysis of the wind farm. However, the information may not be directly available through the SCADA and then must be obtained implicitly through other operational variables.

Four operational states have been identified in this analysis, according to the operation in the time interval under consideration (10 minutes):

- Production pure normal: the wind turbine has been producing without stops or derating.
- Production pure derating: the wind turbine has been in derating during the whole interval.
- Production partial: there have been moments of production combined with stopping and/or derating.
- Parked: the wind turbine has been stopped (either idling or standstill) during the entire interval.

As a mere example, Figure 16a shows for wind turbine WT002 how these four operational states have been identified and how (see Figure 16b) this influences the obtained power curve. The power curve is postprocessed (fit according to IEC 61400-12-1 ([37])) from samples identified as production pure normal conditions.

FILTERING

For the rain study, three datasets are created (Figure 15), using filters based on precipitation information when available:

- rain: dataset filtered for values of ”Rainfall average” higher than 0.
- no rain: dataset filtered for values of ”Rainfall average” equal to 0.
- complete: includes ’rain’, ’no rain’ datasets and timestamps without rainfall values.

Funded by the European Union

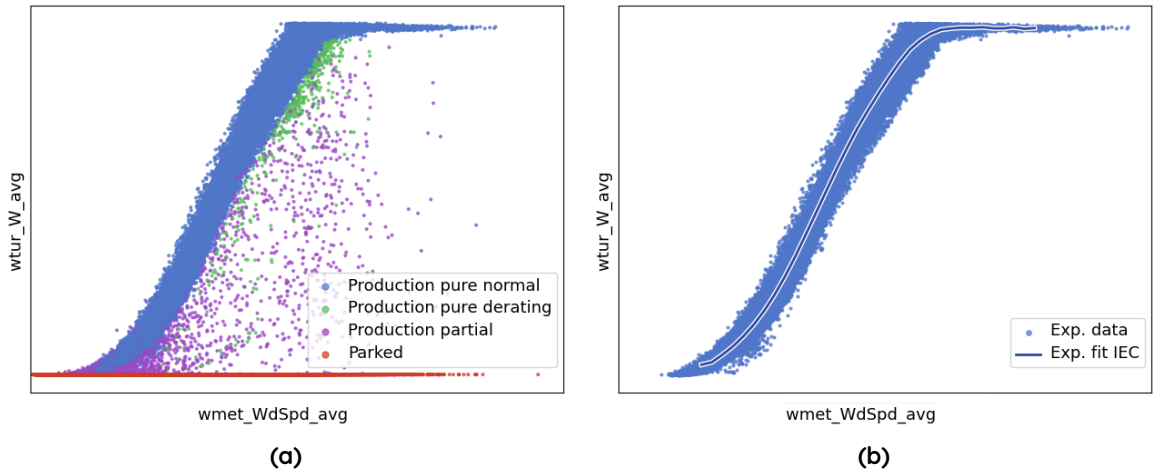

Figure 16. Average power production versus average wind speed for WT002: (a) classification by operational state and (b) data filtered for production pure normal conditions (scatter and IEC fit power curve).

Table 4 shows the number of 10-minute samples in the study period for each turbine individually and for the wind farm. It should be noted that the complete dataset also includes samples with no information about rain conditions. The number of samples for the wind farm analysis is significantly lower because the wind farm simulations requires synchronised normal production states for all wind turbines.

Table 4. Data availability.

	complete	no rain	rain
WT001	145937	99454	20185
WT002	155089	100978	19933
WT003	154556	100867	19507
WT004	69031	35638	6220
Wind farm analysis	26252	15770	2875

Initially, several variables were proposed to ideally classify the data and analyse their correlations with rainfall in greater detail, namely: air density, wind direction, wind shear, turbulence intensity, and wind speed. However, they are ultimately not used in the case study due to the insufficient data, as binning the data by including more classification variables drastically reduced the number of samples per bin. Therefore, these variables have not been used to divide the dataset, but they are considered during the analysis process instead to evaluate their effect and separate it from the impact of precipitation.

4.2.4.2 Meteorological characteristics

In this section, the effect of precipitation is analysed in terms of meteorological magnitudes. Different variables are compared to see if a different behaviour is detected depending on the precipitation. Figure 21 shows the analysis performed on the turbines.

Funded by the European Union

For the meteorological analysis, SCADA data from the turbines have been used, with their measurements obtained at the nacelle. The only metmast signal used was the rain signal (which was previously used to filter the data).

WIND SPEED DISTRIBUTION ANALYSIS

The average wind speed distributions have been obtained for the different wind turbines and the three datasets. As an example, the distributions are shown in Figure 17 for wind turbine WT002, for the complete dataset (Figure 17a), no-rain dataset (Figure 17b) and rain dataset (Figure 17c), and taking into account the turbine operational states.

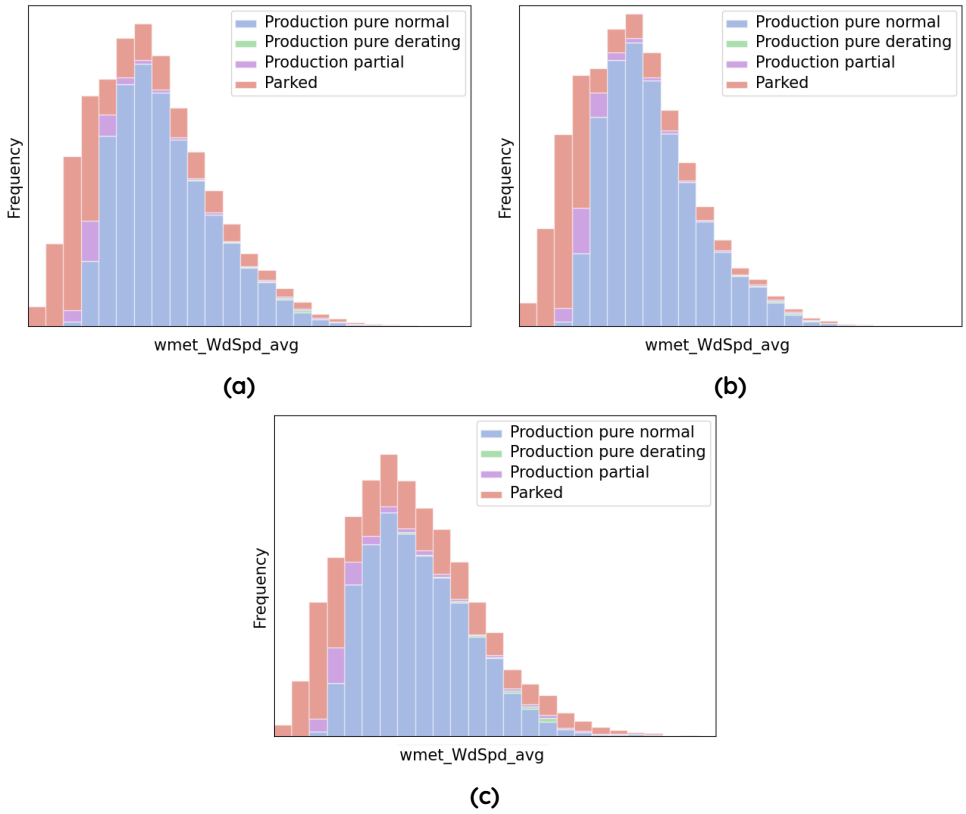

Figure 17. Wind speed distribution and operational states for WT002: (a) Complete dataset, (b) no-rain dataset and (c) rain dataset.

A Weibull probability density function is also fitted to the different datasets, yielding the corresponding scale (A) and shape (k) parameters. Rain dataset presents Weibull scale parameters between 12% and 17 % higher for the rain dataset with respect to the no rain dataset.

It is evident that the performance for the complete dataset and the no-rain dataset are similar. The highest differences between them are related to the operational states. For high wind speeds, the complete dataset shows lower contribution of production pure normal operation. The performance of the rain dataset is clearly different to the rest: the distribution is displaced to higher wind speeds, the variance is higher, and there are higher percentages of parked conditions at speeds above cut-in wind speed.

Funded by the European Union

WIND ROSES ANALYSIS

The wind roses are shown in Figure 18a for the full dataset, Figure 18b for the no-rain dataset and Figure 18c for the rain dataset, again for WT002. It can be observed that the distribution of occurrences and the prevailing wind directions depend on precipitation. Similar trends are observed for the rest of wind turbines in the wind farm.

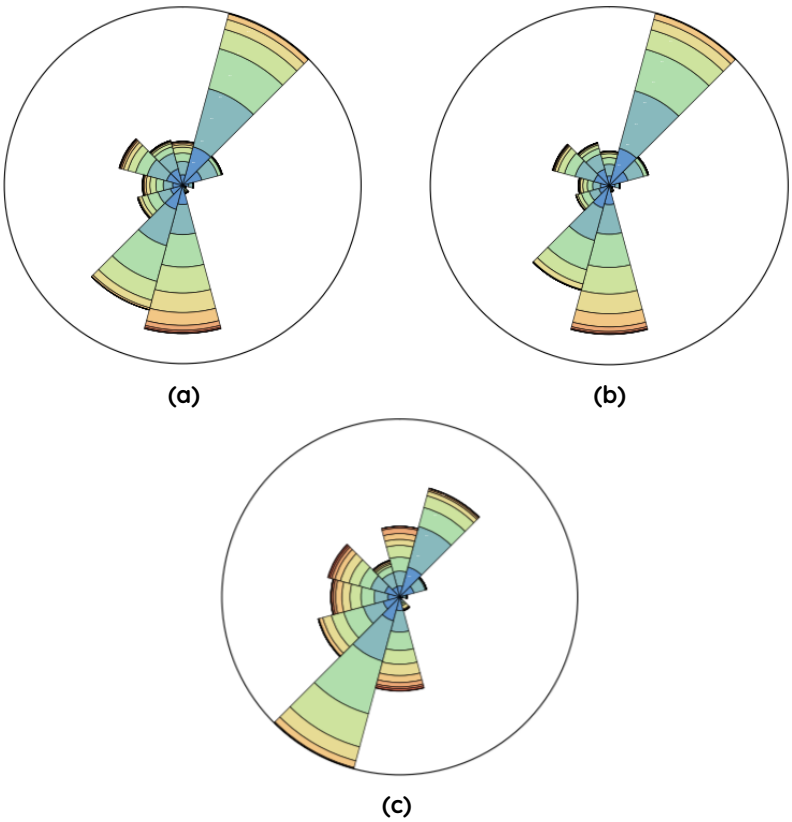

Figure 18. Wind roses for WT002: (a) Complete dataset, (b) no-rain dataset and (c) rain dataset.

AIR DENSITY EFFECT

Air density significantly impacts wind turbine performance; it is directly proportional to the power available in the wind. Denser air means more energy can be extracted, and this density changes with pressure and temperature. Density is not a value that appears in the original wind farm SCADA data, but it can be calculated from the air temperature and pressure recorded at each wind turbine by the following expression:

$$\rho = \frac{1}{T}\left[\frac{B}{R_0}\right], \tag{4.1}$$

where;

- T is the measured absolute air temperature averaged over 10 min [K],
- B is the air pressure corrected to hub height, averaged over 10 min [Pa], and

Funded by the European Union

- R_0 is the gas constant of dry air 287.05 J/kg·K.

Figure 19 shows the air density distribution for the different datasets: complete, rain and no rain. The boxplot shows the median (green horizontal line), mean (green triangle) and inter-quartile range (25th–75th percentiles), while whiskers extend to the 1st and 99th percentiles. The difference shown in air density between datasets was minimal (<1%) and is not considered to reach practical significance for the wind turbine performance.

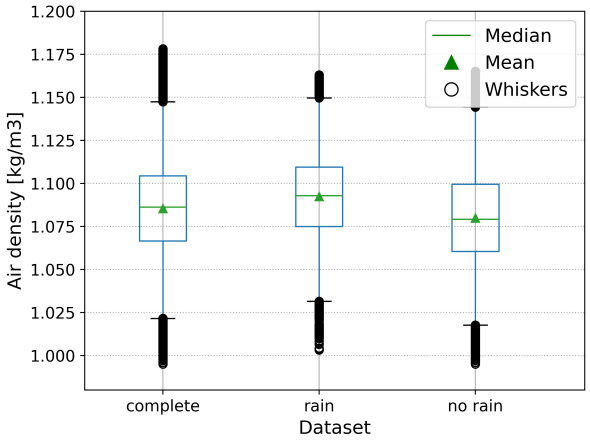

Figure 19. Air density distribution (WT002) for the different datasets.

TURBULENCE INTENSITY EFFECT

The effect of the turbulence intensity in the power curve has been a topic of interest for the wind energy and it has been extensively studied by the industry and the academia ([48, 59, 7]). Turbulence intensity is calculated from SCADA ten-minute data using the standard deviation and average wind speed signals. The first option for the methodology is to include the turbulence intensity in the binning process in order to analyse the effect of this variable combined with the precipitation. However, the specific dataset used as case study could not be split into different levels of turbulence intensity due to the insufficient amount of data for the analysis.

Figure 20 shows the reference turbulence intensity values for each of the three datasets at each of the four wind turbines in the wind farm. It can be seen how the turbulence intensity is higher in rainy than in non-rainy conditions in the four wind turbine positions.

4.2.4.3 Analysis of rain impact on wind turbine performance

The analysis of the performance of wind turbines is focused on pure normal production state. Consequently, the previous datasets (complete, rain and no rain) are filtered in order to evaluate the normal production state samples.

Funded by the European Union

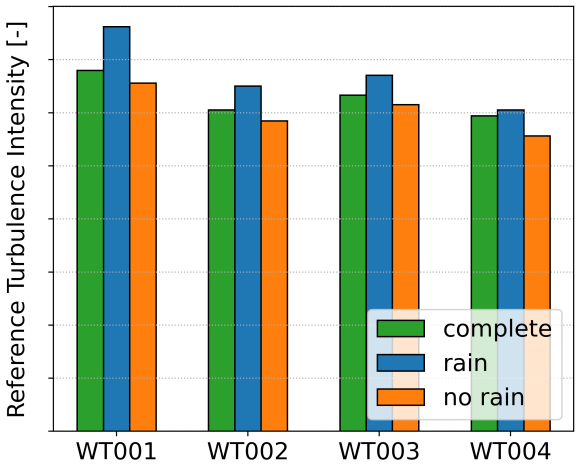

Figure 20. Differences in reference TI for different datasets by wind turbine: complete (green), rain (blue) and no-rain (orange) datasets.

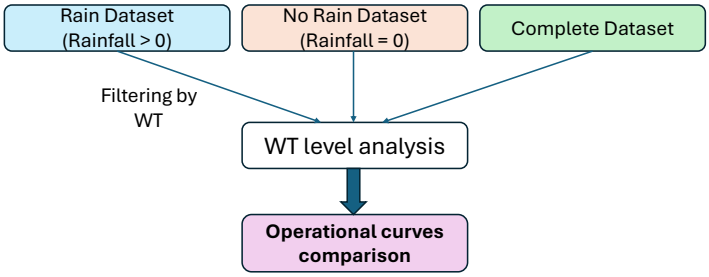

Figure 21. Diagram of rain impact analysis at wind turbine level.

The statistics of operational signals are included in the analysis. In terms of standard deviation of power production, see Figure 22a , the behaviour observed for the rain dataset is coherent with the increase of turbulence intensity with respect to the other datasets. Regarding the average rotational speed in the rotor, the curve for the data set with rain is slightly displaced to the left with respect to the other curves and slight differences are observed at higher speeds (close to rated wind speeds).

The measured IEC fit power curve for the various datasets shows differences for the rain dataset in Figure 23a: higher power values for the lowest wind speeds and lower values for higher wind speeds. However, this behaviour is similar to the effect of the turbulence intensity could have.

Funded by
the European Union

The alternative option for cases with limited data and evident differences in terms of turbulence intensity is to use the procedure included in IEC 61400-12 Annex M ([37]) for the normalisation of power curve data according to the turbulence intensity. This method normalises power curve data to a reference turbulence intensity, and can be applied to the different datasets with and without rain events, in order to compare the power curve results using equivalent turbulence intensity level. Figure 23b shows such normalised results (zero turbulence intensity) for the three datasets for wind turbine WT002. The differences observed in the measured power curve at low wind speeds for the rain dataset (Figure 23a) have been reduced in the normalised curve. Consequently, these differences in the IEC fit power curve were directly explained by the effect of the turbulence intensity. However, the normalised TI results obtained for the specific rain dataset show a behaviour that differs from the other power curves close to rated wind speed. Similar trends are observed for the rest of wind turbines in the wind farm. Therefore, it is clear that the behaviour of the turbines analysed is different depending on the datasets, i.e. on the rain conditions, and this effect is not directly related to the effects of concurrent turbulence intensity change.

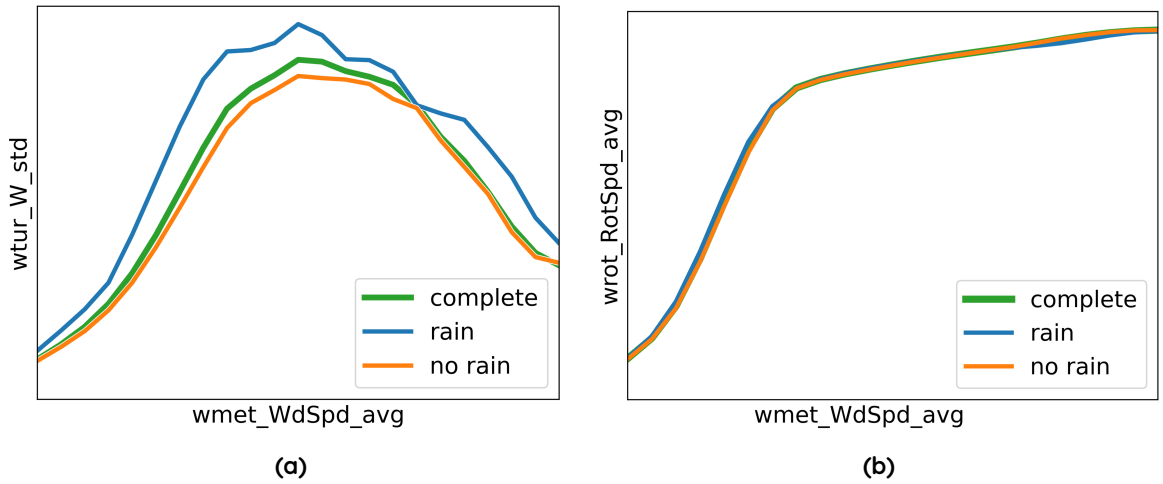

Figure 22. (a) Standard deviation of power production, and (b) average rotor speed vs wind speed for different datasets: complete (green), rain (blue) and no rain (orange).

4.2.4.4 Analysis of rain impact at wind farm level

The analysis at wind farm level is based on the comparison between the real data of the wind farm and the results from simulations to analyse a potential impact of rain on wake effect. A parametric study has been carried out, see Figure 24, to evaluate whether an impact is observed in the results for the datasets considered, with different data according to rainfall. Two different assumptions have also been taken into account for the turbine data, related to the study conclusions at the turbine level: use of manufacturer power curve data (OEM) or use IEC fit power curve (per wind turbine and dataset).

The analysis at wind farm level focuses on identifying whether wake simulation should be performed similarly for the different datasets according to rainfall. The wind farm model parameters that have been taken into account for the simulation can be divided into groups:

Funded by the European Union

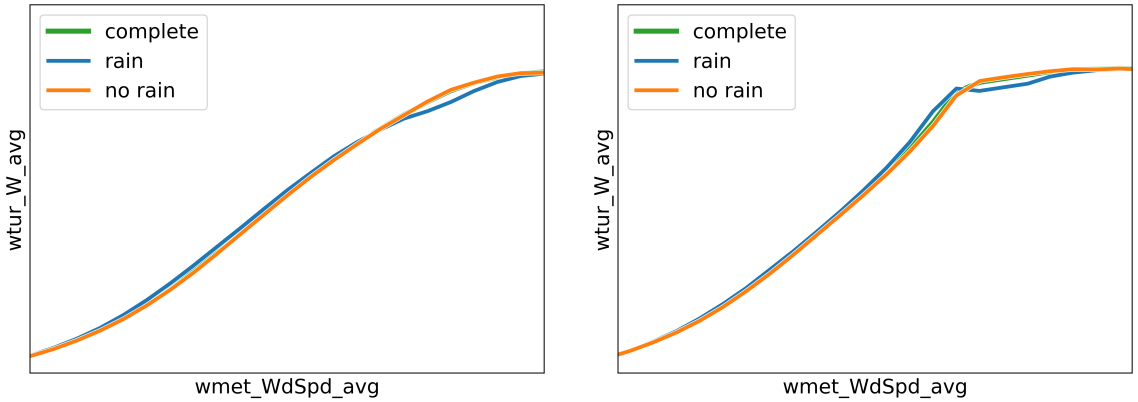

Figure 23. Power production for wind turbine WT002: (a) IEC fit; (b) TI_0 power curve. Complete (green), rain (blue) and no-rain (orange) datasets.

- Parameters related to the characterisation of the **flow map** in the wind farm. The baseline scenario is performed assuming homogeneous flow (same wind speed, wind direction for all wind turbine positions). Heterogeneous flow refers to the wind conditions being non-uniform across the entire wind farm area. The heterogeneity is influenced by terrain, vegetation and atmospheric conditions. Specifically, the number of sectors for the characterisation of the flow heterogeneity in terms of wind speed is the main parameter considered: 10, 36, 72 and 90 sectors are evaluated ([10]).
- **Wake deficit parameters** The default parameters for the wake deficit model (see below) are used for the basic analysis and then the impact of the calibration of these values is analysed.
- **Wind turbine power curve impact**. OEM and IEC fit power curves.

Funded by the European Union

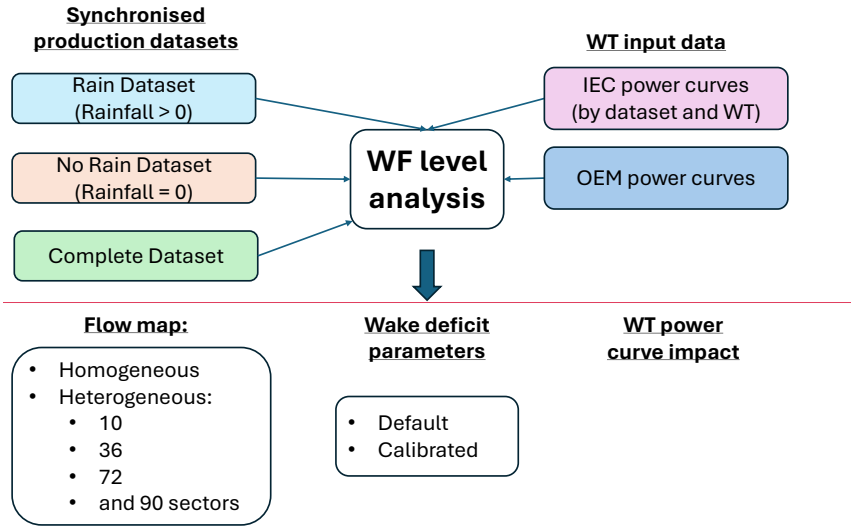

Figure 24. Diagram of rain impact analysis at wind farm level.

WIND FARM SIMULATION SET UP

Simulation process

For the different combinations of datasets, power curves and number of sectors of the heterogeneous flow (see Figure 24), the process for the wake calculation is similar.

1. The heterogeneous flow of the wind farm is characterised for a determined number of sectors (this step is not necessary when homogeneous flow is considered).
2. From SCADA data, free-stream wind speeds, wind directions and turbulence intensities are extracted according to the heterogeneous map. These series are used for the simulation of the SCADA registries.
3. The comparison of the simulation against the real data is performed through a set of error metrics: Root Mean Square Error (RMSE), mean absolute error (MAE) and the bias. These errors are evaluated for individual wind turbines and general at the wind farm level, for both wind speed and power production.
4. Finally, the calibration of the wake parameters is performed and the metrics evaluation is repeated.

The metrics results and additional figures comparing SCADA timestamps against the simulations have been used to evaluate the impact of rainfall, as shown in the following sections.

Input datasets

Synchronised data in which the turbines are in production pure normal operating conditions have been filtered out, as this is the baseline situation for wake simulation. This filter significantly reduces the number of time series data that can be used for both characterisation and evaluation in the practical case, as can be observed in Table 4. Again, as in the previous section, three different input datasets have been generated for this analysis depending on the rainfall data: complete, rain and no-rain datasets.

From SCADA data, free stream wind speeds, wind directions and turbulence intensities are extracted (according to the heterogeneous map). These series are used for the simulation of the SCADA samples with the wind farm model.

Wind turbine data

Based on the previous conclusions of the turbine-level study, a comparison is considered necessary between the two power curves considered for the simulation, namely:

- Power and thrust coefficient curves from wind turbine manufacturer (OEM).
- Measured IEC power curve and C_T curves. The thrust curve has been considered equivalent to that from the manufacturer, since there is no information available to estimate it from operation.

Baseline wake simulation

The simulations for this study are calculated using FLORIS version 4.2.2 ([51]), with default parameter and the selected models:

- Deficit model: Gauss [alpha=0.58, beta=0.07, ka=0.38, kb= 0.004]
- Deflection model: Gauss [alpha=0.58, beta=0.07, ka=0.38, kb= 0.004, ad=0.0, bd= 0.004]
- Turbulence model: Crespo-Hernandez [initial=0.1, constant=0.5, ai=0.8, downstream=-0.32]
- Combination model: sum of squares free stream superposition

HOMOGENEOUS MAP RESULTS

First, the results for the simplest simulation assuming homogeneous flow are obtained. As shown in Figure 25, significant bias errors are observed for both turbines WT001 and WT004. Comparatively, these errors are larger for the rain dataset.

The affection figures show the normalised wind speed values with respect to the free-stream velocity of the wind farm in radial coordinates (Figure 26a). The angular coordinates correspond to the wind direction. In this case, the simulation (yellow dots) uses a homogeneous map and consequently, the values in the free sectors (white background) are 1.0, while the SCADA spline fit for this turbine shows lower values. It is also observed that these values vary with wind direction, so it is assumed that the heterogeneous flow characterisation (Figure 26b) will need to be divided into several sectors.

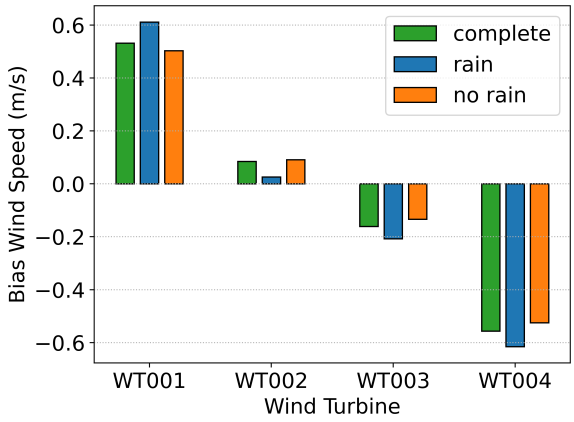

Figure 25. Bias in wind speed by wind turbine for complete (green), rain (blue) and no-rain (orange) datasets.

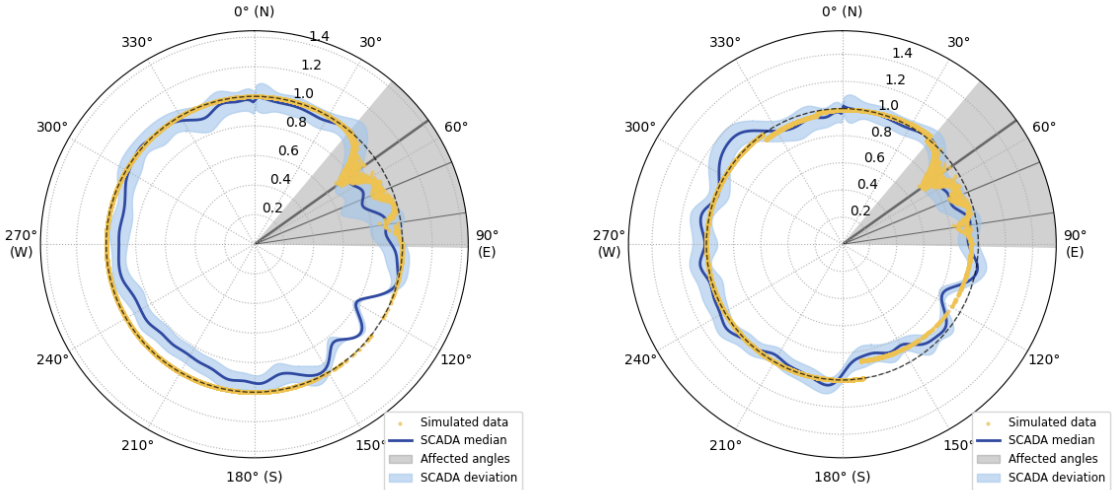

Figure 26. (a) Normalised wind speed comparison for the complete dataset (wind turbine WT001): (a) Homogeneous flow (b) Heterogeneous flow, 10 sectors.

In general, this homogeneous type of wind farm simulation is not considered valid for the wind farm under study.

HETEROGENEOUS MAP SIMULATION

The study of the heterogeneous map characterisation is based on the number of sectors of the map. The values considered for the analysis include: 10, 36, 72 and 90 sectors.

By comparing to the previous simulation with homogeneous flow, it is clearly shown that, even using a 10-sector map, the normalised wind speed heterogeneous simulations are closer to the SCADA data than the homogeneous assumption (Figure 26).

Funded by the European Union

The results in terms of RMSE of wind speed for the wind farm (the analysis per wind turbine is not included for the sake of conciseness) can be seen in Figure 27. This figure shows that errors clearly decrease from 10 to 36 sectors and then remain practically the same at 72 and 90 sectors.

The results in terms of adequate number of sectors are considered site-dependent. For the current case study, it is important to note that the number of samples for the rain dataset (29a) is clearly smaller than for the rest (Figure 28a and Figure 28b).

The extracted heterogeneous map should resemble the median for the SCADA normalised wind speed at the affection figure. Comparing this line for the different datasets shows that the approximation for the complete and without rain datasets is similar in both cases (see Figure 28 for 36 sectors).

It should be noted that a difference is observed between the SCADA median for these datasets and the one for the rain dataset (Figure 29a) in several directions (60-150 degrees, 300-330 degrees), which coincide with the directions with the lowest number of occurrences in the wind rose (see Figure 18c). The simulation approximates quite well the SCADA data (Figure 29b) for the rain dataset and wind turbine WT003, both in free stream sectors (white background) and affected sectors (grey background).

The value of 36 sectors is selected to continue the study. This is a compromise solution with a sufficient number to capture the variation trend of the flow heterogeneity, avoiding too small sectors (a sufficient number of samples is necessary for the identification of flow conditions).

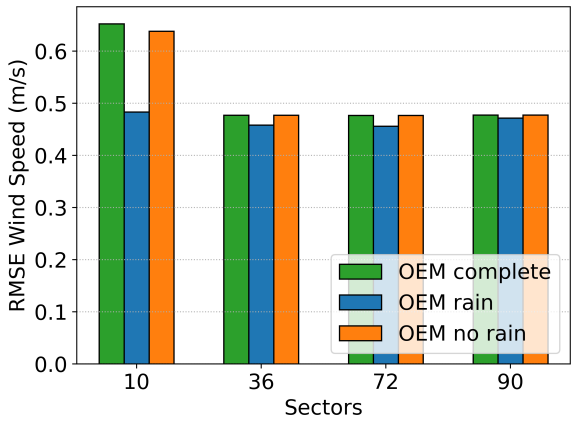

Figure 27. RMSE wind speed vs number of sectors (heterogeneity).

WIND TURBINE POWER CURVE IMPACT

As mentioned above, the wind farm simulations are calculated for power curves from the wind turbine manufacturer (OEM) and IEC curves measured on each of the turbines.

Funded by the European Union

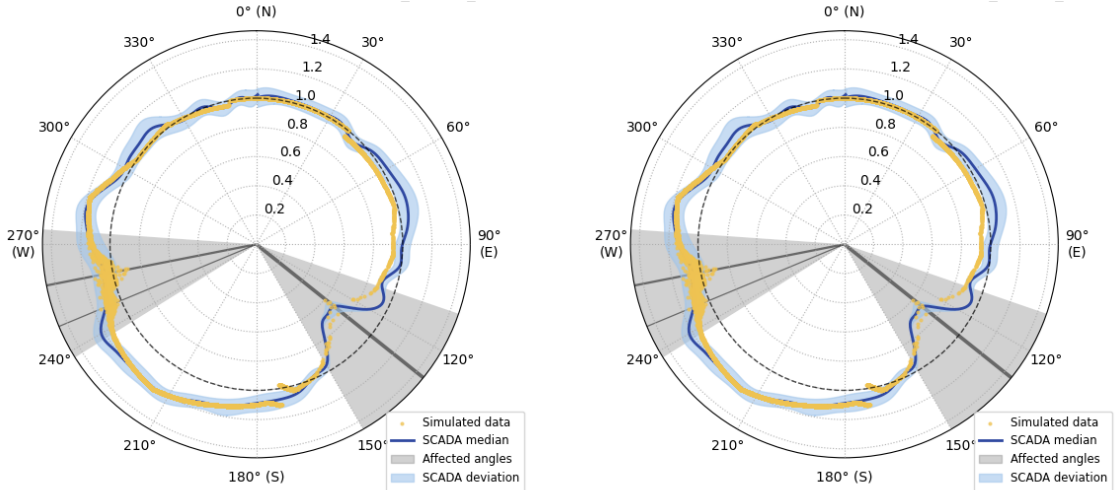

(a) (b)

Figure 28. Normalised wind speed comparison using 36 sectors for heterogeneous flow (wind turbine WT003) with (a) complete dataset and (b) no-rain dataset.

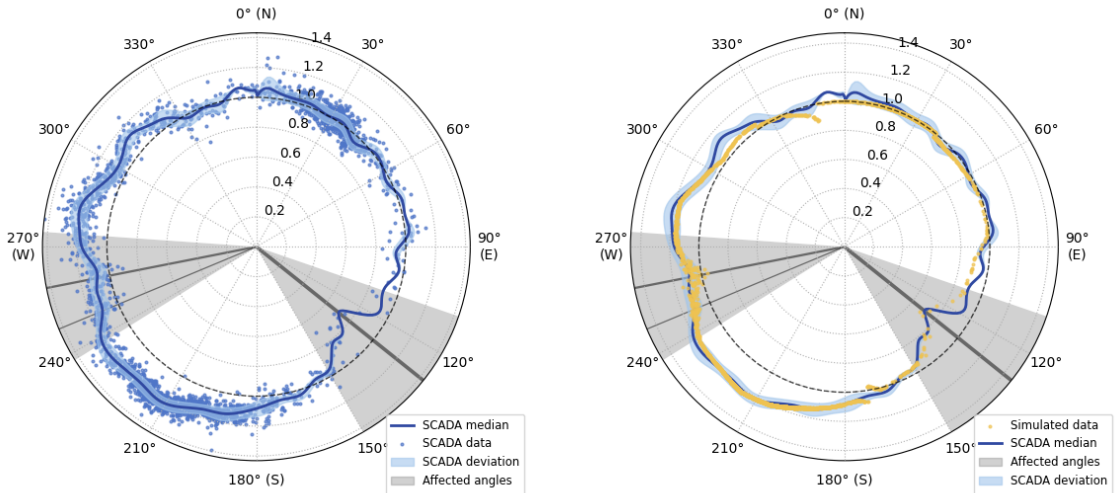

(a) (b)

Figure 29. (a) Normalised wind speed SCADA data using 36 sectors for heterogeneous flow (wind turbine WT003) and (b) normalised wind speed comparison between simulation and SCADA data (same wind turbine and number of sectors).

Funded by the European Union

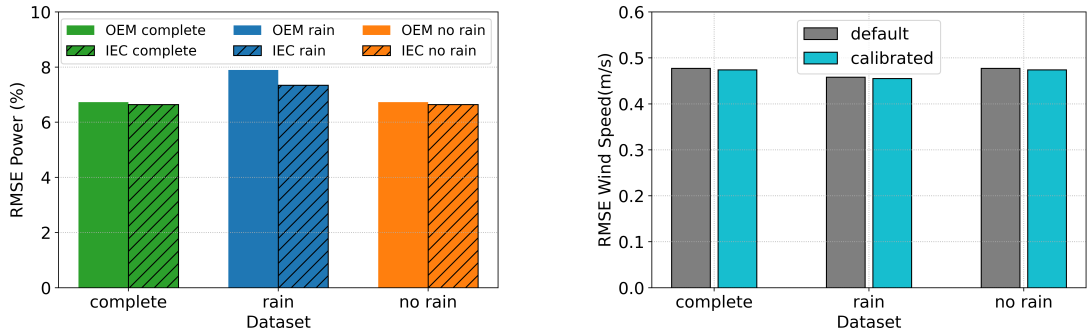

(a) (b)

Figure 30. (a) Power RMSE for OEM and IEC power curves (36 sectors), (b) Wind speed RMSE for default and calibrated wake parameters (36 sectors).

The wind speed results are equivalent even if the power curves are modified, since the wake depends on the thrust coefficient data, which in this case could not be characterised from the data, and implies a limitation of the study. It would be necessary to have an independent thrust coefficient characterisation for the different datasets to assess whether it has an impact at the farm level. The farm simulation results in terms of power additionally depend on the power curves of the turbine models. It is observed that errors in the farm simulation are considerably reduced for the rain dataset by using the measured IEC power curves (Figure 30a). For the other datasets, the error reduction in terms of power is negligible.

CALIBRATION OF WAKE MODEL PARAMETERS

The calibration is performed using an optimisation algorithm that modifies the deficit model values in FLORIS to minimise the wind speed error between simulation and real SCADA data. This calibration is performed for a set of 90 representative wind directions. A finer sector grid is used in order to better capture the wake behaviour. Wake model calibration serves to improve estimates in the affected sectors, i.e., areas with a grey background in the affection figures (Figures 26, 28 and 29).

The improvement achieved through calibration is negligible in terms of wind speed RMSE (Figure 30b). The main reason is that the default parameters generate results that are fairly close to the actual behaviour, so the room for improvement has been very small.

This behaviour is similar for the different datasets (rain, no-rain and complete). An obvious limitation is the limited number of samples for studying the wake effects in the rain dataset. For instance, Figure 29a shows a very small number of SCADA samples between 120 and 150 degrees (affected sector).

4.2.5 Conclusions

The main output from the study is the development of the methodology for analysis of the precipitation impact on wind farm performance. Some conclusions have been reached to this respect.

First of all, it is necessary to have a representative number of samples both for the study of meteorological conditions and for the analysis of the performance of the turbine and the wind farm. Depending on the site climate conditions, i.e. how often it rains, the analysis of rain impact on wind farm performance may therefore require a longer measurement period.

Air density and turbulence intensity should be accounted for in the analysis of rain effects, particularly when comparing power curves, as both factors significantly influence the performance of the wind turbines. Normalising power curves to zero turbulence intensity provides a practical approach for facilitating such comparisons by isolating the influence of turbulence.

The characterisation of the heterogeneity of the site could be necessary for a proper wind farm simulation, and the number of wind direction sectors used should be consistent with the SCADA data. This heterogeneous characterisation should be performed independently for the different datasets (complete, rain, no-rain), in order to evaluate whether differences are observed. Similarly, the calibration of wake parameters independently with the different datasets allows the robustness assessment of such parameters with respect to rainfall.

Other conclusions drawn from the specific analysis of the case study include the following:

The effect of air density in the case study was found to be negligible, with no major differences observed between the rain and no rain datasets. In contrast, turbulence intensity exhibited a more significant impact, as the rain dataset was associated with higher values of mean velocity and reference turbulence intensity.

The effect of the rain can be observed in terms of differences in rotational speed and power production close to rated wind speed. The impact is also observed in power curves normalised to the turbulence intensity (IEC 61400-12 Annex M) in regions close to rated wind speed.

Slight differences have been observed for the heterogeneous maps of the different datasets. Some of the differences may be due to lack of data, especially in wind direction sectors with few occurrences. More data would be required to characterise the heterogeneous flow behaviour within the wind farm in a more reliable manner.

The use of IEC-fitted power curves tailored to each dataset and turbine enhances the power estimation for the wind farm in the case study. Although wake parameter calibration was applied across the different datasets, its impact on the error metrics was found to be negligible in this context.

Given the current scope, the impact observed in this case study cannot be generalised to other sites. Applying this methodology to a larger number of wind farms would be necessary to draw broader conclusions regarding the effects of precipitation on wind turbine and wind farm performance.

Rain category [mm/h]	No. of 10min obs
No rain (0,1]	26703
Light (1,10]	3425
Heavy (10,50]	981
Very heavy (50,∞)	6

Table 5. Event counts of rain categories at Site A, according to 2.5 years of data.

4.3 FOXES analysis

4.3.1 Introduction

As discussed in Section 4.1, the existing literature does not give a clear answer to the question how rain affects the power production and wake effects in wind farms.

Engineering wake models are usually governed by simplistic analytical equations that depend on wind speed, the turbine's thrust coefficient, and turbulence intensity. Precipitation, and also other possibly relevant parameters like air density or temperature do not enter these equations, hence a direct modelling and modification of the wake model appears impossible.

Hence, the data that was provided within the project was analyzed in order to determine the phenomenological requirements for a wake model modification in the presence of rain. For this purpose two different operational sites located in Southern Europe were analyzed, with a focus on a potentially modified power production by isolated turbines, and changes in the observed wake effects.

4.3.2 Data analysis

4.3.2.1 Commercial Farm A

At the time of evaluation, 2.5 years of measurement data was available at Site A, which was described in detail in sections 4.2.3 and 4.2.4. The number of rain event observations on a time scale of 10 minutes for four categories of rain intensity are listed in Table 5. Figure 31 visualizes the distribution of these rain events as a function of wind speed. Clearly the abundance of heavy and very heavy rain events is low, but also the number of light rain events per wind speed bin introduces large statistical uncertainty.

The mean power curves of at the site for the four introduced rain categories are compared in Figure 32. No significant influence of the rain or the rain intensity on the power curve behaviour can be concluded from this analysis from the available data.

4.3.2.2 Commercial Farm B

The wind farm layout and a typical wake situation at the Site B are visualized in Figure 33. The wind rose and the rain statistics are shown in Figs. 34 and 35, indicating a slight change of the mean wind direction under rain conditions.

The mean values of the measured air density, temperature, turbulence intensity and wind speed are listed in Table 6 for dry and rainy conditions. Notice the observed increase of the mean wind speed during rain.

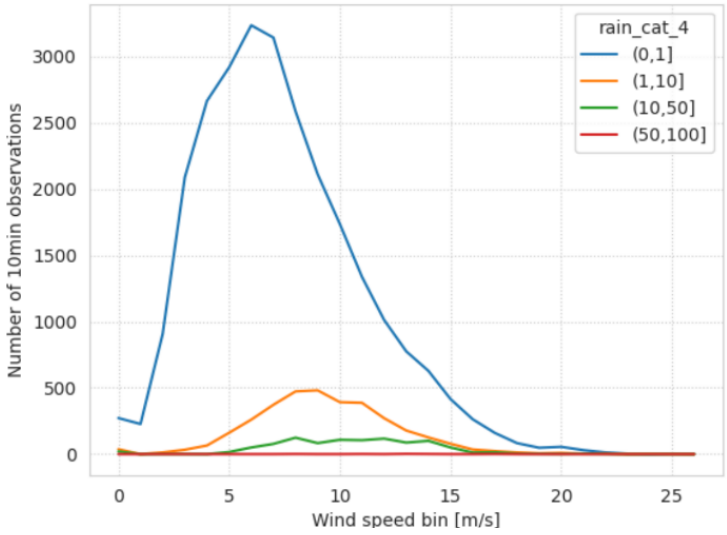

Figure 31. Event counts of rain categories from Table 5 at the Site A site, according to 2.5 years of data.

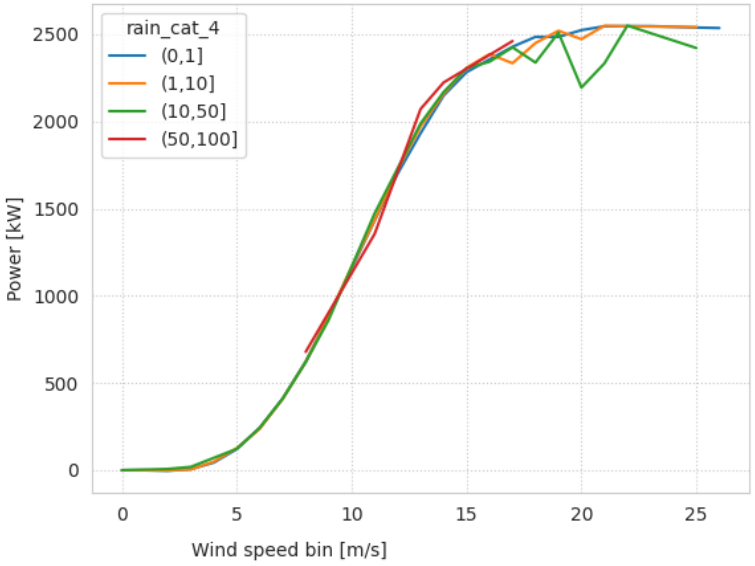

Figure 32. Rain effects on the power curve at the Site A.

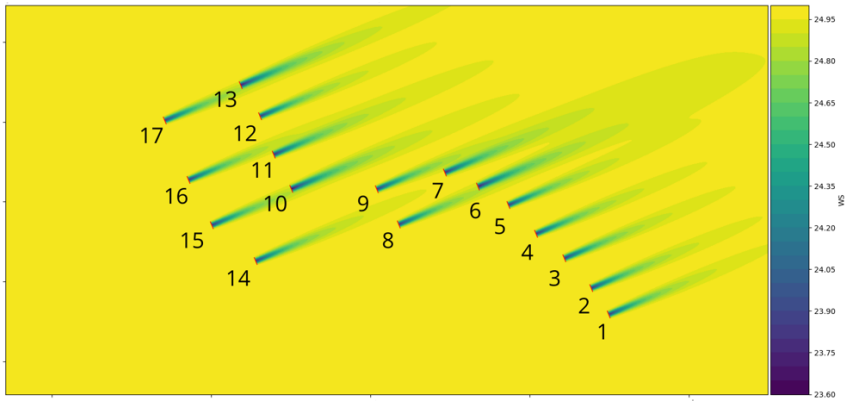

Figure 33. Wind farm layout and turbine labeling at Site B, and a wake visualization for the main wind direction.

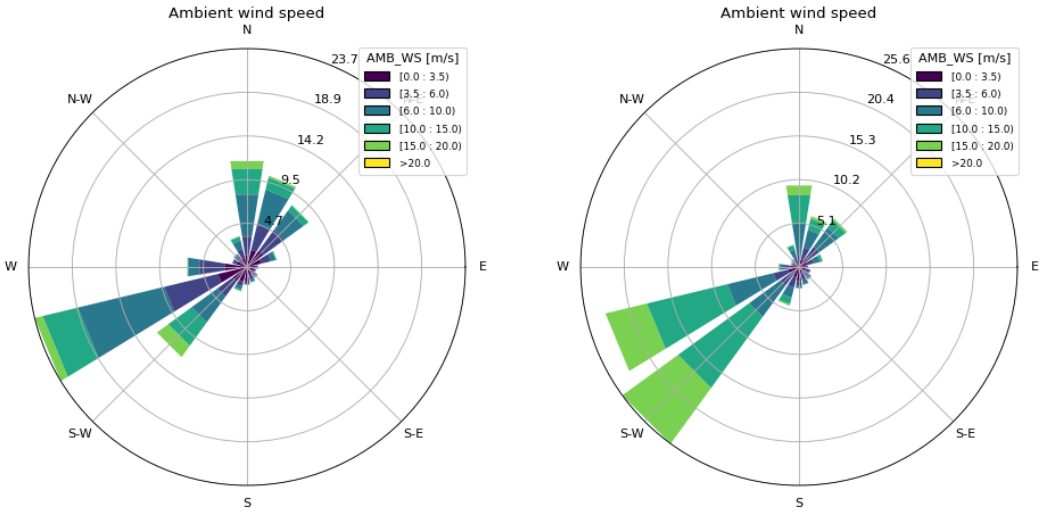

Figure 34. Wind statistics at Site B, total time series (left) and during rain (right).

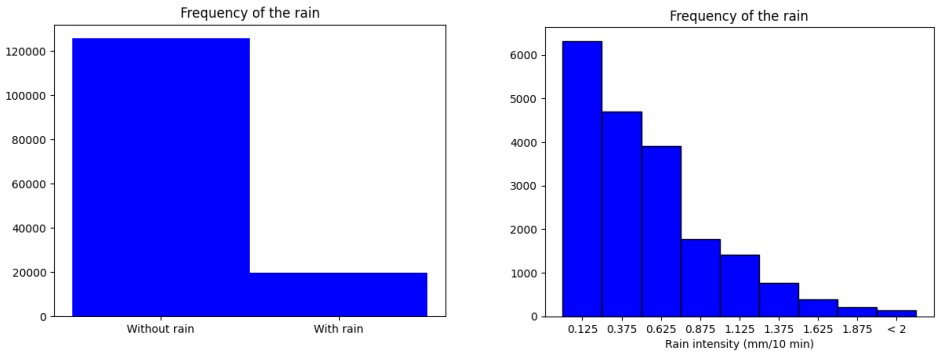

Figure 35. Rain statistics at Site B. The second axis shows the total counts in the available time series data.

	General	With rain	Without rain
Measured density (mean)	1.085 kg/m^3	1.097 kg/m^3	1.084 kg/m^3
Mean of the temperature	284.67 K	279.88 K	285.42 K
Mean of the TI	17 %	17 %	17 %
Mean of the wind speed	6.37 m/s	9.93 m/s	5.82 m/s

Table 6. Mean parameters at Site B.

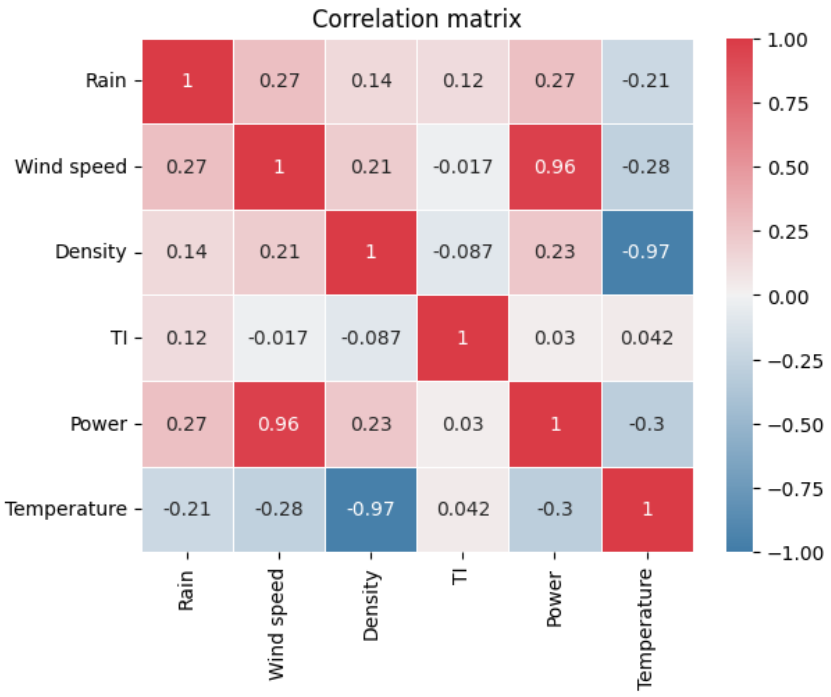

Figure 36. Parameter correlation matrix at Site B.

The correlation matrix of the relevant parameters is shown in Figure 36, based on about 2.5 years of overlap between SCADA and met mast data. Hourly rain intensity was interpolated on the SCADA time stamps, inducing a possibly large uncertainty factor. Clearly wind speed and mean power are correlated, as well as air density and temperature. The correlation of rain intensity and turbulence intensity is low, but a slight positive correlation between rain and wind speed as well as with air density was observed.

The SCADA data was filtered for data sanity, furthermore box filters were applied in ws-power and pitch-power spaces in order to exclude clearly deviating control states, following [69].

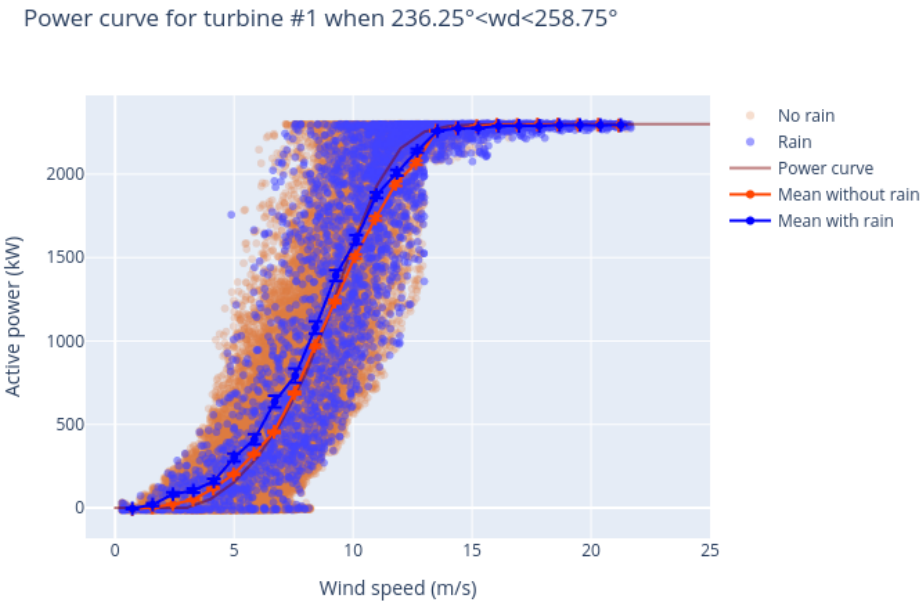

Figure 37. Rain effects on the power curve of turbine 1 at Site B.

A typical result for the power curve evaluation is shown in Figure 37, indicating a slightly increased power production during rain. This trend is consistent for most turbines in the wind farm. However, due to the large spread and the small statistical sample size the significance of this finding is questionable. It is worth mentioning that the wind speed from SCADA data was density corrected for this analysis. The anemometers could have been influenced by rain and also existing turbulence intensity variations have not been considered during the generation of this result.

As a next step, the bootstrapping method was applied to evaluate the statistical significance of the findings. Figure 38 shows a result of the power difference between dry and rainy conditions for a subset of the turbines in the wind farm. The 95% confidence intervals always also include no power difference. Hence it remains difficult to conclude on a significance with all the considered uncertainties.

Considering wake effects, figures 39 and 40 show a comparison of two pairs of turbines in waked situations. Again the sample size of rainy conditions is too small for significant conclusions about the influence of rain on wake effects.

Figure 38. Power in dry conditions minus power in rainy conditions at Site B. Error bars indicate 95% confidence intervals.

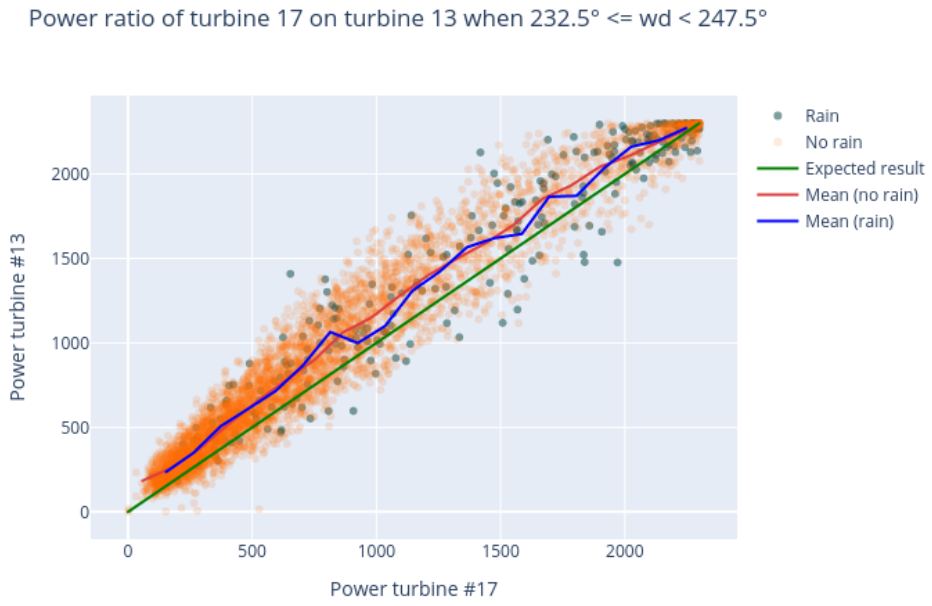

Figure 39. The power comparison of turbines 13 and 17 at Site B, with and without rain, in units of kW.

Funded by the European Union

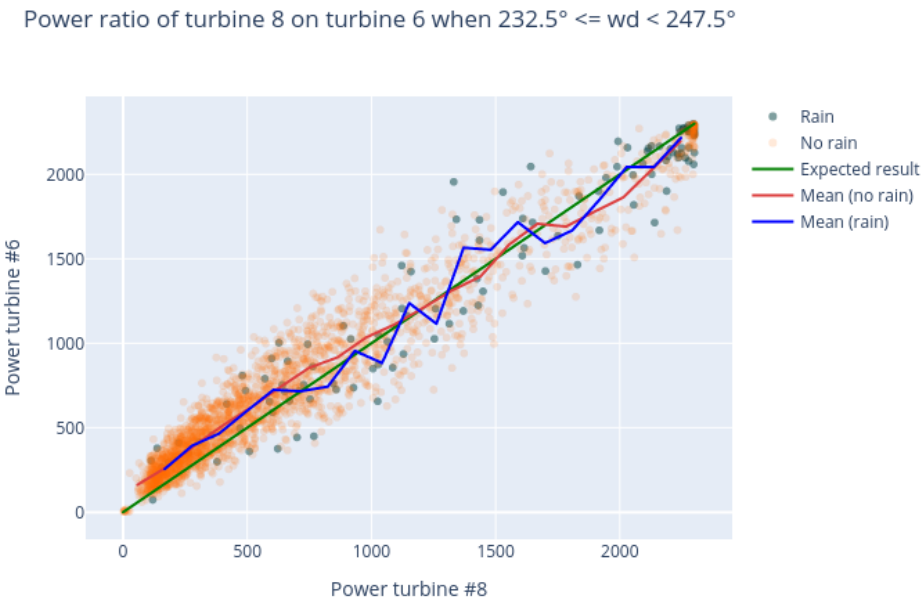

Figure 40. The power comparison of turbines 6 and 8 at Site B, with and without rain, in units of kW.

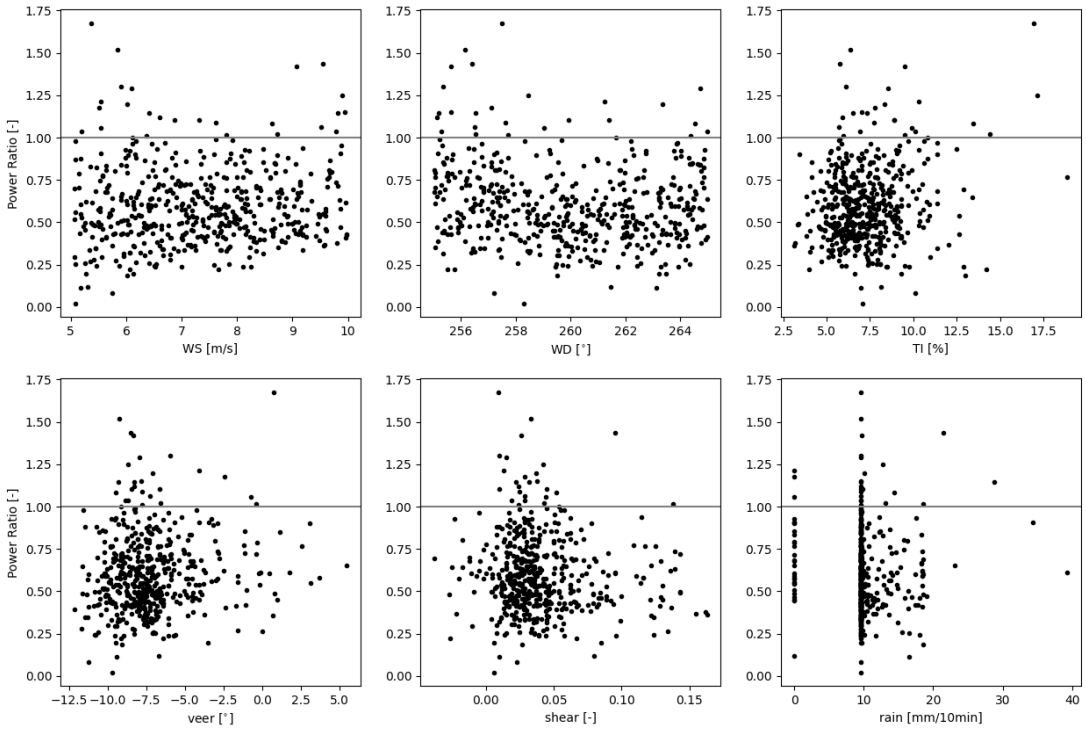

Figure 41. Correlation between atmospheric variables and the power ratio between two aligned turbines.

Funded by the European Union

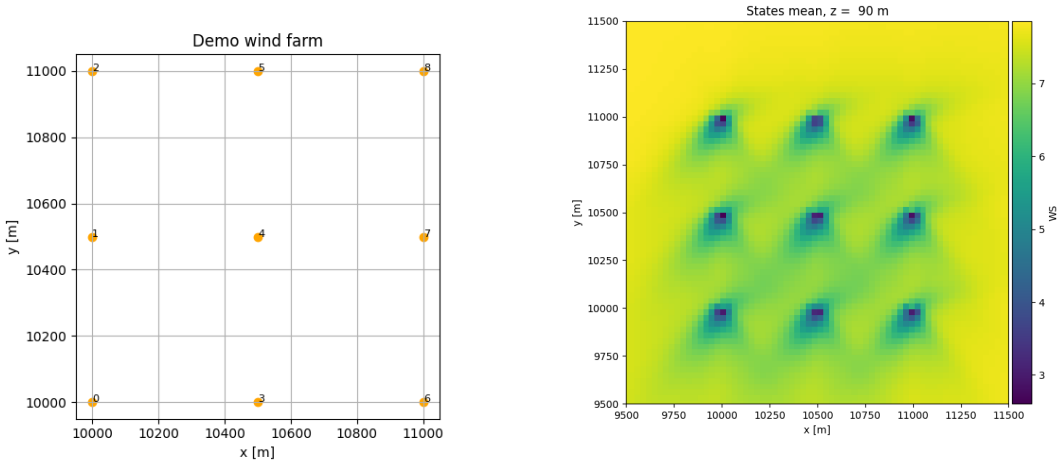

Figure 42. Left: Layout of the demonstration wind farm, fictional. Right: The mean flow over the studied time series.

4.3.2.3 Alpha Ventus & FINO1

In addition to investigation of Site A and B data, data from Alpha Ventus and the FINO1 met mast were used to find a relation between precipitation and the wake deficit. Data from 2016 was acquired with wind speed, wind direction and turbulence intensity at 90m, precipitation at 20m and shear and veer calculated between 33m and 90m. As a proxy for the wake deficit, the power ratio between two turbines is computed, and the data is filtered for a 10° bin around the wind direction in which these turbines are aligned.

Figure 41 displays the correlation between six atmospheric variables and the power ratio of the two aligned turbines. Unfortunately, no clear correlations between any of these pairs was found. Only the wind direction appears to have a slight correlation due to full and partial wakes, but even here the scatter is high. Even WS and TI, which in literature have often been studied as variables affecting the wake deficit magnitude, don't show a clear relation here. Lastly, the rain data does not seem correct, with many values collapsing on 10 mm/10min, indicating unreliable data. Unfortunately, this lead to the conclusion that this data set is unsuitable for further analysis.

4.3.3 Erosion wake effect implementation

Erosion damage reduces the performance of the wind turbine blades. This yields a modification of the thrust and, eventually, a decrease in the produced power. Hence in the context of wake modeling based on engineering wake models such effects can be modeled by alterations of the power and thrust curves.

A lookup-based approach has been implemented that interpolates the power and thrust curves between the undamaged and damaged states in the wind farm and wake modeling software FOXES [62, 23].

If damage information is available in the form of time series data for each turbine, this method incorporates the erosion effect into wake and power calculations in a fully vectorized manner. Alternatively, the model is also applicable in the context of a control-based sequential time-step evaluation.

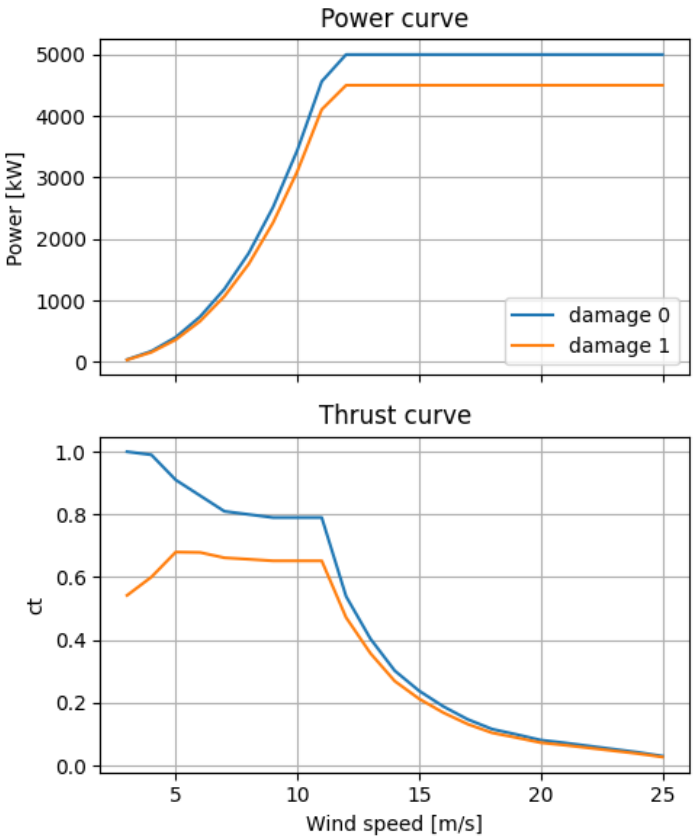

Figure 43. Assumed power and thrust curve changes under damage, fictional. Notice that these curves are unrealistic, since the controller can compensate for the erosion effect above rated wind speed. For the sake of simplicity such effects were ignored in this demonstration.

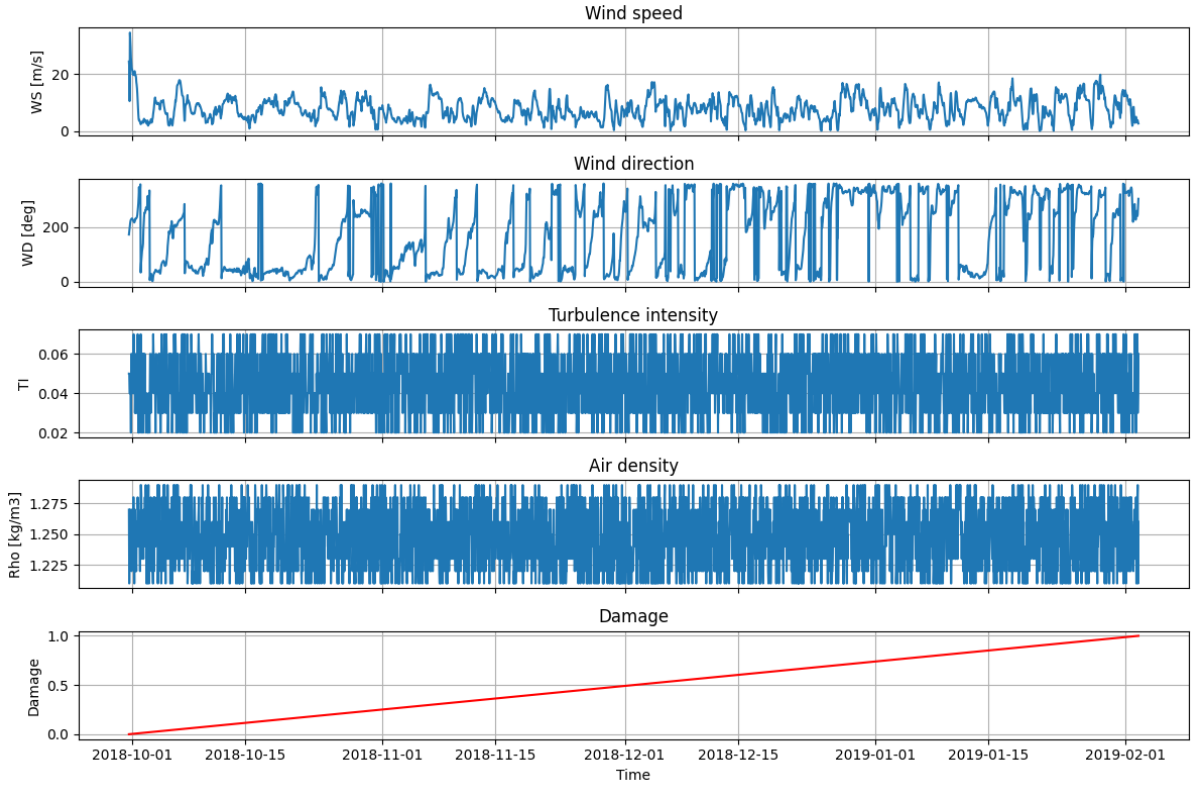

Figure 44. Assumed time series with linearly increasing damage, fictional.

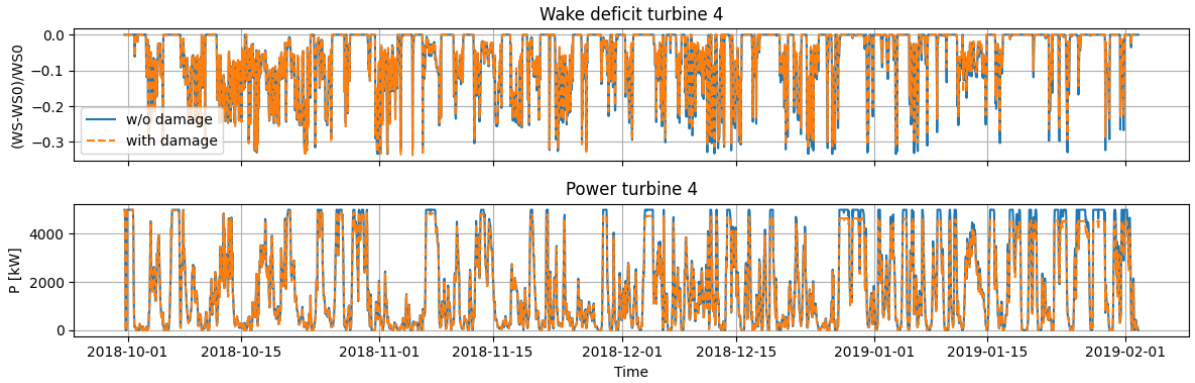

Figure 45. Results of the damage modeling demonstration run.

Funded by the European Union

The implemented functionality is demonstrated in the following proof-of-principle wind farm case setup. The latter is based on the fictional wind farm site shown in Fig. 42 consisting of 9 wind turbines in a regular layout and the inflow conditions of Fig. 44, representing a time series with 3000 entries. The turbine type is a modified version of the NREL 5MW turbine. Its thrust and power curves are interpolated between the damage 0 and damage 1 curves shown in Fig. 43, depending on the value of the dimensionless parameter damage in the time series. For demonstration purposes, the damage values are linearly increasing from 0 to 1 with time in this example, c.f. Fig. 44.

Figure 45 shows the effect of including the damage parameter into the calculation. The wake deficit and the power yield of turbine 4, c.f. Fig. 42, are increasingly affected by the linearly growing erosion damage.

4.3.4 Conclusion

In conclusion, the observed differences between dry and rainy conditions at the commercial farms A and B appear not significant enough to serve as a base for model building. Additionally, the data from the Alpha Ventus wind farm and the FINO1 met mast were analyzed, but did not provide additional insights.

Based on the available data, it seems impossible to specify in which ways the wake model predictions should be altered due to the presence of rain. On the contrary, according to our analysis it cannot be ruled out that the influence of rain and precipitation can be safely ignored in the context of wind farm yield evaluation with engineering wake models.

Concerning erosion damage modeling, a lookup-table based approach has been implemented in the wind farm and wake modelling software FOXES [62, 23] and its functionality has been demonstrated in a fictional proof-of-principle case.

5. MICROSCALE MODELS

Microscale wind resource assessment (WRA) in complex terrain (CT) is crucial for identifying suitable sites for wind farms (WF). Mesoscale, analytical and linearised flow models struggle with terrain complexity, leading to higher fidelity approaches such as CFD for microscale modelling. Wind turbine (WT) wakes, downstream regions of reduced wind speed and increased turbulence, significantly affect the performance of downstream turbines, resulting in reduced energy production and increased structural loads. Wakes and CT interaction is influenced by factors such as topography, atmospheric stability, and WT characteristics.

Understanding the wake-topography interaction is critical for WF operators during site planning. Studies such as the Perdigao case in Portugal have extensively instrumented sites to understand flow behaviour under WT wakes, providing valuable data for model development and validation. The wake behaviour under different atmospheric stability conditions was studied at this site using LiDAR technology, showing local peaks in the velocity deficit profiles of 70% at 1D (rotor diameter), and decreasing to 50% at 3D under neutral conditions. This study concluded that wake propagation is highly complex and strongly dependent on terrain orography and the stability conditions.

This work investigates the wind resource at the CT site of the Alaiz experimental WF, first without the influence of the WF, and then modelling theoretical WTs using the Actuator Disk (AD) method. This work provides a better understanding of the wind flow in CT sites, and its behaviour with the wake of wind turbines wake.

5.1 Methodology

This study analyses the highly complex topography of the Alaiz experimental WF. Alaiz is in a high altitude (elevation 1,100 m) CT´site located at 15 km SE from Pamplona (Navarre, Spain). The size of the farm is 30 km x 30 km and is suitable for the study of high-resolution mesoscale-to-microscale models with strong coupling between terrain and thermal stratification. The prevailing wind directions are from the north and from the south. To the north of the WF there is a large valley at an elevation of around 700m. To the south, the terrain is complex with the presence of some WFs; the closest one is situated 2 km south. The WF has four reference met masts (MP1, MP3, MP5 and MP6) 118 m tall, situated at the north of six wind turbine positions (A1 to A6).

The Alaiz experimental WF site was simulated using the OpenFOAM Finite Volume Method (FVM) open-source CFD code. The vegetation effect was modelled using the aerodynamic roughness height (z_0). Neutral atmospheric stability was modelled using a logarithmic inlet wind profile and including the Coriolis force. The WTs of the WF were modelled with the AD method. The k-ϵ-f$_P$ eddy viscosity model (EVM) was used to avoid the wind speed deficits underestimation of the original k-ϵ EVM when considering ADs. Experimental data representing neutral atmospheric conditions was used to validate the model. Finally, the influence of a virtual WF with NREL5MW WTs located in the Alaiz experimental WF available positions was studied.

The following steps were taken in this study:

- Mesh sensitivity study of a single AD.

Funded by the European Union

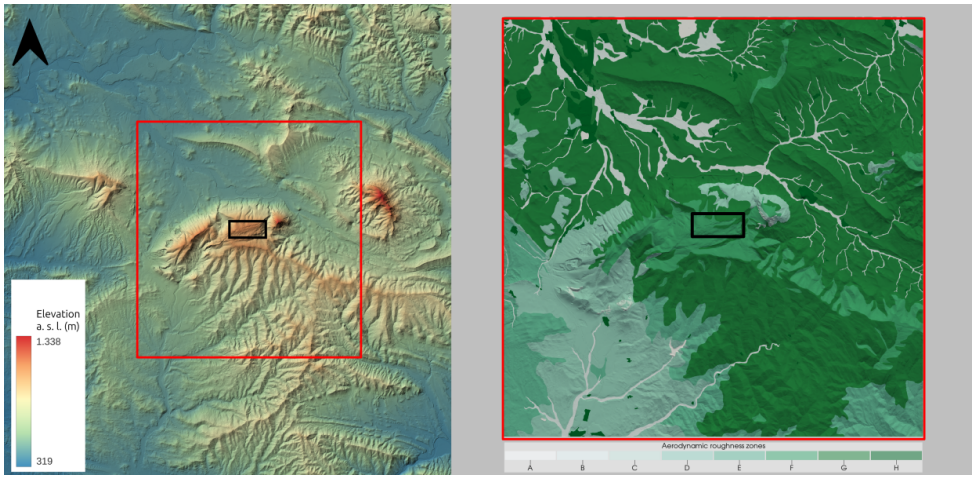

Figure 46. Map of the Alaiz experimental WF (black rectangle) site in elevation above sea level (a.s.l.) (40 km x 40 km) (left). Potential vegetation zones modelled using aerodynamic roughness heights (20 km x 20 km) (right).

- Mesh sensitivity study of the CT case.
- Comparison of k-ϵ and k-ϵ-f$_P$ EVMs in a highly CT case.
- Highly CT simulation.
- Highly CT simulation with a virtual WF consisting of 6 WTs.

5.1.1 Topography and geometry

The Alaiz experimental WF site has a highly complex topography (Figure 46 (left)). In order to study and model the effect of topography on wind flow, it is necessary to characterise the complexity of the terrain. High-resolution geometry and a subsequent high-resolution mesh for the computations are required. Furthermore, the characterisation of the vegetation diversity (Figure 46 (right)) by means of aerodynamic roughness height is considered that also demands to subdivide the geometry.

The high-resolution geometry is generated from a high-resolution Digital Terrain Model (DTM) obtained from LiDAR flights with a resolution of 2 m. The extent of the modelled terrain is 20 km by 20 km, with the WF located in the centre of the domain (black rectangles on Figure 46).

5.1.2 Met masts and wind turbines

The available experimental data used to calibrate the model corresponds to a period prior to the installation of the WF. The maximum instrumented height is 118 m above ground level (AGL). During this period there were two different types of met masts: the permanent met masts (MP) and the calibration met masts (MC). The MC met masts were located where the WTs would be installed. The MP met masts are still in place. The locations of the met masts can be seen in Figure 47.

For this study, the data from the met masts MP1, MP3, MP5, MC1, MC2 and MC3 was available. The available data from these met masts concern wind speed and direction at four different heights (118 m, 102 m, 90 m and 78 m AGL) instrumented with wind vanes and cup anemometers.

Funded by the European Union

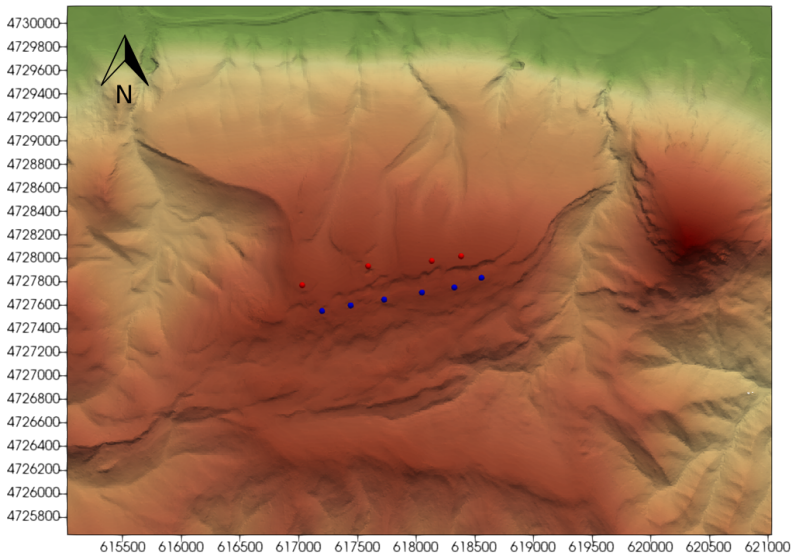

Figure 47. Alaiz experimental WF layout (ETRS89-UTM30N coordinate reference system)

5.1.3 Simulation Setup

A Reynolds-averaged-Navier-Stokes (RANS) approach was used for all the simulations. Incompressible steady-state simulations were performed using the Semi-Implicit Method for Pressure-Linked Equations-Consistent (SIMPLEC) algorithm. Second order linear-upwind schemes were used for both the momentum and turbulence equations.

The k-ϵ-f$_P$ EVM with a variable C_μ value, influenced by the tuning constant C_r is used in the calculations. Previous studies have shown that the conventional $k-\epsilon$ eddy viscosity model (EVM) tends to underestimate velocity deficits when simulating wind turbine wakes with ADs, while the $k-\epsilon-f_P$ EVM provides more accurate estimates. In [45], the C_r value of this EVM was tuned to 4.5 using Large Eddy Simulations (LES) for the NREL5MW WT, which is also used in this study for consistency.

To deal with the non-orthogonal cells due to the highly complex topography of the site, 3 non orthogonal correctors were used to ensure the convergence of the simulations. A residual control of 1e-6 was set up for all the equations after studying the effect of this choice on the variables of interest (wind speed at hub height).

5.1.4 Neutral Atmospheric Stability

Neutral atmospheric conditions were considered for these simulations and thermal phenomena were not considered. The neutral atmospheric stability was modelled by the idealised logarithmic wind profile. A turbulence intensity of 10% was considered. The Coriolis force was also considered using a source term assigned to all cells in the computational domain to account for the horizontal and vertical components of the Coriolis force induced by the Earth's rotation. A planetary rotation period of 23.934 h/day and a latitude of 42.7° (according to the WF location) were assigned to set up the source term, resulting in a Coriolis parameter of 0.729x10-4 1/s. The inclusion of the Coriolis source term with an idealised logarithmic wind profile showed a good agreement with the experimental data in the CT site of Perdigao [67].

5.1.5 Wind Turbines Modelling

The WTs are modelled using the AD method with a variable scaling approach [44]. This approach makes it possible to perform a dynamic calibration of the WF when there are several WTs downstream. This is not the case in this study, but in order to improve the study of the WF wake effect on other WFs in the vicinity in future work, this AD method has been chosen.

5.1.6 Experimental data for validation

The experimental data used for model calibration and validation covers the period prior to the installation of the WTs, from August to December 2010. Only one wind speed and direction (north) is simulated.

With no sonic anemometers or ground temperature data available, the Monin-Obukhov length [50] calculation isn't feasible. Simplified methods such as Pasquill-Gifford classification [54] result in significant data loss when synchronising towers. Therefore, the available data from both the north and south wind directions are split and the average wind speed and direction for the north direction is calculated, assuming neutral atmospheric conditions.

5.2 Simulations

Mesh sensitivity studies for AD and CT are performed, followed by a comparison between the k-ϵ and k-ϵ-f$_P$ EVMs in CT conditions without considering wakes. Subsequently, the CT model is calibrated and validated using experimental data before finally modelling the WTs wakes in the CT.

5.2.1 Actuator Disk Mesh Sensitivity Study

Although mesh sensitivity studies have been carried out in previous studies [45], this study investigates the mesh requirements when considering the k-ϵ-f$_P$ EVM with a WT modelled by the AD method due to the use of a different meshing strategy (unstructured meshes).

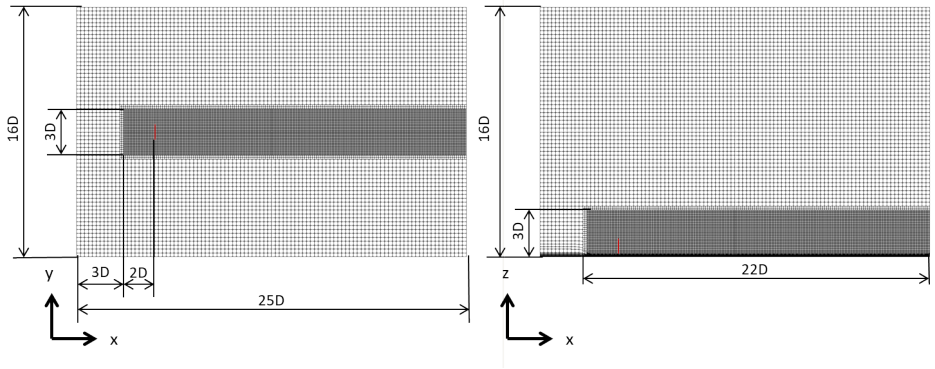

Figure 48. AD mesh characteristics depending on rotor diameter (D). AD selected cells in red.

Figure 48 shows the mesh refinement region (RR). The mesh background is defined as a function of the rotor diameter (D) of the NREL5MW WT [38]. Three different background sizes are studied, maintaining a refinement ratio (r) of 2 (Table 1). The RR has a refinement level of 2, 10 surface layers are used with a constant expansion ratio of 1.12. The Global Convergence Index (GCI) method [57] with a safety factor (F_s) of 1.25 is used for this study.

Table 7. AD mesh characteristics.

Mesh	Back-ground size	1st layer size [m]	Cells/D	N. Cells
A	0.5	1	8	208,477
B	0.25	2	16	1,437,401
C	0.125	4	32	10,660,139

The GCI calculation involves adimensionalising the wind speed integrated over the rotor area with the freestream speed integrated over the rotor area at various wake distances (proportional to D). Mesh B has a GCI below 0.6% while Mesh C has a GCI below 0.2 %. In [45] it is recommended to use at least 8 cells per rotor diameter in the AD area when using k-ϵ-f_P EVM with structured meshes, but it shows small deviations from the two others finer meshes studied with 16 and 32 cells per rotor diameter in the AD area. After carrying out this study with unstructured meshes and seeing some common conclusions with the work of other authors, the features of mesh B (16 cells per rotor diameter) were selected for the subsequent WF simulations due to its balanced GCI/cell number ratio and agreement with the finest mesh.

5.2.2 Complex Terrain Mesh Sensitivity Study

A mesh refinement study based on the GCI method was carried out to define the CT mesh features. Two RRs are considered (Figure 49), RR1 (refinement level 2) and RR2 (refinement level 3); focusing on the area of interest (the WF site). Additionally, a surface refinement level of 3 is applied to the topography surface.

Funded by the European Union

The mesh background size is defined according to D (Table 8), 10 surface layers with a constant expansion ratio of 1.12 and a constant first layer thickness of 4 m are used. The first surface layer thickness is different from that defined for mesh B in the AD mesh sensitivity study in Section 5.2.1, as aerodynamic roughness heights up to 2 m are going to be considered.

Three meshes are studied keeping a refinement ratio (r) of 2. The hub height wind speed at met masts MC1, MC2 and MC3 is considered for this study. The GCI for mesh C is less than 2.72 % for all the met masts studied, these mesh features are selected for the calculations.

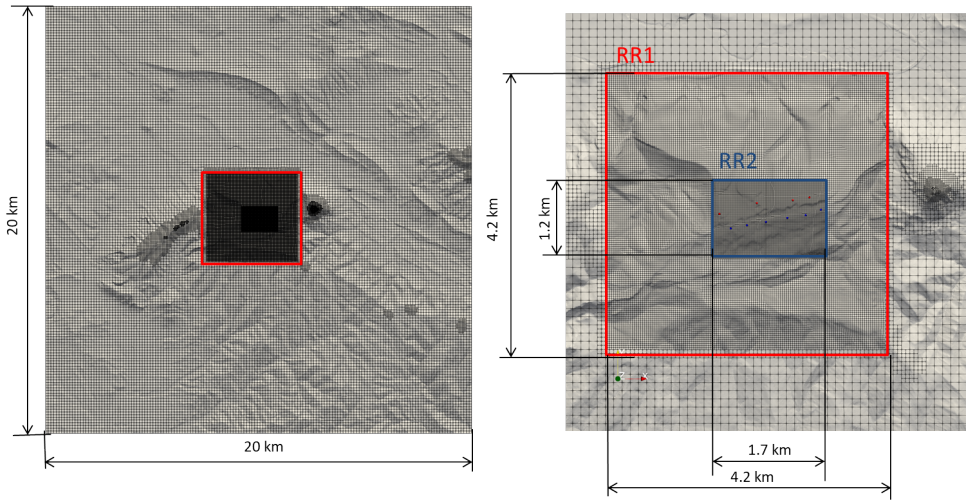

Figure 49. Terrain mesh characteristics. General overview (left) and zoom at WF location (right).

Table 8. CT mesh characteristics.

Mesh	Background	N. Cells	$U_{H,MC1}$ [m/s]	$U_{H,MC2}$ [m/s]	$U_{H,MC3}$ [m/s]
A	4 D	991,347	13.089	13.239	12.741
B	2 D	3,968,840	12.675	12.644	12.118
C	1 D	16,718,041	12.608	12.5882	12.012

5.2.3 $k-\varepsilon$ and $k-\varepsilon-f_P$ EVMs Comparison in Highly Complex Terrain

The $k-\varepsilon-f_P$ EVM is a variable C_{mu} EVM based on the $k-\varepsilon$ EVM. This modified EVM is used in the modelling of WTs by ADs in order to better predict the velocity deficit in the WT wakes. However, the use of this EVM instead of the constant C_{mu} EVM could question its suitability for cases where WTs are not modelled by ADs. Both EVMs were compared and showed a good agreement (Figure 50) in wind speed (U), turbulent kinetic energy (TKE) and wind direction for the different met masts, leading to the selection of the $k-\varepsilon-f_P$ EVM for all the simulations.

5.2.4 Complex Terrain Model Validation

The CT flow model was calibrated to match the experimental data in terms of wind speed and direction and to validate its suitability for the subsequent simulation.

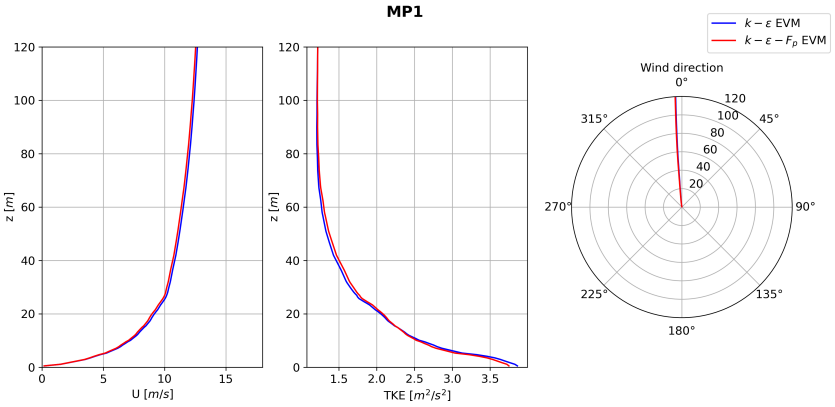

Figure 50. $k - \varepsilon$ and $k - \varepsilon - f_P$ EVMs comparison at met mast MP1 site. The radius of the polar plot (right) refers to the height AGL.

Six met masts were used to validate the model: MP1, MP3, MP5, MC1, MC2 and MC3. For all the met masts except for the MP5, the estimated wind speed is within the experimental uncertainty range. The maximum wind speed deviation from experimental data occurs at the MP5 met mast at 102 m AGL with an overestimation of 0.768 m/s, while the maximum wind direction deviation is of 12.02º and occurs at the MP1 met mast at 78 m AGL (Figure 51). The turbulence intensity value at hub height is around 10 % for all the met masts locations.

In Figure 52 the met masts at WTs positions (MCs) show a high U_x component (X axis goes from West to East, Y axis from south to north and Z is the vertical axis). The met masts at westerly positions show a higher westerly wind component due to the flow acceleration in that direction (270 °) caused by a topographic depression to the west of the WF (Figure 53). The further east the WT is located, the less the met masts are affected by this topographic feature.

5.2.5 Complex Terrain with Wind Farm Influence

In this phase, the CT flow model incorporates the Alaiz WF influence by positioning the virtual NREL 5MW WT in each of its six available locations. The AD mesh strategy defined in Section 5.2.1 is applied within the context of the CT mesh strategy defined in Section 5.2.2.

The calibrated model wind speeds at hub height at the MCs locations (Section 5.2.4) are used to define the C_p and C_T for the modelled WTs in the WF simulations.

The results are presented in the direction of the free stream velocity (north to south) as a function of a dimensionless distance (D^*). These dimensionless coordinates are associated with the x_{UTM30N} values in terms of D distances from the position of WT1 (MC1), which is the southernmost located WT.

The CT wake is compared with and without the influence of the WF layout. Figure 54 shows the natural wake speed deficit in CT at hub height (90 m AGL). The contribution of each WT to the natural wake of the terrain can be seen at $2.5D^*$ (wind speed deficits up to 29.46 %). At $5D^*$it is no longer possible to distinguish the contribution of WT5 and WT6 to the global wake in CT (wind speed deficits up to 18.53 %).

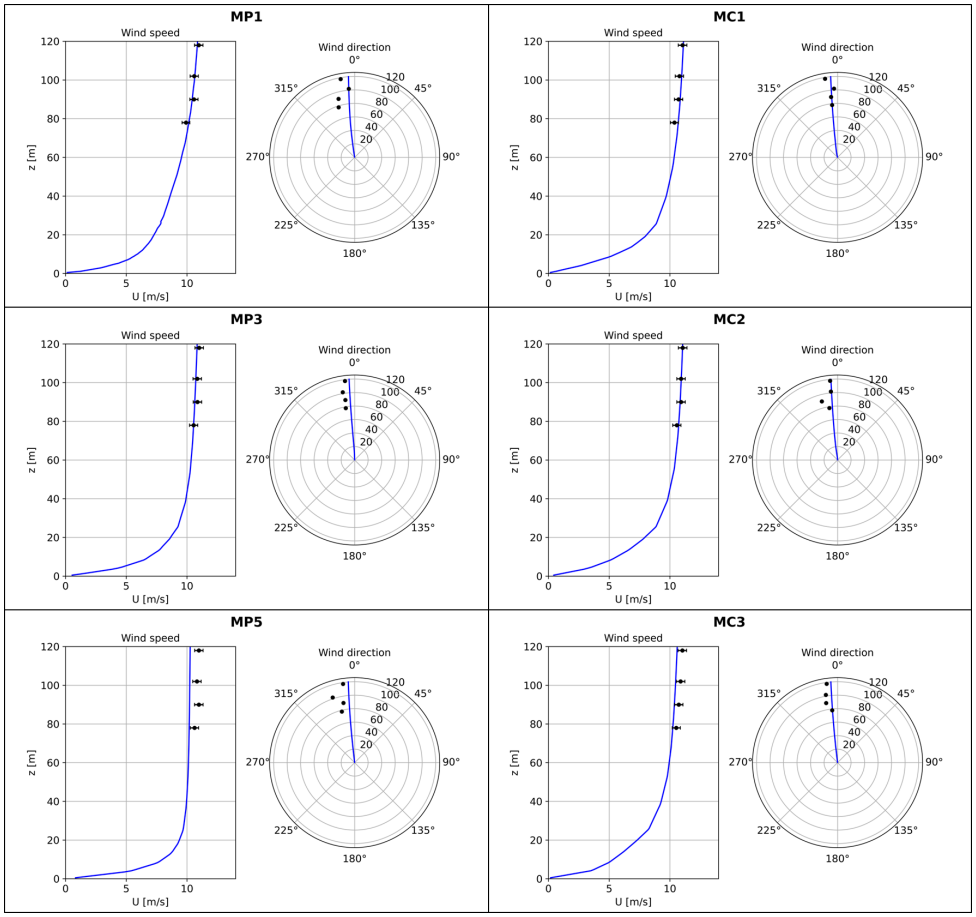

Figure 51. Evolution of wind speed and direction with height (up to 120 m) at met masts site; and experimental data (black dots with error bars). The radius of the polar plots refers to the height AGL.

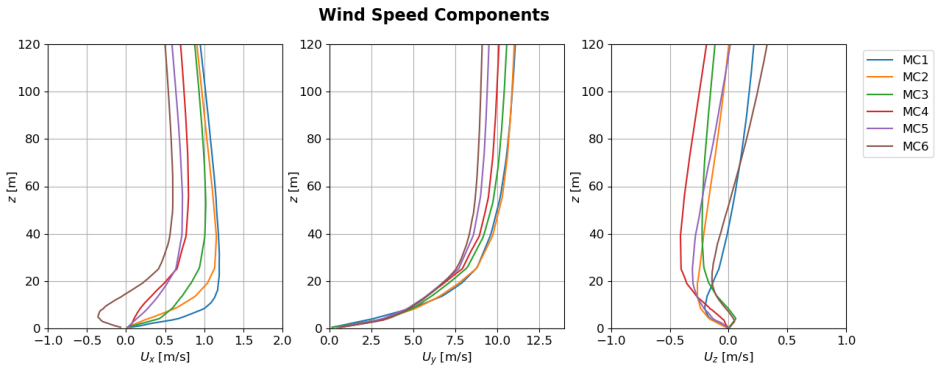

Figure 52. Wind speed components of the met masts.

At $10D^*$ the contribution of each WT is not noticeable and a generalised wind speed deficit appears . At $20D^*$, $25D^*$ and $50D^*$ it is no longer possible to distinguish the contribution of each WT to the global wake. At $75D^*$ (9450 m), there is a complete recovery of the wake in the transects concerning the WT1, WT4, WT5 and WT6. While there is still a noticeable wind speed deficit in the transects concerning the WT2 and WT3, the wake of the natural terrain is not fully recovered.

Funded by the European Union

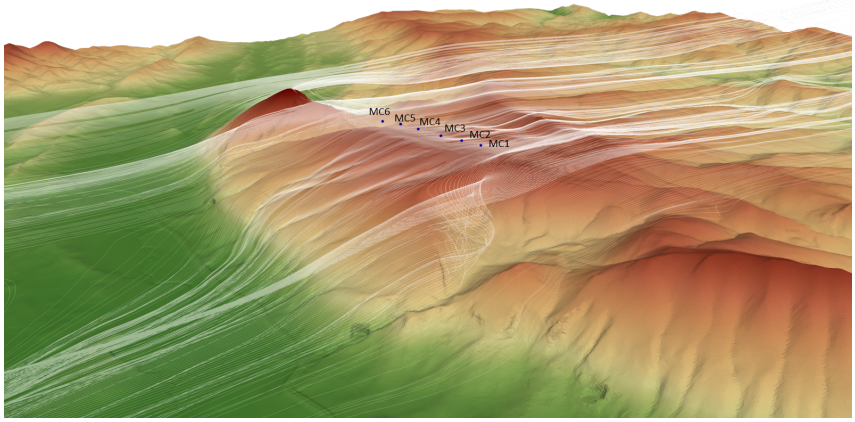

Figure 53. Flow streamlines in the WF vicinity.

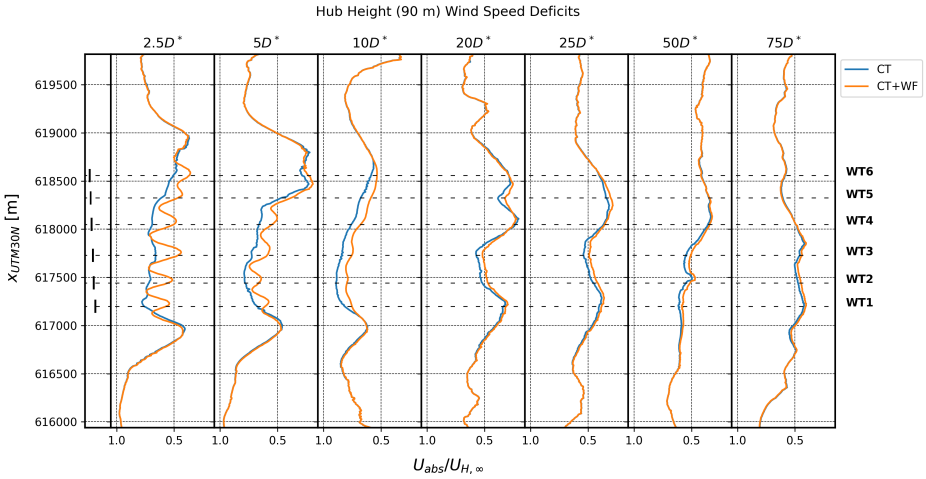

Figure 54. Normalised absolute velocity along x_{UTM30N} coordinates AGL for the CT without (CT) and with (CT+WF) WF at hub height.

A slight wake deflection can be seen in Figure 54, where the velocity deficit peaks at $2.5D^*$ do not agree with WTs transects, there is a deviation of the minimum velocity peaks to the east. This can be explained by the effect of a topographic depression in the south of the WF, where a high flow circulation is generated (Figure 53) leading to a larger westerly wind speed component (Table 52). This phenomenon can be also seen in Figure 55, where the natural terrain wake contribution of the western terrain depression is observed in the form of a wind speed deficit leading to an increase in the west wind component.

The locations to the south of the experimental WF would be the most affected by the wind speed and direction conditions, and the theoretical WTs considered in this study. The studied potential sites are located at above $10D^*$ to the south and there is height a.s.l. reduction above 100 m.

Some of the possible back WTs (BWT) locations at $10D^*$ suffer from large wind speed deficits when considering the WF wakes. Figure 56 shows some of the most affected possible BWTs. The wind direction does not show a large deviation, whereas the wind speed is reduced by about 1 m/s at heights above 20 m AGL.

Funded by the European Union

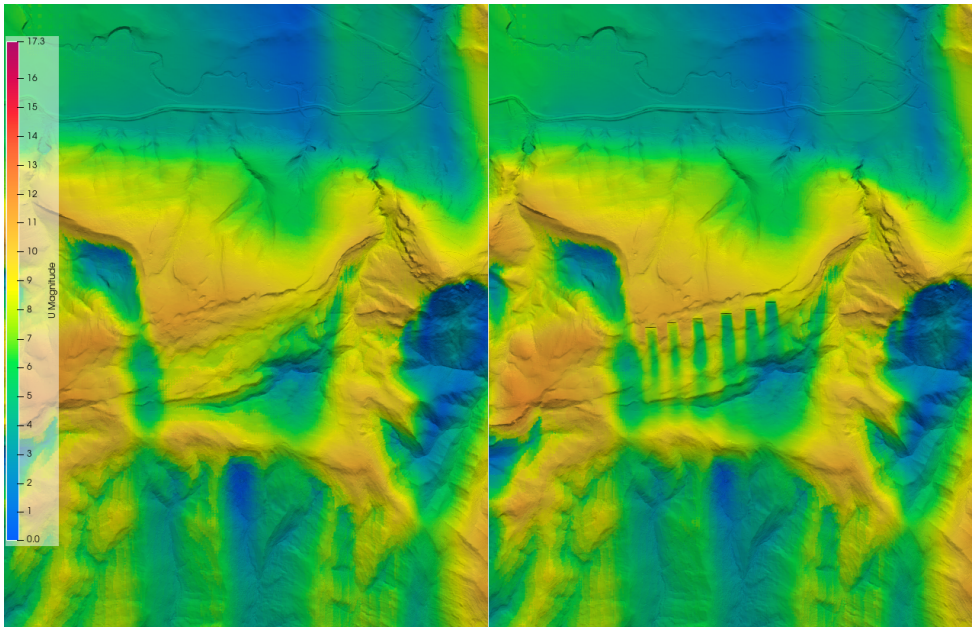

Figure 55. Velocity field (90 m AGL) without the influence of a WF (left) and accounting for the WF influence (right).

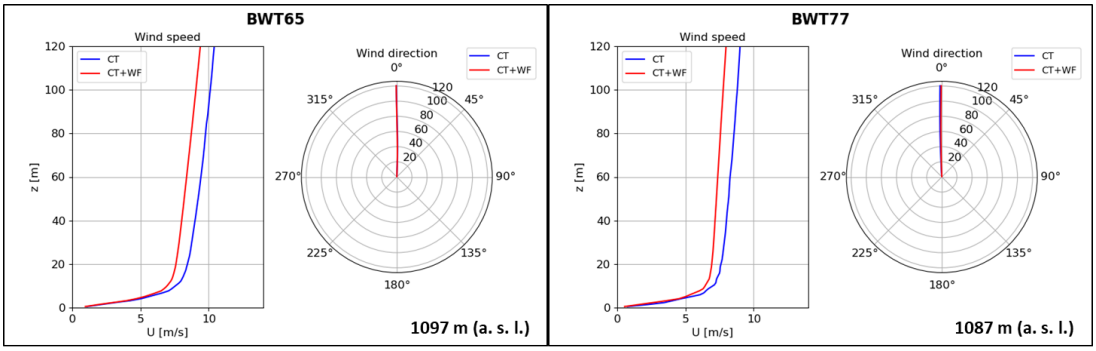

Figure 56. Wind speed and direction of some positions of the possible BWTs locations to the south of the experimental Alaiz's WF. The radius of the polar plots refers to the height AGL.

5.3 Conclusions

The flow in the CT location around the Alaiz experimental WF was simulated and validated with experimental data. The effect of using $k - \varepsilon - f_P$ EVM in cases where WTs wakes are not modelled was compared with $k - \varepsilon$ EVM, which gave similar results in terms of wind speed, direction and TKE. This justified its suitability in the calculated cases shown in this work. The CT flow model was calibrated and validated in terms of wind speed and direction with the available met masts experimental data, showing a good agreement. The wake dissipation of a virtual WF setup with the theoretical NREL5MW WT in the available positions of the Alaiz experimental WF was studied as a function of terrain complexity.

Funded by the European Union

The virtual WF contribution to the natural terrain deficit of velocities and the wakes dissipation was studied at different distances downwards, up to $75D^*$ (9450 m); in the different WTs transects. The WT1, WT4, WT5 and WT6 transects in CT showed a full wake recovery at $75D^*$. The slight WF wake deflection in CT was attributed to a topographic depression to the west of the WF, which increases the westerly wind component.

The methodology used covered only one wind speed and direction, with theoretical WTs. Consequently, the scope of the investigation was restricted to a particular wind condition, yielding a substantial amount of data for WRA. The theoretical effect of the WF layout on other possible WTs sites in the vicinity was investigated and showed that the theoretical WTs would lead to a reduction in wind speed of up to 1 m/s at the potential BWTs sites to the south of the experimental WF (at above $10D^*$).

Furthermore, higher fidelity computations (Large Eddy Simulations) with more reliable wake models (ALM) should be performed in future works to verify the conclusions of this study.

6. FAST.FARM MODELS

This section describes wake development investigations using the open-source code FAST.Farm. The selected site is at Båtskär (Finland) using a data set from a previous research project (Business Finland funded project which took place from 2020 to 2022).

6.1 Båtskär site description

The site is located 16 km south of Mariehamn, in the Åland islands. It is comprised of 6 turbines, all located on islets with a maximum elevation above sea level of 10 metres. An illustrative layout and site location can be found in Figure 57 along with a reference image taken from Turbine 4 (Figure 59). The closest turbines on the main islet (turbines 1, 2 and 3 on Stora Båtskär) lie within 350 to 400 metres of each other or alternatively 4.7D to 5.6D, whilst the whole farm is placed within a 1.1 km distance (15D) due to the geographical constraints.

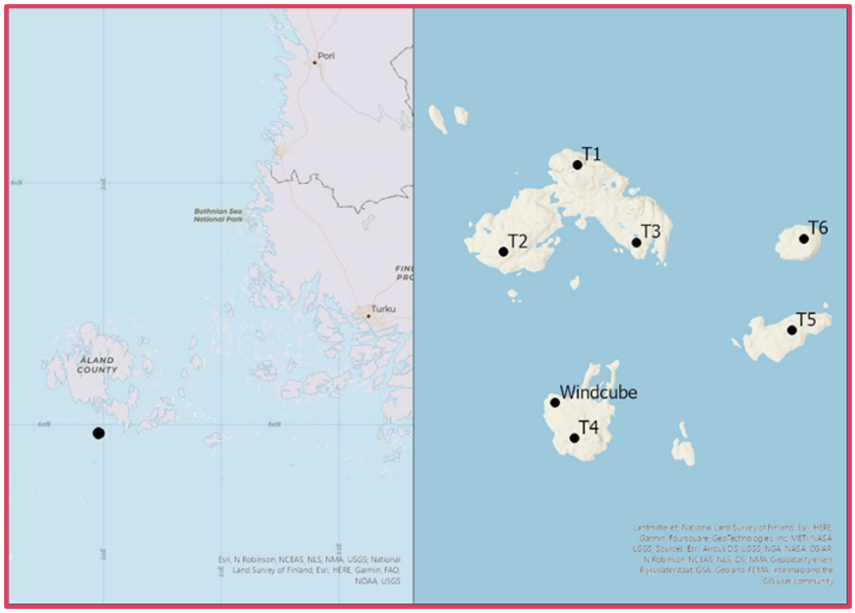

Figure 57. Stora Båtskär Site

All turbines are of the model Enercon E70, with a rated capacity of 2.3 MW and a rated wind speed of 15 m/s. This model presents a hub height of 65 metres and a rotor diameter of 71 metres. The site was instrumented from December 2020 to December 2021 with equipment for measuring the wake effects primarily on turbines 1 and 2. This corresponds to the dominant wind direction from the South-West, where Turbine 1 is in the wake of Turbine 2. These were the main instrumented turbines during this campaign, with SCADA data available for the entire site. Furthermore, complementary measurements available from the Windcube vertical profiling lidar (seen in Figure 57) which is located at ground level on the Lilla Båtskär islet or nearby Turbine 4. A summary of all of the instrumentation on site is presented in Table 9.

The dominant wind direction can be seen in Figure 58. Therefore, the main analysis will be conducted for the direction 220 to 230 degrees to align with the main waked direction for Turbine 1.

Table 9. Measurement instrumentation for 2020-2021 Båtskär campaign

Location	Measurement instrumentation
Turbine 1	Nacelle-mounted forward-facing LIDAR Ambient air measurement Generator signals Blade strain gauge
Turbine 2	Nacelle-mounted forward-facing LIDAR Nacelle-mounted backward-facing LIDAR Generator signals Blade strain gauge
Lilla Båtskär	Windcube vertical profiling LIDAR
All turbines	SCADA measurement data

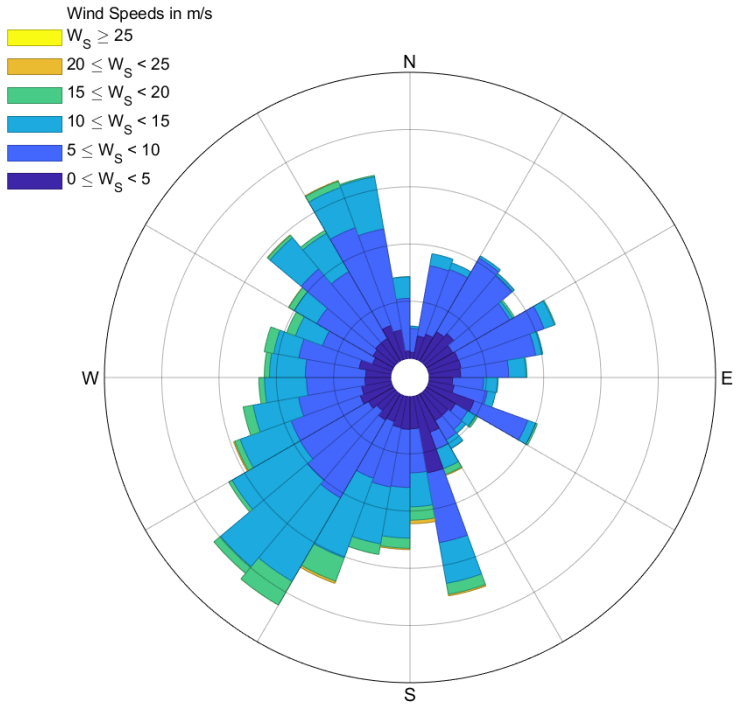

Figure 58. Wind rose for Båtskär site

Figure 59. Stora Båtskär view from Turbine 4

6.2 Dataset analysis

During the previous project, the dataset was investigated to confirm the presence of wake effects in the turbine output power data. An analysis of the power deficit was carried out across all of the turbines for varying wind speeds. This analysis utilised the site-wide SCADA data demonstrating that power deficit can be observed compared to the remaining turbines on the wind farm along the predominant wake directions. This is most noticeable along the full-waked direction with power losses up to 40% of the free-stream performing turbines. The power loss is also negligible above 12.5 m/s, close to the rated wind speed of 15 m/s.

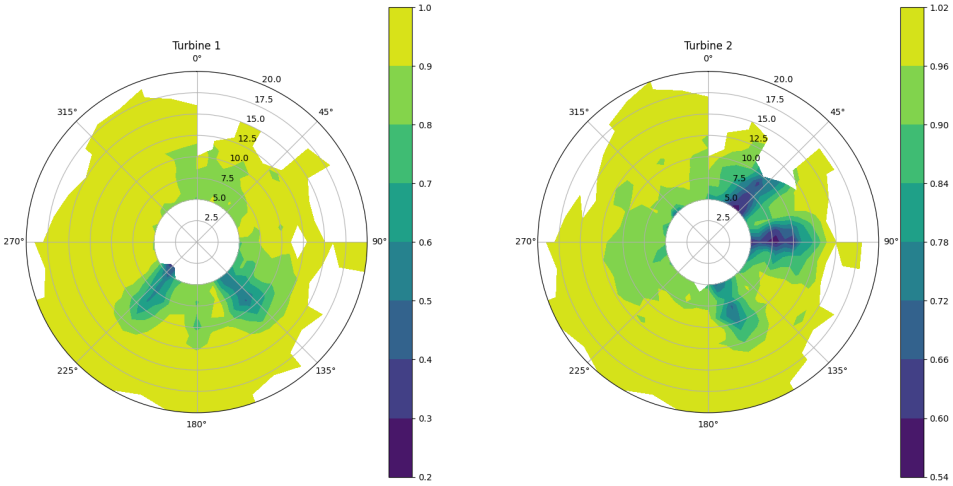

Figure 60. Power deficit for Båtskär turbines 1 and 2 relative to best performing turbine

However, this study did not take into account the effects of other atmospheric parameters. In this study, we evaluate how varying atmospheric parameters affects the visibility of the wake effects. Wakes lead to higher turbulence which can clearly be observed in the data when there is a divergence in the turbulence observed by turbines 1 and 2, as seen in Figure 61.

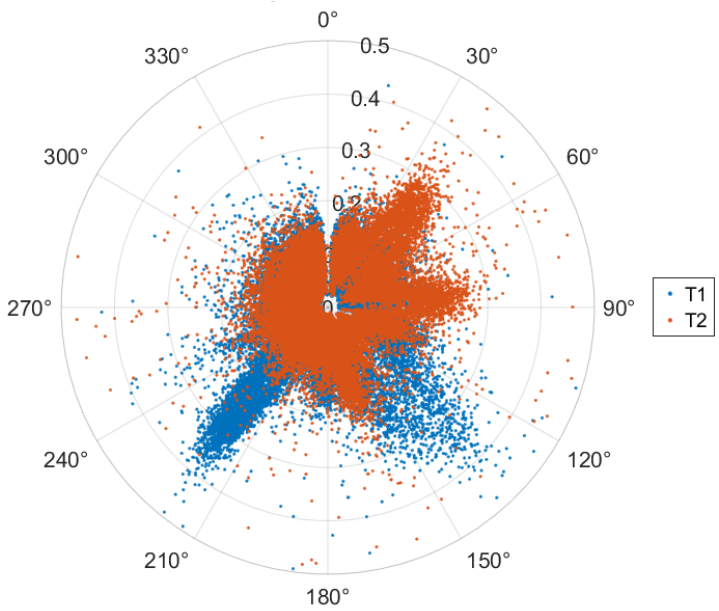

Figure 61. Turbulence intensity with varying wind direction for turbines 1 & 2

Funded by the European Union

But, how do different input conditions observed by turbine 2 affect the wakes or power losses which we can see at turbine 1? From the the trends in Figure 62, the power loss gradually reduces the closer the turbine gets to rated wind speed and power which aligns with the observations of the previous study. The level of turbulence already in the atmosphere also affects the wake or at least the power loss we can see at turbine 1. The power deficit also becomes negligible for turbulence values above 10%, at least from the available dataset. Finally, variations in the shear exponent do not seem to affect the power losses seen by turbine 1.

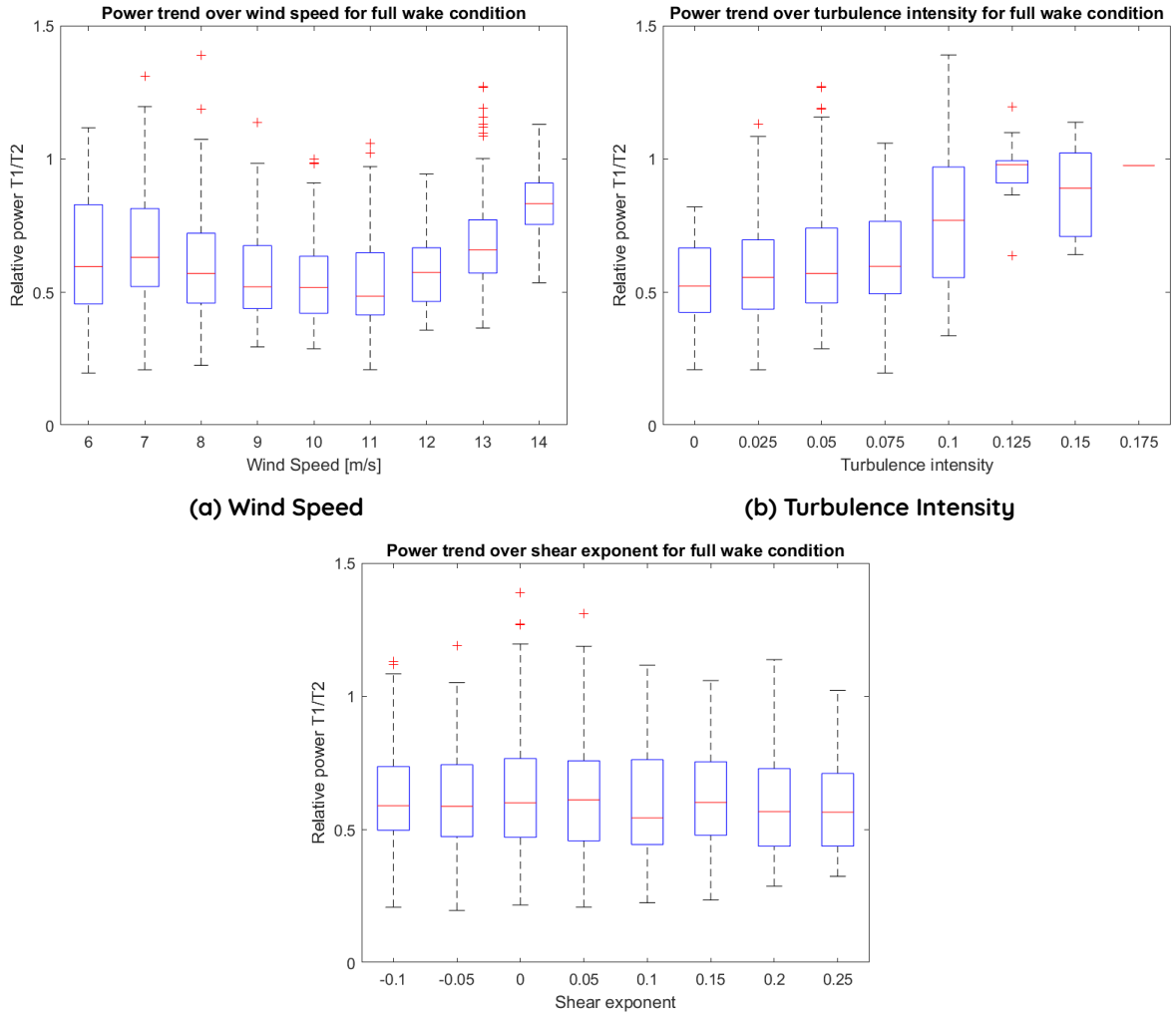

(a) Wind Speed

(b) Turbulence Intensity

(c) Shear exponent

Figure 62. Power deficit for T1 relative to T2 for varying inflow conditions. The red line indicates the median. The box covers the 25th to 75th percentiles while the whiskers cover all data not considered outliers.

Funded by the European Union

6.3 FAST.Farm simulations

Following on from the data analysis, the study compares the results found with FAST.Farm simulations in order to further investigate the effect of atmospheric conditions on power loss for a single-waked turbine.

FAST.Farm [39] is a mid-fidelity tool for simulating the behaviour of wind turbines coupled with the wake effects seen in wind farms. It is a physics-based implementation which builds on the OpenFAST single-turbine simulation software developed by the National Renewable Energy Laboratory (NREL). The main outputs it provides are the wind turbines' power production and structural loading whilst subject to the wakes present in the wind farm.

Being a mid-fidelity tool, FAST.Farm offers a good compromise between being able to perform simulations rapidly versus the accuracy of highly detailed models. It uses the Dynamic Wake Meandering (DWM) model as a basis to solve the wake effects for a turbine, with further modifications and array effects which have been validated against large-eddy simulations (LES), amongst which is SOWFA. Similarly, synthetically generated inflows are an efficient way to analyse the sensitivity to different atmospheric conditions, for which TurbSim was used for this study.

The aim of these simulations is to find how well FAST.Farm can represent the variation in atmospheric conditions and their effect on the power loss in waked turbines. This involved designing a test matrix which included the most commonly occurring conditions in the dataset where each parameter was varied independently. Table 10 shows the parameters which form the test matrix.

Table 10. Input parameters for FAST.Farm simulations

Parameter	Value range
Wind Speed [m/s]	7.5 8.5 9.5 10.5 11.5
Turbulence Intensity [%]	5 7 9 11
Shear Exponent [-]	-0.05 0.05 0.15 0.25

The wind farm configuration was modelled for two different wind directions. Firstly a full impingement direction from the South-West where turbine 1 is in the full wake of turbine 2. The second case is a baseline where both turbines are in free flow, primarily from the North-West. This analysis will primarily focus on the former of the two cases. The OpenFAST model was previously generated during the TUTTE project [36].

In order to generate the atmospheric conditions, TurbSim was used as the precursor ambient inflow simulation. TurbSim was chosen in order to maximise the number of cases which could be tested with the minimum required computational resources. These precursor simulations, which are then coupled with the FAST.Farm, utilised the Kaimal spectral turbulence model with scaling from the IEC 61400-1 standard. Six simulations in TurbSim were used across six random turbulence seeds for a total simulation time of 1000 s where the first 400 second transient period was removed.

6.4 Results

This section will focus on the trends which can be observed as a result of varying the inflow parameters and compare these with the trends extracted from the experimental data. For the purposes of this comparison, the experimental dataset has been filtered to encapsulate the parameter selection chosen for the simulations. The filtering of the dataset therefore respects the parameter ranges set for the simulations, however, it does not guarantee a one-to-one correspondence between specific cases.

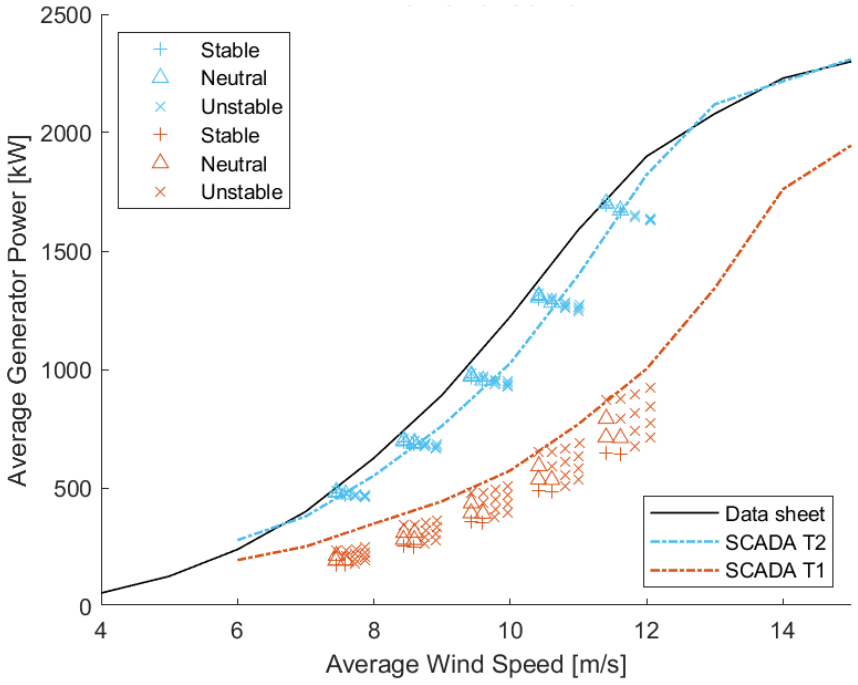

Figure 63. Power curve for the full-wake condition from the South-West and simulation data points for Turbine 1 (waked) and Turbine 2 (un-waked)

Figure 63 shows the generator power for both turbines 1 (red) and 2 (blue) operating in stable, neutral and unstable conditions. The categorisation into these stability classes is based on Dörenkämper (2015) [22], whereby the distinction between classes can be made based on turbulence intensity. While other methods for this type of classification exist, such as Rajewski et al (2013) [55], these were not suitable in this case due to the lack of high-resolution temperature data at the site.

Firstly, for the freestream turbine (T2), we see strong alignment with the experimental data gathered at the Båtskär site. With cases that fall into the stable and neutral criteria, we observe slight over-prediction of the generated power. On the other hand, the unstable cases show larger variation trending towards under-predicting. This variation is most likely caused by these cases covering a wider span of atmospheric conditions within the selected criteria which are most prevalent at the site.

Funded by the European Union

Secondly, for the waked turbine (T1), it is generally observed that the simulated power loss is greater than that of the SCADA data. Furthermore, with increasing wind speed, we see a larger variance and looser clustering of the output power. Since all of the experimental conditions are below the rated wind speed of the turbine, this outcome aligns with the findings in Shaler et al. (2020) [64], where for lower wind speeds an average over-prediction of 15.5% of the losses was shown in waked conditions.

Inspecting the different stability cases, we see that for the stable conditions the generated power tends to be on the higher than the average of the measured data. Conversely, for the waked turbine the stable cases generally present the highest losses in the simulations. On the other hand, the unstable cases for the waked turbine demonstrate a better recovery from the power losses. These patterns match those observed in the experimental data, whereby the relative power loss seen in Figure 62b decreases with higher values of turbulence intensity.

Funded by the European Union

7. WIND FARM FLOW CONTROL

7.1 Introduction

Leading-edge erosion (LEE) corresponds, as its name suggests, to the erosion that appears in the leading edge of wind turbines blades. This erosion is caused by particles that are suspended in the air (like rain or dust, for example) and can be a relevant issue, as it leads to blade damage (Figure 64). Actually, if this damage is not well addressed, it can have undesirable consequences. On the one hand, it can affect the operation and maintenance costs of the wind turbine, in terms of inspections and field repairs [56]. On the other hand, it can reduce the energy produced by the wind turbine [47, 53], although further validation with real data is needed to quantify this loss more reliably.

Offshore sites are, in general, more prone to LEE, due to four main particularities in marine environments:

- Stronger and steadier wind speeds [9]
- Higher rain rate rainfalls [13]
- Presence of sea-salt aerosols [47]
- Reduced noise restrictions [31]

LEE modifies, in essence, the shape of the aerodynamic profile, which affects its aerodynamic behaviour. This causes a loss in power production [61, 52], especially at below rated wind speeds, where the control system of the wind turbine traditionally looks for the optimum operating point (maximum power) of the clean blade.

Figure 64. Wind turbine blade with LEE

Funded by the European Union

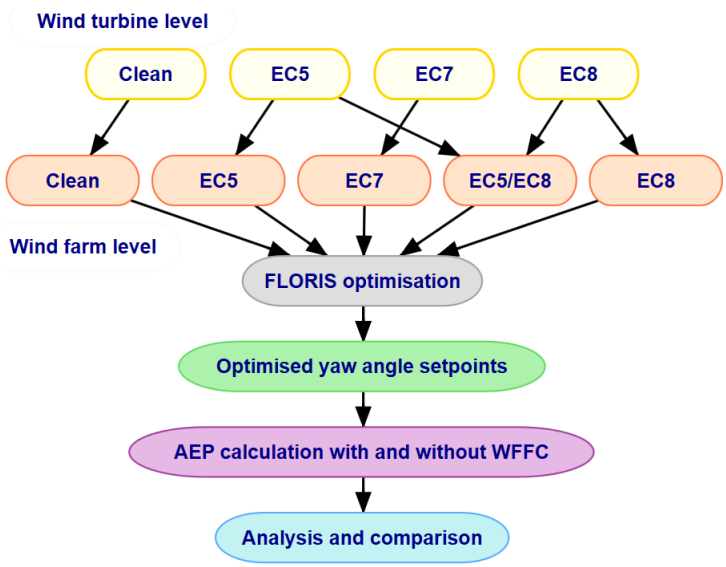

Figure 65. Methodology flow diagram

However, LEE not only reduces the power production of the turbine, but also the thrust force at the rotor, although little attention has been paid to this phenomenon in the literature. This thrust force contributes to the wake a wind turbine produces. Hence, a rotor with eroded blades produces a weaker wake than a rotor with clean blades [68]. This implies a modification in the overall performance of the wind farm, as weaker wakes cause less deficit in downstream wind turbines. Therefore, in principle LEE could have a relevant impact on wind farm flow control (WFFC) strategies, whose main objective is the optimisation of the wind farm performance as a whole taking into account aerodynamic inter-turbine interactions. The verification of this hypothesis is the main goal of this section, in which wake steering WFFC strategies are addressed.

7.2 Methodology

The methodology carried out in this work is shown as flow diagram in Figure 65 and, as can be observed, it is composed of six main steps.

The first step consists of defining the erosion levels that are going to be used in the study. In AIRE project [32] several erosion categories have been defined, but only three of them are applied herein for the sake of simplicity. Erosion category 5 (EC5) represents low-erosion level, erosion category 7 (EC7) represents medium-erosion level and erosion category 8 (EC8) represents high-erosion level. All eroded blade zones have the same C form with a transition to the clean profile of 45° (Figure 66), as explained in [58].

Funded by the European Union

These erosion categories are defined by three different parameters: h_e, u_e and l_e (Figure 66). In this case, h_e has been selected as 0.12% of the blade chord length for EC5 and EC7 categories, and 0.2% for EC8. u_e and l_e, which are considered equal in the present work (i.e. same eroded distance in pressure and suction zones), are 5% of the blade chord length for EC5, and 8% for EC7 and EC8. These erosion parameters are summarised in Table 11.

It is worth mentioning here that these erosion categories are only applied to the last 30% of the blade, as it is the blade zone with the highest linear velocity. In this zone, erosion level is considered constant with the blade length [58, 15].

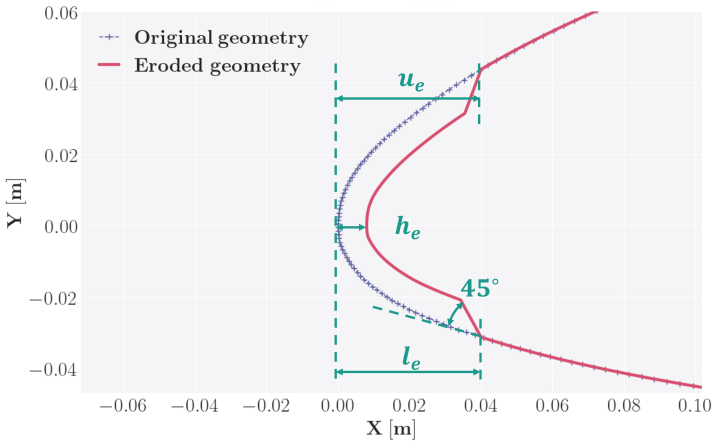

Figure 66. Erosion categories definition

Based on these erosion categories, the corresponding polars are calculated using OpenFOAM CFD software [35]. With them, four different wind turbine aeroelastic models are built, one for each erosion category and another one for a wind turbine with no erosion (called "Clean" in Figure 65). These four models are built in OpenFAST [34] and are used to obtain the power and thrust curves for each erosion category, which are inputs for the wind farm modelling tool, together with other parameters, like hub height, rotor diameter, wind rose, etc.

Table 11. Properties of blade erosion categories

Erosion category	h_e [%/c]	u_e [%/c]	l_e [%/c]	Max. efficiency loss [%]
5	0.12	5	5	22.47
7	0.12	8	8	38.72
8	0.20	8	8	66.60

Funded by the European Union

In Figure 67 the generated power and thrust coefficient curves for each erosion configuration are shown. As can be observed, there are little differences between the clean, EC5 and EC7 profiles, especially at below rated wind speeds. However, wind turbine performance with EC8 blades presents significant differences, which indicate performance is highly sensitive to h_e parameter. From 6 m/s to 15 m/s wind speed, the power produced by the turbine is much lower than for the other three configurations, and it actually reaches rated power at a higher wind speed (15 m/s instead of 12 m/s). Besides, the thrust coefficient is also much lower at below-rated wind speeds (near 0.5 instead of 0.8). This means the wake will also be notably weaker with this erosion configuration.

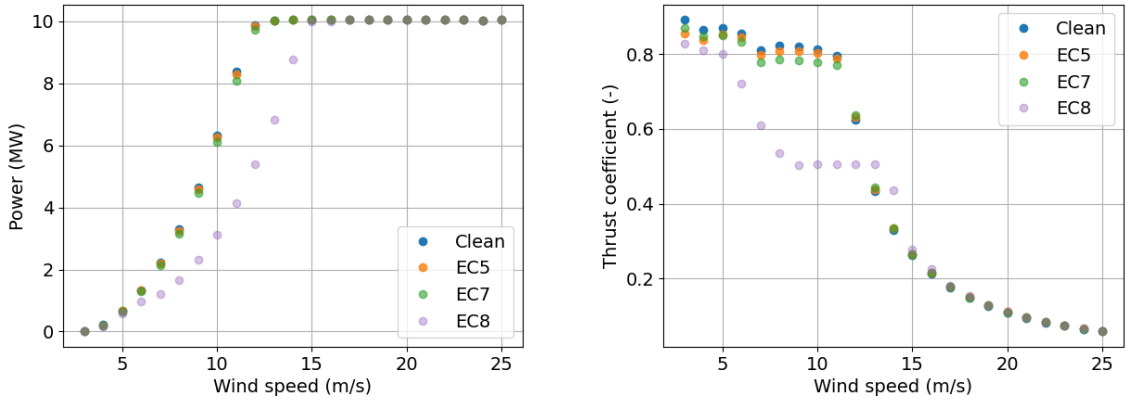

(a) Power curve **(b) Thrust coefficient curve**

Figure 67. Power and thrust curves for clean (blue), EC5 (orange), EC7 (green) and EC8 (purple) erosion categories

Funded by the European Union

As shown in Figure 65, the second step in the methodology consists of building the wind farm models. To do so, FLORIS [33] is used. The wake model used is the Gaussian model [8] with default wake parameters. Yaw angle setpoint limits haven been set between 0° and 20° ,although simulations by using variable yaw setpoint ranges from -20° to 20° have also been performed to check the sensitivity of the results to these parameters. Cosine loss exponent for yaw has been set to 3, based on OpenFAST simulations.

Five different wind farm models are built. One for each erosion configuration (clean, EC5, EC7 and EC8) and a fifth one, called EC5/EC8, which represents a mixed wind farm of wind turbines with EC5 or EC8 erosion categories. In order to select which turbines have EC5 and EC8 erosion levels, wind farm layout is combined with the site wind rose. Wind turbines that are most of the time in unwaked conditions are given EC8 (high erosion) and the rest of wind turbines are given EC5 (low erosion).

Then, as third step in the methodology, optimum yaw angle setpoints for each wind farm configuration, and for each wind speed and direction, are calculated using FLORIS. With these yaw angles, annual energy production (AEP) for the cases with WFFC for each configuration is calculated, as well as the AEP for the cases without WFFC.

Last, obtained results are analysed and compared, in order to quantify the differences between each casuistry.

7.3 Case study

In this section, the methodology described in Section 7.2 is applied to a practical case, in order to check its validity and study the results.

7.3.1 Definition

The analysed case study is defined by the following information:

- The selected wind farm is the virtual offshore TotalControl Reference Wind Power Plant [3], which is located in the west coast of Denmark (Figure 68a) and has the layout shown in Figure 68b. It consists of 32 DTU 10MW Reference Wind Turbines [6].
- Site wind resource data have been used [42, 40, 41] (Figure 69). For comparison purposes, resource data from another site have also been used to check the impact of site conditions on the results. Ulsan, in South Korea, has been selected as this second site ([18]), since its wind rose is very different to the site one (Figure 70).

  For the TotalControl site, most likely wind directions are between NW and SW (Figure 69). Therefore, for the mixed EC5/EC8 wind farm, wind turbines from T01 to T16 (two leftmost columns) are considered to have EC8 (high erosion) and turbines from T17 to T32 (two rightmost columns), EC5 (low erosion).

  As seen in Figure 69, the wind rose of the site does not have a remarkable predominant wind direction and most probable wind speeds are quite high. On the other hand, Ulsan site wind rose (Figure 70) is very directional and has a lower mean wind speed[1].

[1]For the sake of simplicity, the mixed EC5/EC8 wind farm configuration is maintained for Ulsan site wind resource.

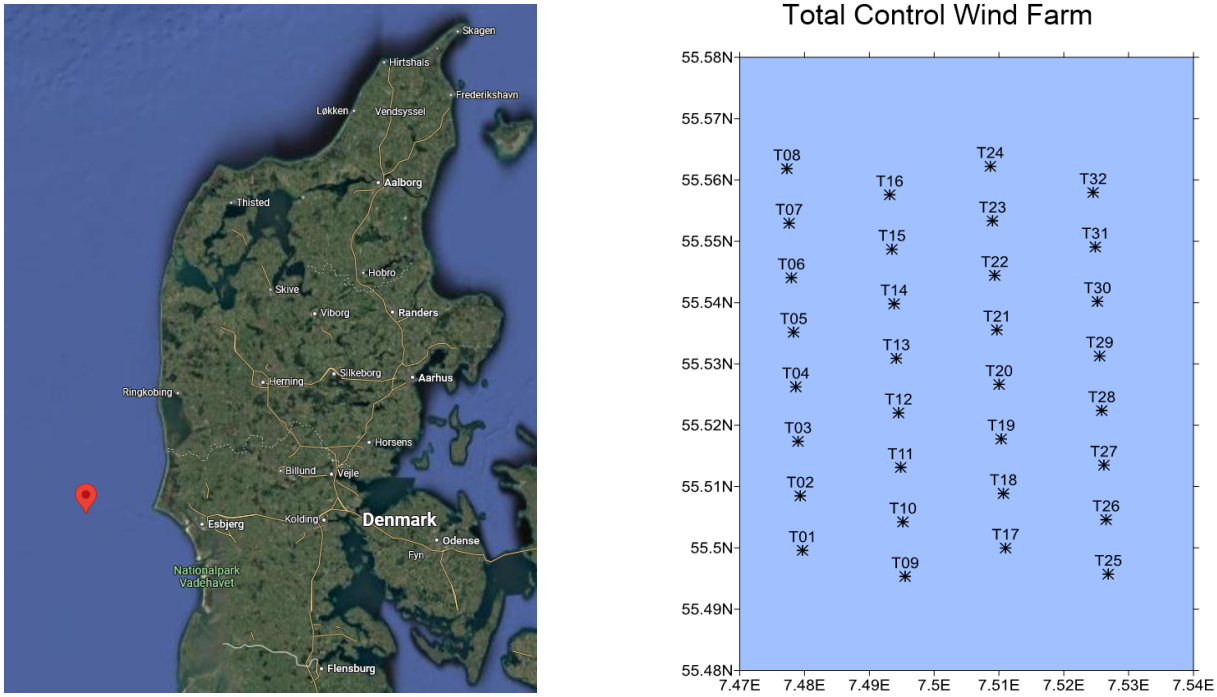

(a) Wind farm location **(b) Wind farm layout**

Figure 68. TotalControl Reference Wind Power Plant

- Erosion takes place on blade profile FFAW3241.
- As explained above, wind turbines are modelled using OpenFAST and wind farms using FLORIS. Yaw optimisation is also done using FLORIS.

7.3.2 TotalControl wind distribution

In this subsection results for the original wind distribution of the TotalControl wind farm site are presented and analysed.

7.3.2.1 Optimised yaw angle setpoints

In Figure 71 the optimised yaw angle setpoints of three turbines are shown with respect to wind direction for the case of 7 m/s. The turbines selected are WT01, WT20 and WT32, which represent three different wind farm zones. WT01 (south-westernmost turbine), for example, has 0° yaw angle setpoint for northern and eastern wind directions, as there are no wind turbines downstream and hence, there is no need for wake steering. However, for wind directions where there are downstream turbines (marked as grey-shaded areas in the figure; green-shaded areas represent upstream turbines), optimised yaw angle setpoints take non-zero values, in order to steer the wake and minimise its impact on downstream turbines. In any case, the most important thing to notice here is that most of the optimised yaw angle setpoints are very similar for every erosion configuration.

Funded by the European Union

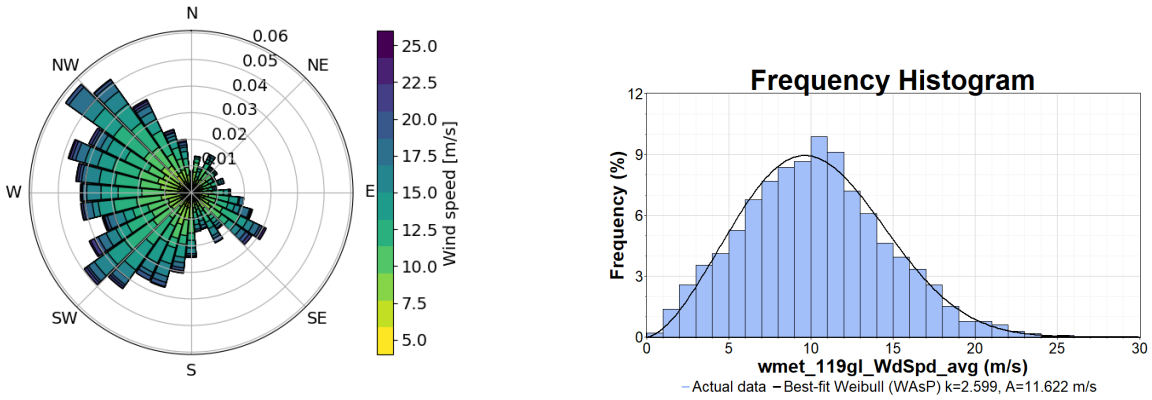

(a) Wind rose (b) Weibull distribution

Figure 69. TotalControl Reference Wind Power Plant wind rose (a) and Weibull distribution (b)

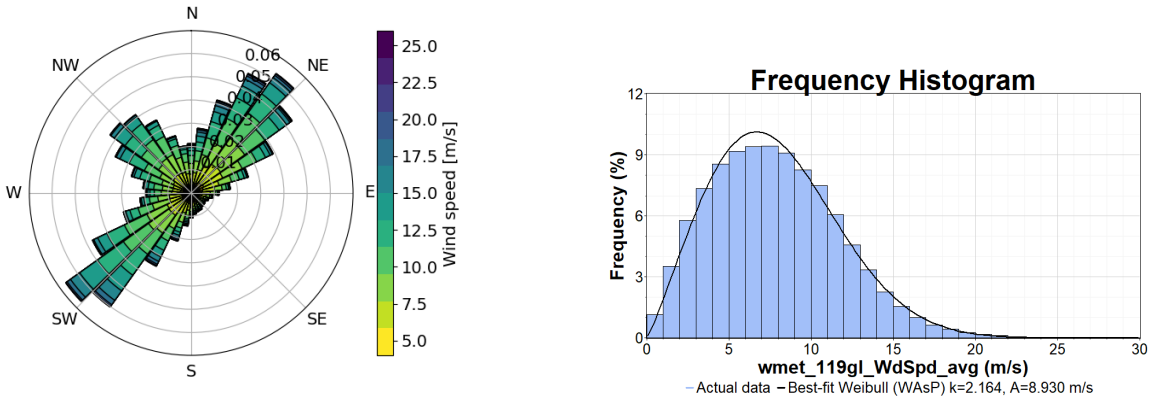

(a) Wind rose (b) Weibull distribution

Figure 70. Ulsan wind rose (a) and Weibull distribution (b)

The biggest differences that can be appreciated are between the mixed wind farm (EC5/EC8) and the rest of wind farm erosion configurations, for some specific wind directions. For instance, for WT01 (with high erosion within the mixed configuration), EC5/EC8 wind farm optimised yaw angle setpoints for western wind directions are higher than for the rest of configurations. This might happen due to the fact that there are less eroded wind turbines downstream. These turbines are able to produce more energy, hence it makes sense that upstream machines (more eroded) are more yawed to minimise wake affection in EC5 wind turbines and therefore maximise the overall wind farm power. For wind turbines WT20 and WT32 (with low erosion in that mixed wind farm configuration), the opposite happens. For eastern wind directions, optimised yaw angle setpoints for mixed EC5/EC8 configuration are in general slightly lower than for the other configurations. The reason might be that there are more eroded turbines downstream and, in consequence, the optimisation algorithm tries to maximise the power of less eroded wind turbines upstream (that means smaller yaw angle setpoints), as wakes are not going to further penalise the energy produced by the overall wind farm. Actually, it can be seen that the graphs for WT01 and WT32 are symmetrical for all configurations, except for the mixed one, for the reasons explained above.

Funded by the European Union

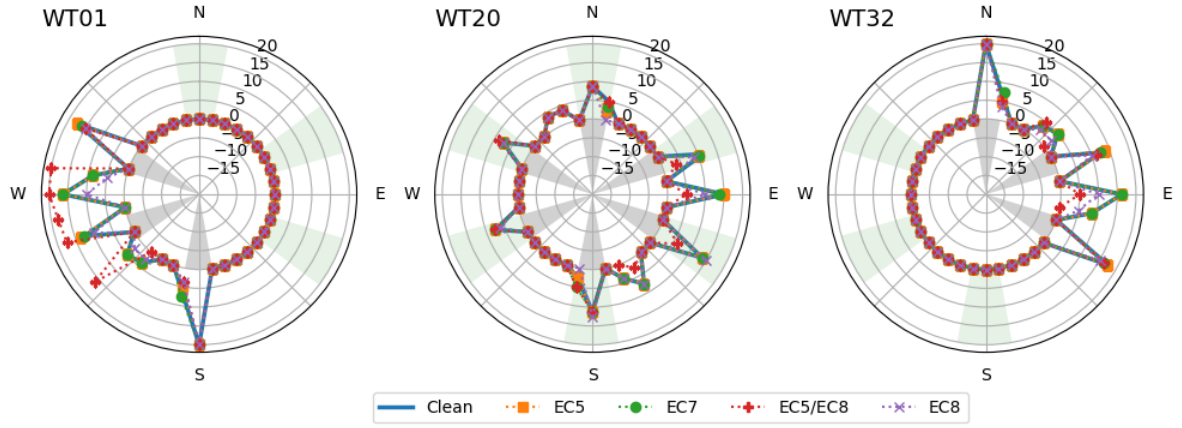

Figure 71. Optimised yaw angle setpoints for 7 m/s wind speed. Grey-shaded areas represent sectors with downstream turbines and green-shaded areas, sectors with upstream turbines

There are also some slight differences between EC8 and lower erosion categories (EC5 and EC7), for very specific wind directions (west for WT01 and east for WT32), but they are considered not to be very significant.

These conclusions are also drawn for the rest of wind turbines and wind speeds, and changing optimised yaw angles limits in FLORIS does not affect the conclusions either. This way, it can be concluded that optimised yaw angle setpoints for a homogeneously eroded wind farm are very similar as the erosion category evolves, and noticeable differences appear only if there are significant differences in the erosion category between wind turbines.

7.3.2.2 Annual energy production

Annual energy production (AEP) for every wind farm erosion configuration has also been calculated, with results shown in Table 12, for both with and without WFFC cases.

Table 12. AEP comparison for different wind farm erosion configurations (TotalControl wind distribution)

WF erosion type	AEP - no WFFC [GWh]	AEP erosion loss - no WFFC [%]	AEP - WFFC [GWh]	AEP erosion loss - WFFC [%]
Clean	1623.73	-	1650.20	-
EC5	1615.70	0.49	1641.84	0.51
EC7	1598.52	1.55	1623.71	1.61
EC5/EC8	1387.11	14.6	1405.53	14.8
EC8	1149.18	29.2	1159.33	29.7

Table 13. AEP wakes loss and WFFC gain for different wind farm erosion configurations (TotalControl wind distribution)

WF erosion type	AEP wake loss - noWFFC [%]	AEP gain with WFFC [%]
Clean	7.58	1.60
EC5	7.54	1.59
EC7	7.46	1.55
EC5/EC8	6.94	1.31
EC8	6.85	0.88

As expected, the greater the erosion level, the lower the AEP value is, regardless if it has or not WFFC. Actually, AEP losses due to erosion are small for EC5 and EC7 configurations, with values between 0.5% and 1.6%, which is aligned with the results seen in the power curve (Figure 67a) and in the literature [58]. The other two configuration cases (EC5/EC8 and EC8) present a much greater loss, with values between 14% and 30%, which is also in line with the power curve seen in Figure 67a. It is interesting to notice here again that, between EC7 and EC8 erosion categories, only h_e parameter has changed, increasing from 0.12% to 0.2% of the blade chord length. Therefore, the high sensitivity of AEP losses to this parameter is confirmed. Furthermore, in spite of having very similar values, AEP losses due to erosion are slightly higher for the cases with WFFC.

As erosion increases, wakes become weaker too, and so does the AEP loss due to wakes in the case with no WFFC (Table 13), which is in line with [68]. However, these AEP wake loss values remain quite similar among different erosion configurations. By contrast, the AEP loss due to overall effect of erosion (Table 12) can attain higher percentages and presents more disparate values among erosion configurations. In this sense, it can be said that, for this case study, high erosion levels affect much more power production than induced wake.

On the other side, as mentioned before, the AEP gain when applying WFFC is slightly reduced as erosion increases. For the clean, EC5 and EC7 configurations, a gain of nearly 1.6% is achieved, whereas for EC5/EC8 and EC8 configurations values are notably smaller (1.3% for EC5/EC8 and less than 0.9% for EC8). From these data, it can be clearly seen that, as erosion increases, wakes are reduced, which causes a lower potential benefit of WFFC, although for low and medium erosion levels this is barely noticeable.

7.3.3 Ulsan wind distribution

In this subsection results for the Ulsan site wind distribution are presented and compared with the ones obtained for the original wind distribution of the site.

7.3.3.1 Optimised yaw angle setpoints

FLORIS yaw optimisations do not depend on the wind rose, hence optimised yaw angle setpoints obtained for this wind distribution are the same ones as in the previous section (Figure 71).

7.3.3.2 Annual energy production

With this wind distribution, energy results are notably different, as the wind farm layout has not been optimised for these dominant wind directions. This means that wakes have, in general, higher impact than in the previous case. This, together with lower wind speeds, makes that AEP values are always lower than for the case with the TotalControl wind distribution, as observed in Table 14.

Table 14. AEP comparison for different erosion configurations (Ulsan wind distribution)

WF erosion type	AEP - no WFFC [GWh]	AEP erosion loss - no WFFC [%]	AEP - WFFC [GWh]	AEP erosion loss - WFFC [%]
Clean	1050.98	-	1067.04	-
EC5	1043.44	0.72	1059.24	0.73
EC7	1028.90	2.10	1044.04	2.16
EC5/EC8	862.93	17.9	874.36	18.1
EC8	678.18	35.5	684.29	35.9

Table 15. AEP wakes loss and WFFC gain for different wind farm erosion configurations (Ulsan wind distribution)

WF erosion type	AEP wake loss - noWFFC [%]	AEP gain with WFFC [%]
Clean	9.44	1.50
EC5	9.40	1.49
EC7	9.27	1.45
EC5/EC8	8.61	1.31
EC8	7.97	0.89

AEP losses due to wakes are obviously higher, but again, all the configurations have similar values, except EC5/EC8 and EC8, which have slightly lower values. Despite these differences, the trend is the same as with the original TotalControl wind rose. AEP gains with WFFC are similar compared to the previous site (see Table 15. AEP loss due to erosion is small (between 0.7% and 2.2%) for EC5 and EC7 wind farm configurations and much bigger for EC5/EC8 and EC8 (18% and 36%, respectively), as can be seen in Table 14. Therefore, conclusions extracted from the case with the original wind distribution can be applied to this site conditions too.

7.4 Conclusions

In this work, an analysis of the LEE impact on wake steering static WFFC strategies has been carried out, taking into account different erosion categories, wind farm erosion configurations and wind distributions. From the control point of view, the main conclusion is that the calculated optimised yaw angle setpoints are very similar for every erosion configuration, if the erosion level in all turbines is similar. By contrast, if there are large discrepancies in the erosion category within the wind farm, yaw angle setpoints may be different for some wind directions.

From the wind farm performance point of view, several interesting conclusions have been extracted. First of all, and as expected, the energy produced by eroded wind farms is lower than the energy produced by the clean farm. For low and medium erosion levels, this AEP reduction is small, but it can increase up to very significant values if the erosion is high enough. On the other hand, the energy lost by wakes in the case without WFFC is similar in every erosion configuration, although it gets slightly lower as erosion increases. In consequence, static yaw optimisation for wake steering improves the energy produced by the wind farm by a similar amount for each erosion configuration, but this gain gets smaller as erosion increases.

Funded by the European Union

8. CONCLUSIONS

Mesoscale

For the development of the erosion risk atlas in WP4 and case studies at commercial sites in WP5, wind speed and precipitation estimates from the mesoscale model WRF will be used. In Task 3.1, a sensitivity study was carried out that evaluated different model configurations on their ability to reproduce measured wind speeds and precipitation rates. Data from four sites having different terrain complexities and climatological characteristics were used, consisting of two AIRE sites and two publicly available data sets. A new model configuration was identified that accurately estimates the most damaging conditions, i.e. high rain rates in combination with high wind speed. This setup was then used in the production runs of the four commercial sites for one representative year.

Wakes

The development of the methodology for analysis of the rain conditions impact on wind turbine and wind farm performance has been completed, and it has been integrated into a workflow to facilitate the applicability of the analysis at other wind farms. The analysis of a specific wind farm has shown differences in some meteorological variables for the different datasets analysed, particularly in terms of turbulence intensity. An effect on turbine performance has been identified in terms of the power curve. Finally, in the wind farm analysis, the wind farm simulation results have been improved with the use of measured IEC curves, while the wake parameters have had similar results regardless of the presence of rain. However, it is considered necessary to study more wind farms to determine whether the observed effects can be generalized.

Microscale

The influence of a highly complex terrain has been analysed in the present work. A micro-scale model of the complex terrain surrounding the Alaiz experimental wind farm has been developed and validated against experimental data.

The $k - \varepsilon - f_P$ eddy viscosity model provides more accurate estimations when actuator disk is employed to model wind turbine. Its suitability for complex terrain simulations was compared against the $k - \varepsilon$ model and similar results in terms of wind speed, direction and turbulent kinetic energy. This justified its suitability in the calculated cases shown in this work.

The micro-scale model was calibrated and validated in terms of wind speed and direction with the available met masts experimental data, showing a good agreement.

In addition a virtual wind farm setup of 5 NREL5MW wind turbines was analysed in terms of wake dissipation. The virtual wind farm contribution to the natural terrain deficit of velocities and the wakes dissipation was studied at different distances downwards, up to $75D^*$ (9450 m); in the different wind turbines transects. The WT1, WT4, WT5 and WT6 transects in complex terrain showed a full wake recovery at $75D^*$. The slight wind farm wake deflection in complex terrain was attributed to a topographic depression to the west of the wind farm, which increases the westerly wind component.

The theoretical effect of the wind farm layout on other possible wind turbine sites in the vicinity was investigated and showed that the virtual wind farm would lead to a reduction in wind speed of up to 1 m/s at the potential sites to the south of the experimental wind farm (at above $10D^*$).

FAST.Farm

The experimental data analysis revealed certain trends that were successfully reproduced using the FAST.Farm model, highlighting its reliability in simulating wind farm performance. Trends of higher wind speeds and increasing turbulence both result in power loss recovery. However, a significant finding was the over-prediction of wake losses, which is consistent with previous studies in the field. To enhance the model's accuracy, integrating the DTU Mann turbulence generator could provide valuable improvements to the wake-added turbulence for offshore conditions such as those seen in this study. Additionally, the uncertainty surrounding the controller design, particularly in relation to power generation, underscores the need for further investigation to optimize performance.

Wind farm flow control

Regarding wind farm flow control, overall it can be concluded that, for the analysed cases, erosion does not have a relevant impact on static wake steering WFFC strategies, as long as high erosion levels do not appear on some wind turbines.

Funded by the European Union

PUBLICATIONS

Please list all the publications of this task here

- Sengers, B., Kassem, H. & Schwegmann, S. (2024, June). Sensitivity of wind resource estimates to microphysics schemes in WRF [Presentation & Poster]. WindEurope Technology Workshop.
- I. Sandua-Fernández, M. Aparicio-Sanchez, E. Cantero-Nouqueret & I. Eguinoa (2025, January). Analysis of leading-edge erosion impact on the design and performance of wind farm flow control [presentation & paper under-review]. DeepWind conference.
- Bretos, D., Campaña-Alonso, G., Méndez-López, B., & Cantero-Nouqueret, E. (2024, June). CFD wind farm evaluation in complex terrain under free and wake induced flow conditions. In Journal of Physics: Conference Series (Vol. 2767, No. 9, p. 092099). IOP Publishing.

REFERENCES

[1] A. T. Abolude and W. Zhou. "Assessment and performance evaluation of a wind turbine power output." In: Energies 11.8 (Aug. 2018). ISSN: 19961073.

[2] AIRE. AIRE Project - Enhancing Wind Power Production. URL: https://aire-project.eu/.

[3] S Andersen et al. Advanced integrated supervisory and wind turbine control for optimal operation of large Wind Power Plants - Reference Wind Power Plant. Tech. rep. Technical Report TotalControl Deliverable, 2018.

[4] H. Arastoopour and A. Cohan. "CFD simulation of the effect of rain on the performance of horizontal wind turbines." In: AIChE Journal 63.12 (2017), pp. 5375–5383. eprint: https://aiche.onlinelibrary.wiley.com/doi/pdf/10.1002/aic.15928. URL: https://aiche.onlinelibrary.wiley.com/doi/abs/10.1002/aic.15928.

[5] C. Bak, A. M. Forsting, and N. N. Sorensen. "The influence of leading edge roughness, rotor control and wind climate on the loss in energy production." In: Journal of Physics: Conference Series 1618.5 (2020), p. 052050. URL: https://dx.doi.org/10.1088/1742-6596/1618/5/052050.

[6] C. Bak, F. Zahle, R. Bitsche, T. Kim, A. Yde, L. C. Henriksen, M. H. Hansen, J. P. A. A. Blasques, M. Gaunaa, and A. Natarajan. "The DTU 10-MW reference wind turbine." In: Danish wind power research 2013 (2013).

[7] L. M. Bardal and L. R. Sætran. "Influence of turbulence intensity on wind turbine power curves." In: Energy Procedia 137 (Oct. 2017), pp. 553–558. ISSN: 1876-6102. URL: https://www.sciencedirect.com/science/article/pii/S1876610217353699.

[8] M. Bastankhah and F. Porté-Agel. "A new analytical model for wind-turbine wakes." In: Renewable energy 70 (2014), pp. 116–123.

[9] M. Bilgili, A. Yasar, and E. Simsek. "Offshore wind power development in Europe and its comparison with onshore counterpart." In: Renewable and Sustainable Energy Reviews 15.2 (2011), pp. 905–915.

[10] R. Braunbehrens, A. Vad, and C. L. Bottasso. "The wind farm as a sensor: learning and explaining orographic and plant-induced flow heterogeneities from operational data." In: (). URL: https://doi.org/10.5194/wes-2022-67.

[11] B. Cañadillas, M. Beckenbauer, J. J. Trujillo, M. Dörenkämper, R. Foreman, T. Neumann, and A. Lampert. "Offshore wind farm cluster wakes as observed by long-range-scanning wind lidar measurements and mesoscale modeling." In: Wind Energy Science 7.3 (2022), pp. 1241–1262. URL: https://wes.copernicus.org/articles/7/1241/2022/.

[12] M. Caboni and G. van Dalum. "Developing an atlas of rain-induced leading edge erosion for wind turbine blades in the Dutch North Sea." In: Wind Energy Science Discussions 2024 (2024), pp. 1–25.

[13] M. Caboni, H. M. Slot, G. Bergman, D. A. Wouters, and H. J. V. D. M. Meijer. "Evaluation of wind turbine blades' rain-induced leading edge erosion using rainfall measurements at offshore, coastal and onshore locations in the Netherlands." In: Journal of Physics: Conference Series 2767.6 (2024), p. 062003.

[14] Y. Cao, Z. Wu, and Z. Xu. "Effects of rainfall on aircraft aerodynamics." In: Progress in Aerospace Sciences 71 (2014), pp. 85–127. ISSN: 0376-0421. URL: https://www.sciencedirect.com/science/article/pii/S0376042114000785.

[15] A. Castorrini, A. Ortolani, and M. S. Campobasso. “Assessing the progression of wind turbine energy yield losses due to blade erosion by resolving damage geometries from lab tests and field observations.” In: Renewable Energy 218 (2023), p. 119256.

[16] R. D. Corrigan and R. D. Demiglio. Effect of precipitation on wind turbine performance. 1985.

[17] R. D. Corrigan and R. D. DeMiglio. Effect of precipitation on wind turbine performance. (Final report). Tech. rep. NASA Lewis Research Center, Cleveland, OH (United States); Sverdrup, Inc., Middleburg Heights, OH (USA), May 1985. URL: https://www.osti.gov/biblio/5801463.

[18] S. Creane, P. Santos, K. Kolle, D. Airoldi, M. Bakhoday-Paskyabi, M. Biglu, W. Brown, E. Cheynet, L. Ecenarro Diaz-Tejeiro, L. Froyd, et al. IEA Wind TCP Task 49: Reference Site Conditions for Floating Wind Arrays. Tech. rep. IEA Wind, 2024.

[19] M. Dörenkämper et al. “The Making of the New European Wind Atlas – Part 2: Production and evaluation.” In: Geoscientific Model Development 13.10 (2020), pp. 5079–5102. URL: https://gmd.copernicus.org/articles/13/5079/2020/.

[20] E. Douvi, D. Douvi, D. Pylarinos, and D. Margaris. “Effect of Rain on the Aerodynamic Performance of a Horizontal Axis Wind Turbine - A Computational Study.” In: Int. J. Energetica (IJECA) 6.1 (2021), pp. 35–43.

[21] E. Douvi and D. Margaris. “Aerodynamic Performance Investigation under the Influence of Heavy Rain of a NACA 0012 Airfoil for Wind Turbine Applications.” In: International Review of Mechanical Engineering 6 (Sept. 2012).

[22] M. Dörenkämper. “An investigation of the atmospheric influence on spatial and temporal power fluctuations in offshore wind farms.” PhD thesis. University of Oldenburg, 2015.

[23] Fraunhofer IWES. FOXES: Farm Optimization and eXtended yield Evaluation Software. URL: https://fraunhoferiwes.github.io/foxes.docs/index.html.

[24] E. Gaertner et al. Definition of the IEA 15□Megawatt Offshore Reference Wind Turbine. NREL Technical Report NREL/TP□5000□75698. Golden, CO: National Renewable Energy Laboratory, Mar. 2020. URL: https://www.nrel.gov/docs/fy20osti/75698.pdf.

[25] A. Gahlot, L. Sankar, and A. Pichitkul. “Computational Modeling of the Effects of Rain on Wind Turbine Performance.” In: Proceedings of the ASME Turbo Expo 11 (Oct. 2022). URL: https://dx.doi.org/10.1115/GT2022-82500.

[26] A. N. Hahmann et al. “The making of the New European Wind Atlas – Part 1: Model sensitivity.” In: Geoscientific Model Development 13.10 (2020), pp. 5053–5078. URL: https://gmd.copernicus.org/articles/13/5053/2020/.

[27] W. Han, J. Kim, and B. Kim. “Effects of contamination and erosion at the leading edge of blade tip airfoils on the annual energy production of wind turbines.” In: Renewable Energy 115 (2018), pp. 817–823. ISSN: 0960-1481. URL: https://www.sciencedirect.com/science/article/pii/S0960148117308649.

[28] Á. Hannesdóttir, S. T. Kral, J. Reuder, and C. B. Hasager. “Rain erosion atlas for wind turbine blades based on ERA5 and NORA3 for Scandinavia.” In: Results in Engineering 22 (2024), p. 102010.

[29] C. Hasager, F. Vejen, J. Bech, W. Skrzypiński, A.-M. Tilg, and M. Nielsen. “Assessment of the rain and wind climate with focus on wind turbine blade leading edge erosion rate and expected lifetime in Danish Seas.” In: Renewable Energy 149 (2020), pp. 91–102. ISSN: 0960-1481. URL: https://www.sciencedirect.com/science/article/pii/S0960148119319159.

[30] R. Herring, K. Dyer, F. Martin, and C. Ward. “The increasing importance of leading edge erosion and a review of existing protection solutions.” In: Renewable and Sustainable Energy Reviews 115 (2019), p. 109382. ISSN: 1364-0321. URL: https://www.sciencedirect.com/science/article/pii/S1364032119305908.

[31] R. Herring, K. Dyer, F. Martin, and C. Ward. “The increasing importance of leading edge erosion and a review of existing protection solutions.” In: Renewable and Sustainable Energy Reviews 115 (2019), p. 109382.

[32] https://aire-project.eu/. Accessed 12 February 2025.

[33] https://nrel.github.io/floris/. Accessed 12 February 2025.

[34] https://openfast.readthedocs.io/en/main/. Accessed 12 February 2025.

[35] https://www.openfoam.com/. Accessed 12 February 2025.

[36] M. Huttunen, T. Karlsson, J. Carreiro Spencer, and R. Prieto. TUTTE Project Final Report. Project Report. Espoo, Finland: VTT Technical Research Centre of Finland, Dec. 2022. URL: https://cris.vtt.fi/ws/portalfiles/portal/71394029/BF_TUTTE_Final_report_signed.pdf.

[37] International Electrotechnical Commission. “IEC 61400-12-1 ed. 2, Wind energy generation systems - Part 12-1: Power performance measurements of electricity producing wind turbines.” 2017. URL: https://webstore.iec.ch/publication/26603.

[38] J Jonkman, S Butterfield, W Musial, and G Scott. Definition of a 5-MW Reference Wind Turbine for Offshore System Development. Tech. rep.

[39] J. Jonkman, J. Annoni, G. Hayman, B. Jonkman, and A. Purkayastha. “Development of FAST.Farm: A new multi-physics tool for wind farm design and analysis.” In: AIAA Sci Tech. NREL/CP-5000-67528. Golden, CO, Jan. 2017.

[40] M. Koivisto, K. Das, F. Guo, P. Sørensen, E. Nuño, N. Cutululis, and P. Maule. “Using time series simulation tools for assessing the effects of variable renewable energy generation on power and energy systems.” In: Wiley Interdisciplinary Reviews: Energy and Environment 8.3 (2019), e329.

[41] M. Koivisto, G. M. Jónsdóttir, P. Sørensen, K. Plakas, and N. Cutululis. “Combination of meteorological reanalysis data and stochastic simulation for modelling wind generation variability.” In: Renewable Energy 159 (2020), pp. 991–999.

[42] K. Kölle, T. Göçmen, I. Eguinoa, L. A. Alcayaga Román, M. Aparicio-Sanchez, J. Feng, J. Meyers, V. Pettas, and I. Sood. “FarmConners Market Showcases Results: Wind farm flow control considering electricity prices and revenue.” In: Wind Energy Science Discussions 2022 (2022), pp. 1–29.

[43] E. K. Kruse. A Method for Quantifying Wind Turbine Leading Edge Roughness and its Influence on Energy Production: LER2AEP. Tech. rep. DTU Wind Energy, 2019. URL: https://orbit.dtu.dk/en/publications/a-method-for-quantifying-wind-turbine-leading-edge-roughness-and--2.

[44] M. P. van der Laan, N. N. Sørensen, P.-E. Réthoré, J. Mann, M. C. Kelly, and N. Troldborg. “The k-□-fP model applied to double wind turbine wakes using different actuator disk force methods.” In: Wind Energy 18.12 (2015), pp. 2223–2240.

[45] M. P. van der Laan, N. N. Sørensen, P.-E. Réthoré, J. Mann, M. C. Kelly, N. Troldborg, J. G. Schepers, and E. Machefaux. “An improved k- □ model applied to a wind turbine wake in atmospheric turbulence.” In: Wind Energy 18.5 (2015), pp. 889–907.

[46] C. M. Langel, R. Chow, O. F. Hurley, C. van Dam, D. C. Maniaci, R. S. Ehrmann, and E. B. White. "Analysis of the Impact of Leading Edge Surface Degradation on Wind Turbine Performance." In: 33rd Wind Energy Symposium. eprint: https://arc.aiaa.org/doi/pdf/10.2514/6.2015-0489. URL: https://arc.aiaa.org/doi/abs/10.2514/6.2015-0489.

[47] H. Law and V. Koutsos. "Leading edge erosion of wind turbines: Effect of solid airborne particles and rain on operational wind farms." In: Wind Energy 23.10 (2020), pp. 1955–1965.

[48] T. H. Malik and C. Bak. "Challenges in detecting wind turbine power loss: the effects of blade erosion, turbulence, and time averaging." In: Wind Energy Science 10.1 (Jan. 2025), pp. 227–243. ISSN: 2366-7451. URL: https://wes.copernicus.org/articles/10/227/2025/.

[49] L. Mishnaevsky, C. B. Hasager, C. Bak, A.-M. Tilg, J. I. Bech, S. Doagou Rad, and S. Fæster. "Leading edge erosion of wind turbine blades: Understanding, prevention and protection." In: Renewable Energy 169 (2021), pp. 953–969. ISSN: 0960-1481. URL: https://www.sciencedirect.com/science/article/pii/S0960148121000501.

[50] A. S. Monin and A. M. Obukhov. "Basic laws of turbulent mixing in the atmosphere near the ground." In: Tr. Akad. Nauk SSSR Geofiz. Inst 24 (1954), pp. 163–187.

[51] NREL. FLORIS- Wake models. URL: https://nrel.github.io/floris/wake_models.html.

[52] Ö. S. Özçakmak, D. Bretos, B. Méndez, and C. Bak. "Determination of annual energy production loss due to erosion on wind turbine blades." In: Journal of Physics: Conference Series 2767.2 (2024), p. 022066.

[53] K. Panthi and G. V. Iungo. "Quantification of wind turbine energy loss due to leading-edge erosion through infrared-camera imaging, numerical simulations, and assessment against SCADA and meteorological data." In: Wind Energy 26.3 (2023), pp. 266–282.

[54] F. Pasquill. Atmospheric diffusion. 2nd edition. Ellis Horwood, 1974. ISBN: 9780853120155.

[55] D. Rajewski et al. "Crop Wind Energy Experiment (CWEX): Observations of Surface-Layer, Boundary Layer, and Mesoscale Interactions with a Wind Farm." In: B. Am. Meteorol. Soc. 94 (2013), pp. 655–672.

[56] L. Rempel. "Rotor blade leading edge erosion-real life experiences." In: Wind Systems Magazine 11 (2012), pp. 22–24.

[57] P. J. Roache. "QUANTIFICATION OF UNCERTAINTY IN COMPUTATIONAL FLUID DYNAMICS." In: Annual Review of Fluid Mechanics 29.1 (1997), pp. 123–160.

[58] E Saenz, B Mendez, and A Muñoz. "Effect of erosion morphology on wind turbine production losses." In: Journal of Physics: Conference Series 2265.3 (2022), p. 032059.

[59] Y. M. Saint-Drenan, R. Besseau, M. Jansen, I. Staffell, A. Troccoli, L. Dubus, J. Schmidt, K. Gruber, S. G. Simões, and S. Heier. "A parametric model for wind turbine power curves incorporating environmental conditions." In: Renewable Energy 157 (Sept. 2020), pp. 754–768. ISSN: 0960-1481. URL: https://www.sciencedirect.com/science/article/abs/pii/S0960148120306613?via%3Dihub.

[60] A. Sareen, C. A. Sapre, and M. S. Selig. "Effects of leading edge erosion on wind turbine blade performance." In: Wind Energy 17.10 (2014), pp. 1531–1542. eprint: https://onlinelibrary.wiley.com/doi/pdf/10.1002/we.1649. URL: https://onlinelibrary.wiley.com/doi/abs/10.1002/we.1649.

[61] A. Sareen, C. A. Sapre, and M. S. Selig. "Effects of leading edge erosion on wind turbine blade performance." In: Wind energy 17.10 (2014), pp. 1531–1542.

[62] J. Schmidt, L. Vollmer, M. Dörenkämper, and B. Stoevesandt. “FOXES: Farm Optimization and eXtended yield Evaluation Software.” In: Journal of Open Source Software 8.86 (June 2023), p. 5464. URL: https://joss.theoj.org/papers/10.21105/joss.05464.

[63] M. Schramm, H. Rahimi, B. Stoevesandt, and K. Tangager. “The Influence of Eroded Blades on Wind Turbine Performance Using Numerical Simulations.” In: Energies 10.9 (2017). ISSN: 1996-1073. URL: https://www.mdpi.com/1996-1073/10/9/1420.

[64] K. Shaler, M. Debnath, and J. Jonkman. “Validation of FAST.Farm against full-scale turbine SCADA data for a small wind farm.” In: The Science of Making Torque from Wind. 2020.

[65] W. C. Skamarock, J. B. Klemp, J. Dudhia, D. O. Gill, Z. Liu, J. Berner, W. Wang, J. G. Powers, M. G. Duda, D. M. Barker, et al. “A description of the advanced research WRF model version 4.” In: National Center for Atmospheric Research: Boulder, CO, USA 145.145 (2019), p. 550.

[66] S. E. Smith, K. N. Travis, H. Djeridi, M. Obligado, and R. B. Cal. “Dynamic effects of inertial particles on the wake recovery of a model wind turbine.” In: Renewable Energy 164 (2021), pp. 346–361. ISSN: 0960-1481. URL: https://www.sciencedirect.com/science/article/pii/S0960148120314579.

[67] K. Venkatraman, T.-O. Hågbo, S. Buckingham, and K. E. Teigen Giljarhus. “Effect of different source terms and inflow direction in atmospheric boundary modeling over the complex terrain site of Perdigão.” In: Wind Energy Science 8.1 (2023), pp. 85–108.

[68] J. Visbech, T. Göçmen, Ö. S. Özçakmak, A. Meyer Forsting, Á. Hannesdóttir, and P.-E. Réthoré. “Aerodynamic effects of leading-edge erosion in wind farm flow modeling.” In: Wind Energy Science 9.9 (2024), pp. 1811–1826.

[69] L. Vollmer, H. Wurps, and M. Dörenkämper. “Benchmarking engineering wake models for farm-to-farm interactions.” In: Journal of Physics: Conference Series 2767.9 (2024), p. 092095. URL: https://dx.doi.org/10.1088/1742-6596/2767/9/092095.

[70] D. Wetterdienst. Wetter und Klima - Deutscher Wetterdienst - Glossar - N - Niederschlagsintensit. Tech. rep. Deutscher Wetterdienst. URL: https://www.dwd.de/DE/service/lexikon/Functions/glossar.html?lv3=101906&lv2=101812.

[71] Z. Wu, Y. Cao, S. Nie, and Y. Yang. “Effects of rain on vertical axis wind turbine performance.” In: Journal of Wind Engineering and Industrial Aerodynamics 170 (2017), pp. 128–140. ISSN: 0167-6105. URL: https://www.sciencedirect.com/science/article/pii/S0167610517302076.